Summer 7-16-2018

An investigation into remote sensing techniques for describing hydraulic roughness

Smriti Chaulagain
University of New Mexico - Main Campus

Smriti Chaulagain
Candidate

Civil Engineering
Department

This thesis is approved, and it is acceptable in quality and form for publication:

Approved by the Thesis Committee:

Dr. Mark Stone, Chairperson

Dr. Julie Coonrod

Dr. Su Zhang

AN INVESTIGATION INTO REMOTE SENSING TECHNIQUES FOR DESCRIBING HYDRAULIC ROUGHNESS

by

SMRITI CHAULAGAIN

BE, CIVIL ENGINEERING, KATHMANDU UNIVERSITY, 2013

THESIS

Submitted in Partial Fulfillment of the
Requirements for the Degree of

Master of Science
Civil Engineering

The University of New Mexico
Albuquerque, New Mexico

July, 2018

ACKNOWLEDGEMENT

I would like to thank my advisor, Dr. Mark Stone for accepting me as a graduate student. I am thankful for all his support, guidance and trust for completing this work. I would like to thank Dr. Julie Coonrod for her mentorship. Thank you Dr. Su Zhang for his willingness to help and providing me a valuable suggestion to improve my performance.

I express my sincere gratitude to Dr. Daniel Dombroski, Hydraulic engineer, Bureau of Reclamation, Denver, Colorado, for sharing the software without which my work would be incomplete. Thank you for your guidance.

Thank you, my friends and colleagues of University of New Mexico, for inspiration and supports.

Finally, my parents and siblings, thank you for your patience, kindness and supports. I wouldn't have completed this work without your support.

AN INVESTIGATION INTO REMOTE SENSING TECHNIQUES FOR DESCRIBING HYDRAULIC ROUGHNESS

by

Smriti Chaulagain

BE, Civil Engineering, Kathmandu University, 2013

MS, Civil Engineering, University of New Mexico, 2018

ABSTRACT

Riparian vegetation, an indicator of healthy river system, increases the hydraulic roughness and reduces the conveyance capacity of a channel. Vegetation provides dominant drag force influencing the velocity distribution, turbulence intensity and water depth. Thus, the study of hydraulic roughness due to vegetation is essential to determine the characteristics of flow. Traditionally, a constant Manning's roughness value is assigned based on land cover maps and that does not adequately account for vegetation. The roughness due to vegetation are determined on the basis of its parameters like height, density, LAI and flexibility. Remote sensing data (LiDAR, aerial photos or satellite images) are preferred in determining detailed vegetation parameters to time consuming field data. The objective of this research was to evaluate the performance of remote sensing-based methods to estimate hydraulic roughness of vegetation. A Canopy Height Model (CHM) was used in this study to estimate the height of vegetation and an empirical relation (Beer Lambert law) to determine LAI from LiDAR data for Middle Rio Grande reach located at Albuquerque, New Mexico. The two two-dimensional hydrodynamic

models, Sedimentation and River Hydraulics (SRH-2D) model and SRH-2DV, were used in this study. The models were simulated for four different flows (142 m^3/s, 198 m^3/s, 283 m^3/s and 425 m^3/s) for two roughness conditions i.e. constant and dynamic roughness. The results showed the minor changes in hydraulic parameters determined due to constant and dynamic roughness. The overall average dynamic roughness value predicted was more by 0.0008 compared to constant roughness for 283 m^3/s. Due to increase in dynamic roughness, water depth increased by 4 cm reducing the velocity by 1.7 cm/s for 283 m^3/s. Further study is suggested to determine the accuracy of hydraulic roughness estimated due to vegetation parameters derived from LiDAR through calibration of model results.

Contents

List of figures

List of tables

1. INTRODUCTION

Riparian vegetation provides river ecosystem services such as bank stabilization, transfer of nutrients, moderation of temperature, and diverse habitats (van Dijk et al., 2013; Afzalimehr & Dey, 2009; Wilson et al., 2003). Further, hydraulic connectivity supports healthy riparian vegetation (Stromberg et al., 2007). This connectivity largely depends on the inundation and interface dynamics (Stone et al., 2017) which have been altered in most river systems by anthropogenic activities such as dam construction (Poff et al., 1997).

Beyond the aforementioned benefits, riparian vegetation also increases hydraulic resistance, increases the threat of flooding by reducing the conveyance capacity of channels (Uotani et al., 2014), and increases sediment deposition (Vargas-Luna et al., 2015; Wu & He, 2009; Yi et al., 2008). Hydraulic resistance or roughness is the resistance provided by the surface (vegetation, bed materials, bed forms, channel irregularities, etc.) on which a fluid flows (Arcement & Schneider, 1989). Riparian vegetation has a strong influence during high flows during overbank flow conditions. The increase in roughness due to vegetation reduces wave celerity, increases the depth of water, and reduces the water velocity. Thus, the study of hydraulic resistance provided by vegetation is one of the major concerns in environmental river management. As a consequence, a substantial body of research has been conducted to identify the effects of vegetation on hydraulic roughness in relation to hydraulic parameters such as velocity distributions, water depths, turbulence, and vegetation characteristics or parameters including height, density, flexibility, and spatiotemporal aspects.

The roughness value of vegetation is assigned in several ways at different phase. It is defined manually as a function of land cover type (Forzieri et al., 2010) based on predefined roughness values (Chow, 1959) through experts' visual inspection (Stone et al., 2013) in traditional approach but values are calculated in relation to vegetation parameters in new approach implemented in this study. The roughness value from traditional approach is considered as constant roughness whereas dynamic roughness for new approach. To improve the accuracy in constant roughness, spectral images are used for mapping of vegetation. A large number of studies have proposed resistance laws for the estimation of dynamic roughness depending upon the vegetation parameters. These vegetation parameters can be physically measured in field (Gillihan, 2013) but this method is time consuming and not feasible for larger areas. Alternatively, remote sensing-based data provide benefits over the field data in that aspect and improves the accuracy in terms of both temporal and spatial extend which was applied in this study. The vegetation characteristics (height and Leaf Area Index (LAI)) were then used to parametrize a dynamic hydraulic resistance equation. The equation developed by the study of Jarvela (2004) was applied to the Middle Rio Grande (MRG) using a two-dimensional hydrodynamic model.

2. RESEARCH OBJECTIVES

The goal of this research was to advance the techniques for describing spatially and dynamically varying hydraulic roughness. To accomplish this goal, I pursued the following objectives:

- Develop a framework for characterizing vegetation using remote sensing data to estimate hydraulic roughness.
- Demonstrate and test the framework using a hydrodynamic model applied to the Middle Rio Grande located in Albuquerque, New Mexico.

3. BACKGROUND

3.1 Hydraulic roughness

The investigation and study of hydraulic roughness and other flow parameters began in the eighteenth century with several modifications in later days. Chezy's formula in 1776 with C as bed and bank roughness ((u= C$\sqrt{Rs}$), where u is the velocity of flow, R is hydraulic radius of the channel and S is the bed slope), Prandtl and Von Karman equation, White-Colebrook formula, Darcy-Weisbach, Sticklers, and Manning's in 1891 are some common formulas or methods for prediction of roughness. However, manning's equation ($u = ({}^{k}/_{n})R^{\frac{2}{3}}\sqrt{s}$, where u indicates the velocity of water, k=1.486 for imperial units and 1 for SI units, and *n* denotes the Manning's roughness coefficient) is most widely used to compute hydraulic roughness of open channel systems. Manning's formula is developed by Robert Manning in 1891 (FathiMaghadam & Kouwen, 1997). Generally, the Darcy-Weisbach friction factor, f, and Chezy's constant, C, are related to Manning's, n, by $n = (\sqrt{\frac{f\, y_n^{1/3}}{8g}})$ and $C = R^{1/6}/n$ respectively, where y_n is the normal water depth. Those approaches do not include the effect of vegetation. In 1949, Ree & Palmer defined the hydraulic roughness as a function of hydraulic parameters (velocity, U, and hydraulic

radius, R) and included vegetation. This empirical relation, which is called the n-UR relation, was revised by US Soil Conservation Service (SCS, 1954) for grass-lined channel. The method was further studied (Temple et al., 1987) and criticized (Kouwen et al., 1981). Kouwen et al. (1981) claimed that the method is not valid for smaller slope (less than 5%) and for short and stiff vegetation. The difficulty in getting a unique relation of n-UR even for uniform vegetation types (Wilson & Horritt, 2002) made this method difficult to implement. This led to further investigation in understanding the effect of vegetation on flow.

Hydrodynamic modeling often requires simplification of complex processes. The effect of sediments and vegetation present in the river system is represented by hydraulic roughness. Sediments and bedforms are the dominant factors offering resistance to flow in non-vegetated channels but for vegetated channels, vegetation roughness is also essential because drag force due to vegetation is dominant for vegetated channels (Temple et al., 1987). Furthermore, even though for the high level of flood, roughness due to vegetation (especially short vegetation) tends to remain constant or uniform (Chow, 1959) acting like a rough boundary, vegetation roughness fluctuates due to fluctuation of flood conditions in overbanks (Wu et al., 1999). Also, the increase in submerged momentum absorbing area (MAA) changes the Manning's roughness value with depth (FathiMaghadam & Kouwen, 1997). Therefore, constant Manning's *n* doesn't accurately represent a complex interaction of MAA due to vegetation. MAA is the function of flexural rigidity and is dependent on one-sided stem and leaf area (FathiMaghadam & Kouwen, 1997). Despite these findings, vegetation induced roughness is usually considered uniform (Horritt & Bates, 2002) or highly simplified in hydrodynamic models.

A variety of approaches have been implemented to understand the effects of vegetation. For example, Jarvela (2005) studied the effect of flexible vegetation on the flow structure using a flume setup. The results indicated that shear velocity due to deflection of plant height is important for estimating the velocity profile above flexible plants. The velocity profile also depends on vegetation drag (Wu & He, 2009).

The hydraulic roughness of vegetation varies depending on vegetation spatial variability, vegetation submergence (full or partial) conditions which impacts hydraulic parameters like turbulence intensity, velocity distribution, and the drag coefficient. Wu et al. (1999) conducted flume study to determine the roughness on the basis of flow depth (i.e. submerged or unsubmerged condition) in relation to the drag coefficient and velocity distribution for pine and cedar tree saplings. They found that the roughness coefficient (*n*) decreases with an increase in water depth during unsubmerged conditions. However, for submerged conditions, the roughness coefficient increases or remains constant near the channel bed and reaches an asymptotic constant for further increase in water level (Wu et al. 1999; FathiMaghadam & Kouwen, 1997; Wilson ,2007).

The spatial distribution or density of vegetation is a dominant parameter in determination of hydraulic roughness (FathiMaghadam & Kouwen, 1997; Nepf, 1999; Järvelä, 2002; Järvelä (2004)). The study of FathiMaghadam & Kouwen (1997) indicated that the density of vegetation has greater influence for unsubmerged conditions because vegetation density increases the submerged MAA. Furthermore, the study of Nepf in 1999 indicated that the intensity of turbulence also depends on the density of vegetation. Similarly, Järvelä (2004) focused on estimating hydraulic roughness for leafy and non-

leafy vegetation to estimate the effect of vegetation density as LAI and vegetation height and proposed a model to estimate flow resistance under low flow and relatively low velocity conditions with both stiff and flexible woody vegetation.

Previous studies showed that the variability of vegetation has a significant effect on hydraulic roughness that alters water depth, velocity profile and turbulence intensity. The variability of vegetation is studied in terms of plant characteristics such as LAI, density, height and steam diameter of vegetation. A study of Baptist et al. (2007) showed that the hydraulic roughness of vegetation depends upon the vegetation height (submerged or unsubmerged) and stem density (that induces vegetation drag). Similarly, the approach of Jarvela (2004) gave the relation of hydraulic roughness of vegetation in relation to LAI ($f = 4C_{d\chi}\, LAI\, (\frac{U}{U_\chi})^{\chi}\, \frac{h}{H}$, f is the Darcy friction factor C_d where drag coefficient, U is average velocity of water, h is depth of flow, H is the height of vegetation, $C_{d\chi}$ species-specific drag coefficient, χ is unique particular species constant and U_χ reference velocity). In this approach, LAI was used to represent the density of vegetation. The study of Jalonen et al. (2013) showed that the LAI can be used to represent the density of vegetation.

Uncertainty exists in estimation of hydraulic roughness of vegetation because it depends upon vegetation structural characteristics such as stem thickness, density, vegetation height, and rigidity of stem and leaves as well as flow conditions. Vegetation structure on the other hand varies with the time of year. Even for the same species of vegetation, due to spatial variability stem diameter and density will be different (Busari & Li, 2015). In addition, error in classification of landcover maps and spatial resolution of terrain are other factors which increases uncertainty in flood plain roughness Straatsma & Huthoff (2011).

3.2 Hydraulic roughness from remote sensing data

Remote sensing data can be used to generate useful input data for hydraulic modeling. It is utilized for developing terrain as well as a land cover maps (Dorn et al., 2014). The accuracy of terrain and land cover maps will be higher for the higher spatial resolution of remote sensing data (Casas et al., 2010). The accuracy of land cover depends upon on the proper selection of the method in classifying the image (Forzieri et al., 2010). Three different classification methods are commonly used to classify the image on the basis of land cover i.e. (1) supervised image classification, (2) unsupervised image classification, and (3) object-based image analysis (OBIA) (Jensen, 2016). Remote sensing data are beneficial not only to represent the spatial distribution of vegetation and other land features (building, pavement, wetlands, water, etc.), but also help in determining the vegetation parameters like vegetation height, LAI, and stem density. Aerial images with spectral characteristics are typically analyzed to distinguish vegetation types. Vegetation indices are also used for spectral discrimination of riparian vegetation which is calculated on the basis of bands of image. For example, Normalized Vegetation Index (NDVI) can monitor phonological changes in vegetation (Weiss et al., 2004).

Considerable amount of progress has been made for spectral mapping of vegetation and determination of vegetation parameters in order to define the hydraulic roughness in presence of vegetation. Abu-Aly et al. (2014) analyzed the spatial distribution of vegetation roughness to estimate its effect on hydrodynamic behavior of flow compared to fixed or constant hydraulic roughness (Chow, 1959). LiDAR data were used to create the Canopy height model and followed the approach of Casas et al. (2010) to estimate hydraulic

roughness. Similarly, Dorn et al. (2014) compared vegetation mapping for LiDAR, orthophotos, and Crowdsourced Geodata. They concluded that LiDAR data can be merged with Open Street Map (OSM) to increase the accuracy of roughness mapping. Zahidi et al. (2015) compared vegetation mapping obtained from a combination of Quickbird images and low point density LiDAR. Jeong et al. (2016) used spectral image and LiDAR for mapping riparian vegetation. Furthermore, Forzieri et al. (2010) implemented supervised classification merging Quickbird images and LiDAR for preparing vegetation map as an input for hydrodynamic model. Again, Forzieri et al. (2011) determined the parameters of vegetation like height, diameter of stem, crown diameter, and plant density to find roughness due to vegetation using LiDAR data. Straatsma & Baptist (2008) introduced vegetation parameters (vegetation height and stem density) for determining hydraulic roughness of vegetation from LiDAR data in a 2D hydrodynamic model. All these studies have shown the improvement in result of hydrodynamic model due to representation of vegetation characteristics using remote sensing data.

Even though, the use of LiDAR data for the study of forest and agriculture (Richardson et al., 2009; Solberg et al., 2006; Tseng et al., 2016) is common, they were used less frequently in prediction of vegetation characteristics (height, density, LAI) to estimate hydraulic roughness. Some studies used LiDAR data for determining height of vegetation (Mason et al., 2003; Abu-Aly et al., 2014). However, estimation of density from remote sensing data is rare. The estimation or prediction of dynamic density is a challenging task. The work of Straatsma (2008) and Straatsma et al. (2008) are the only known works to quantify the density of vegetation using LiDAR points, terrestrial laser

scanning, and digital photography. Since this study utilized the LiDAR data to predict vegetation parameters. It provided a novel method to determine roughness of vegetation using remote sensing data to analyze vegetation height and density.

4. MATERIALS AND METHODS

4.1 Study area

The study area extends 7 km from the Montano Road Bridge (henceforth Montano) to the Central Avenue Bridge (henceforth Central) along the Rio Grande in Albuquerque, New Mexico. A USGS stream gage (08330000) is located at the Central site.

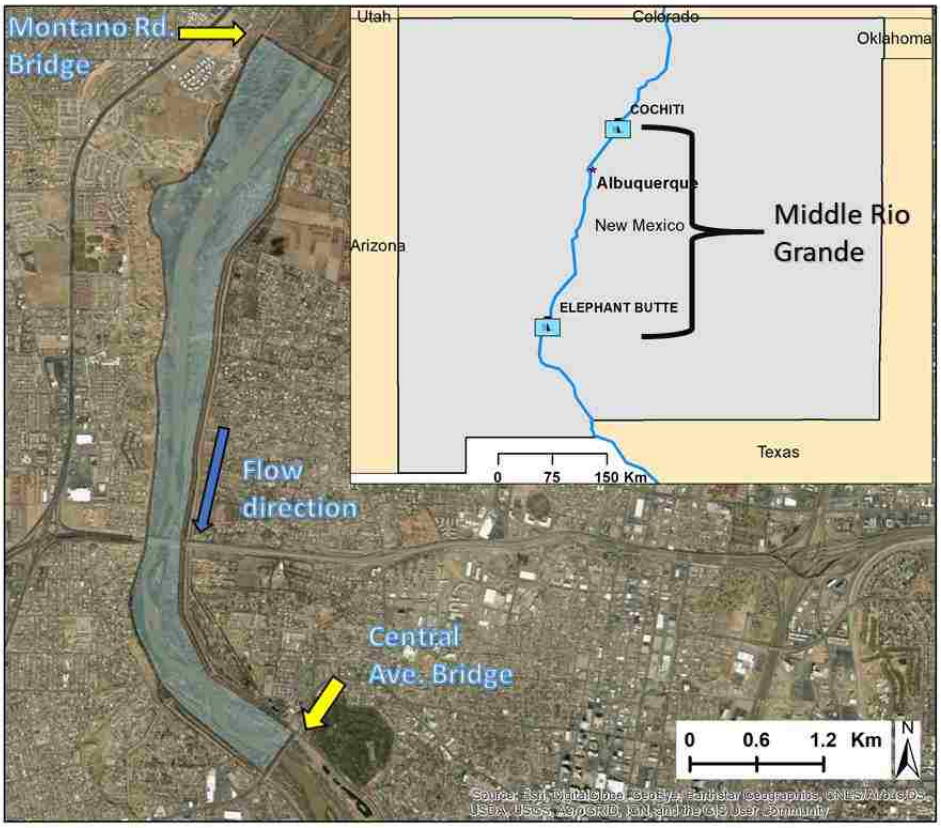

Figure 1: Study area MRG, from Montano Bridge Road to Central Avenue at Albuquerque, New Mexico

Features of the MRG

The portion of Rio Grande from Cochiti Dam to Elephant Butte Reservoir is defined as the MRG. Because of drought, bank stabilization, invasive vegetation, and the establishment of flood control systems, the width of the river has narrowed, meandering has increased, and sand bars have become pervasive. The width of the channel at the Central site was reduced from 365 m in 1935 to 122 m by 2002(Mussetter Engineering, Inc., 2006). The average width of the river is about 183 m, typical depth varies from 0 to 1.5 m, and average bankfull discharge is about 142 m^3/s (Isaacson & Coonrod, 2011). The bankfull discharge is the condition when the channel is at full capacity and just about to spill onto the floodplain (Leopold, 1994). Discharge is highest in May and June due to snowmelt runoff.

The dominant vegetation species along the MRG include native cottonwoods (*Populus deltoids*), coyote willow (*Salix exigua*) salt cedar (*Tamarix ramosissima*) and Russian olives (*Elaeagnus angustifolia*) (Mussetter Engineering, Inc., 2006). However, changes in physical conditions of the river have led to an increase in exotic species including *Tamarix ramosissima* and *Elaeagnus angustifolia*.

The MRG is managed by a combination of local, state, and federal agencies including the Middle Rio Grande Conservancy District (MRGCD), the New Mexico Interstate Stream Commission (ISC), the U.S. Army Corps of Engineers (USACE), and the U.S. Bureau of Reclamation (USBOR). The MRGCD constructed floodways and levee systems in early 1930s. Further to control sediments and stabilize bank lines, jetty jacks were installed. Major dams were constructed across tributaries as well as the main Rio Grande to control floods and sediments.

4.2 Datasets

LiDAR data collected in the year 2010 (March and April) were used in this study. The data were acquired by Leica Geosystems ALS50II LIDAR system mounted with an inertial measurement unit (IMU) and dual frequency GPS receiver, at a flight height of 2511.86 m (8,241 feet) above the ground level. The scan angle for the data varies from 0 to $\pm 29^0$. Cross-section data collected from 2013 and 2014 by USBOR were used as bathymetry for the channel. Revised landcover vegetation mapping done by the U.S. Army Corps of Engineers (USACE) in 2005, Albuquerque District which was originally created by the Upper Rio Grande Water Operations Review and EIS (URGWOPS) in 2002 based on ground method and aerial survey was used as landcover for assigning Manning's roughness values. The vegetation map consists of 93 polygons for the study reach.

4.3 Research framework and approach

4.3.1 Research Framework

The proposed approach combined the land cover and vegetation parameters derived from remote sensing data. Different flood conditions were simulated in the Albuquerque Reach of the MRG using the modified two-dimensional hydrodynamic model, Sedimentation and River Hydraulics (SRH-2D) (Dombroski, 2017). The simulations were conducted for roughness values based on land cover and dynamic roughness obtained from vegetation parameters. An overview of the methods framework is shown in Figure 2.

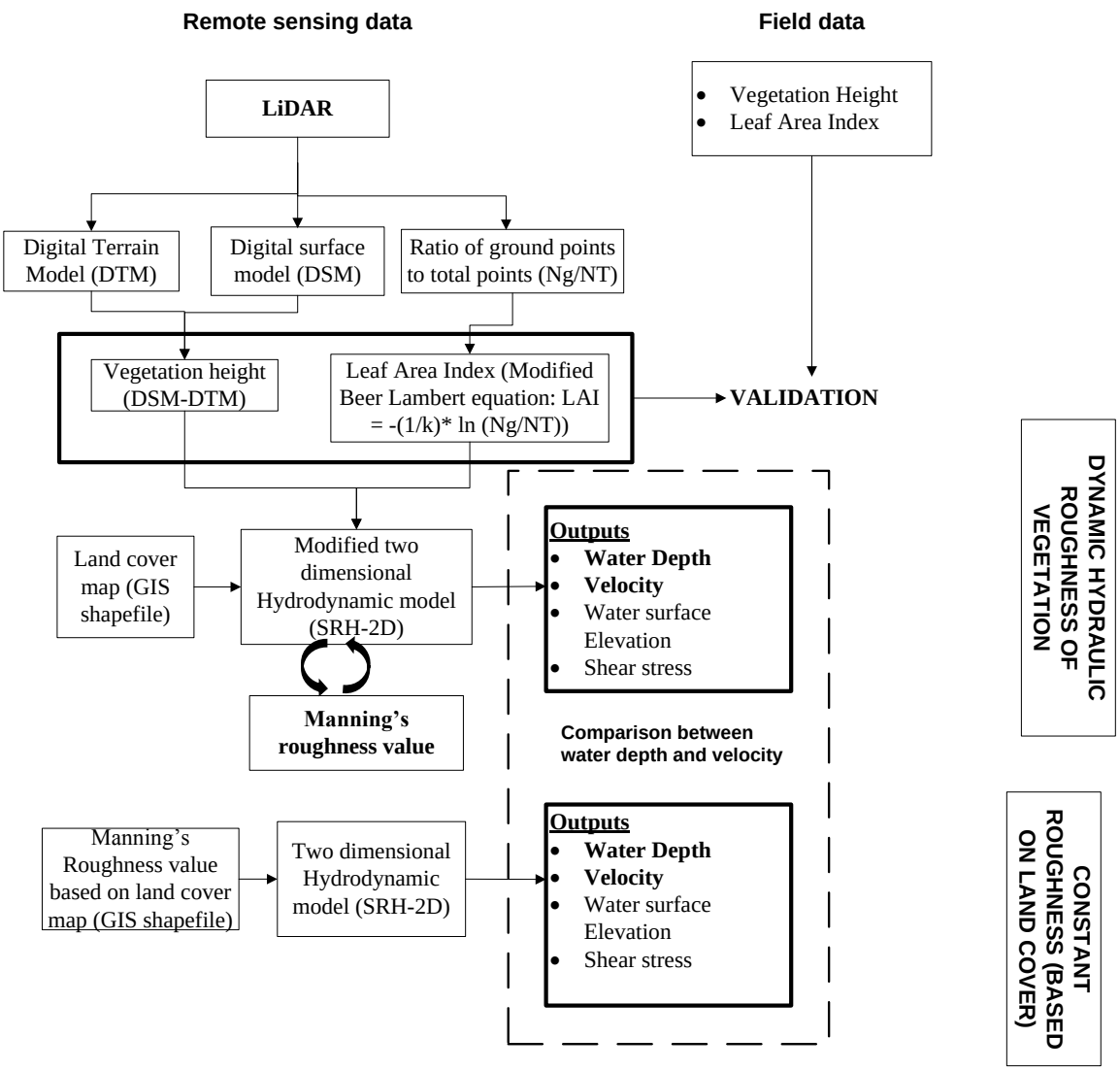

Figure 2: Schematic diagram of method framework

4.3.2 Approach

4.3.2.1 LiDAR data processing

In this study, the approach of Jarvela (2004) was used for analyzing the influence of vegetation parameters on the estimation of hydraulic roughness due to vegetation. In this approach, two parameters i.e. height and LAI of vegetation are required. These

parameters were determined using LiDAR data. The methods for obtaining height and LAI are described below in detail.

Canopy Height Model (CHM)

The CHM was developed using ArcGIS 10.5 from LiDAR data to represent the height of vegetation. CHM is obtained by subtracting the Digital Terrain Model (DTM or bare earth) from the Digital Surface Model (DSM). LiDAR data classified as ground and non-ground points were utilized for creating the DTM and DSM. To create DTM, LiDAR points classified as ground points or last return only were used whereas first return points were used for creating the DSM. The DTM represents the ground surface while the DSM created using only the first return consists of the points reflected by the top of vegetation. Hence the difference between these surfaces normally represents the height of vegetation.

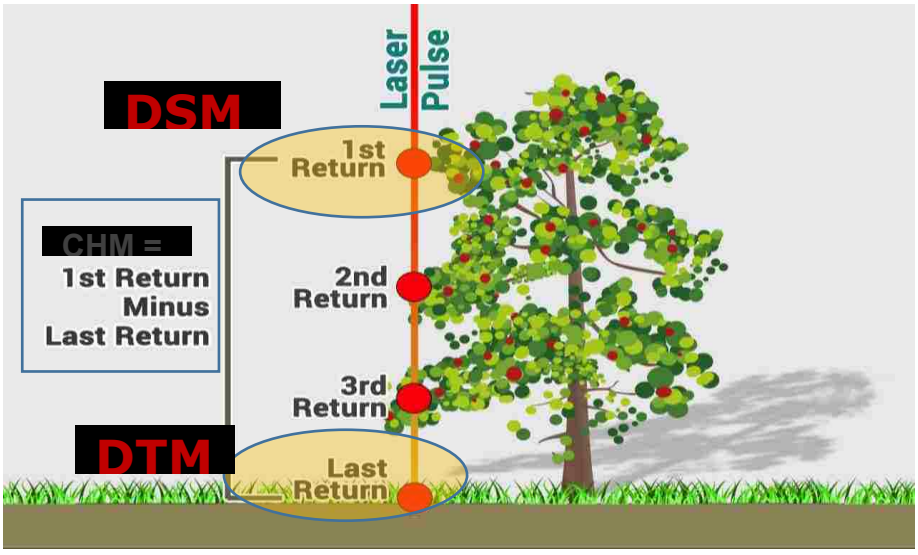

Figure 3: CHM from LiDAR points

While working on LiDAR data to create CHM, some of the outliers were observed and are likely attributable to birds, reflection from water, power lines, towers, etc. These outliers were removed to reduce errors in determining the height of vegetation using LAStools. LAStools is batch-scripted multi-core LiDAR processing tool developed by Dr. Martin Isenburg (Isenburg, 2014). The function of LAStools, lasview was used to have a close view of those points and the las height tool was used to remove those points. The detail steps for creation of CHM model and the codes used for removing the outliers are included in Appendix A.

Estimation of LAI

Besides vegetation height, LAI is another parameter in determination of roughness value. LAI can be estimated directly and indirectly (Breda, 2003). In direct method, LAI is determined in field using active sensors (example: terrestrial laser scanning) or passive optical method (example: AccuPAR LP-80). Indirect method involves the use of remote sensing data like LiDAR, satellite imagery.

The Beer Lambert equation ($I= I_o\, e^{-L/k}$, where I and I_o is the light intensity below and above the canopy respectively., k is extinction coefficient and L is LAI) (Luo et al., 2018; Richardson, Moskal, & Kim, 2009; Solberg et al., 2006; Breda, 2003) is most widely used in determining the LAI of forest. The analogy or modified equation (Richardson et al., 2009; Tseng et al., 2016) of that equation is $LAI = -(1/k)\, \ln(N_g/N_T)$ N_g is the number of ground points, and N_T is all LiDAR returns. The extinction coefficient, *k*, depends on the several factors including distribution of foliage inclination, and structure of leaves (broad or coniferous). In this study, the modified equation was implemented to determine

LAI. The value of k was considered as 0.5 from the study of Breda (2003). ArcGIS 10.5 was used to obtain the ratio of ground points and total LiDAR returns and finally *LAI* was calculated.

Ground Truthing

To check the accuracy or to verify the land cover map, CHM and LAI, field observations were conducted. The data were collected for the transect of 10 m x 10 m representing the range of vegetations types from the entire area of interest. The data of vegetation parameters including height and LAI were collected. The procedure of Gillihan (2013) was followed in this research to measure height and to determine LAI in field. Vegetation height was measured using a hypsometer. The AccuPAR LP-80 passive optical sensor was used to determine the LAI. Figure 4 shows the location where the data were gathered.

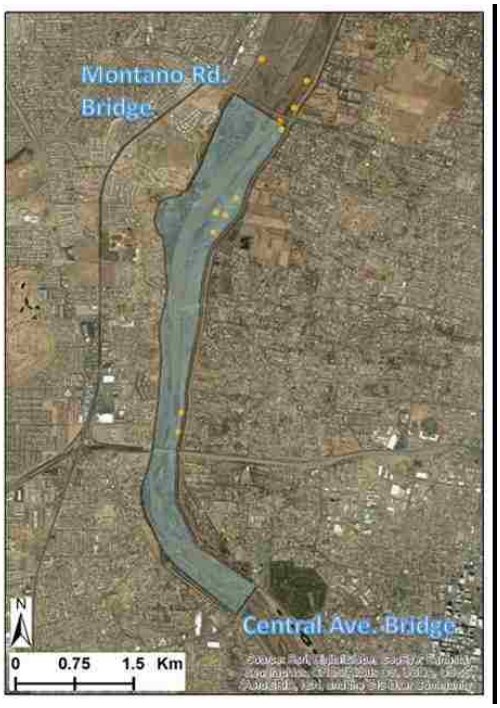

Figure 4: Location of field data collection represented by yellow dots

The height and LAI of the vegetation was prepared in a format that is required for the hydrodynamic model. These parameters were generated into raster format using ArcGIS 10.5. The raster value of height and LAI were aggregated for polygons of each type of vegetation and each polygon was assigned with the average value of height and LAI.

4.3.2.2 Hydrodynamic modeling

The two-dimensional hydrodynamic model SRH-2D, developed by United States Bureau of Reclamation, was selected for simulating under constant and dynamic roughness condition. SRH-2D uses 2D depth average, dynamic wave equation called as St. Venant equation to determine the hydraulic variables and followed finite volume numerical approach (Lai, 2008). The same model integrates a new algorithm (that uses the equation given by Jarvela (2004)) for computing dynamic, spatially-distributed Manning's n (Dombroski, 2017) and this model is called as SRH-2DV (Gillihan, 2013) in this study. The third software Surface-water Modeling System (SMS) version 12.2 graphical user interface developed by Aquaveo LLC, Provo, UT was used for developing a hybrid mesh and SRH-2D is embedded within this software for the simulations whereas SRH-2DV runs independently.

Model setup

The hybrid mesh, quadrilateral mesh to characterize main channel and triangular mesh for floodplain were created for the reach of the MRG. The two-different spatial resolutions were used for the mesh: an average of 5 m spacing for channel and an average of 12 m for floodplain.

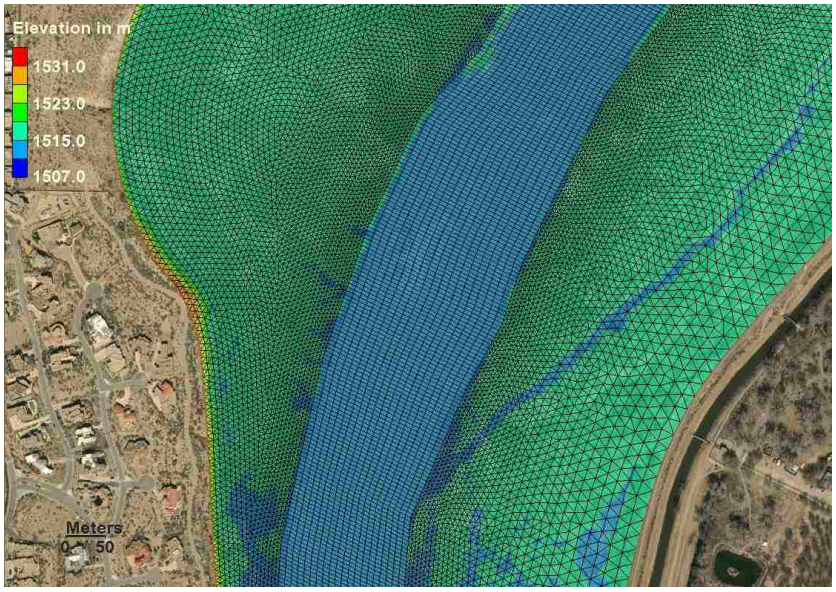

Figure 5: An example of the 2D hydrodynamic modeling mesh with interpolated elevation

The model was simulated for steady state conditions. The four different flows (142 m^3/s, 198 m^3/s, 283 m^3/s and 425 m^3/s) were used for simulation. The water surface elevation (WSE) was assigned as a downstream boundary condition. A rating curve was developed using observations from USGS Gage 08330000 (Rio Grande at Central Street) for flows of 142 m^3/s and 198 m^3/s. Because the rating curve was limited to the maximum possible flood of 255 m^3/s (9,000 cfs), the boundary conditions for 283 m^3/s (10,000 cfs) and 425 m^3/s (15,000 cfs) were obtained using a one-dimensional model (using HEC-RAS 5.0.3). The 1D model was simulated for steady conditions for discharges ranging from 28.32 m^3/s (1000 cfs) to 425 m^3/s (15,000 cfs) to with an increment of 28.32 m^3/s and was calibrated with necessary adjustment of roughness value to determine the WSE for 283 m^3/s and 425 m^3/s.

Model parameters:

The SRH-2D model was applied using two methods for assigning roughness values: (1) manually assigned roughness based on land cover; (2) dynamically calculated using vegetation parameters. All necessary inputs for both models (SRH-2D and SRH-2DV) were same expect the roughness value.

a. Constant roughness

For SRH-2D, constant Manning's roughness value was provided based on land cover. The value of vegetation height and LAI were the inputs for SRH-2DV that were used to calculate dynamic roughness.

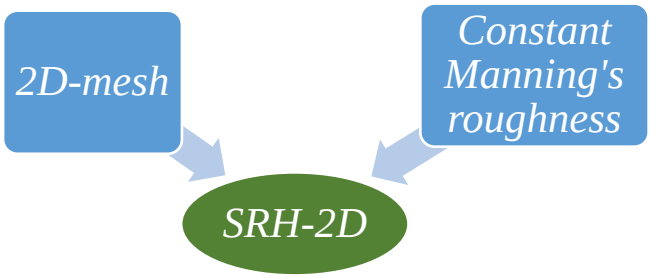

Figure 6: Inputs for SRH-2D

The roughness values based on land cover used in this study are summarized in Table 1 whereas Figure 7 shows the polygons of land cover for vegetation types.

Table 1: Manning's roughness values for based on land cover (Adair, 2016)

Land cover types	**Manning's roughness value**
Sand dunes	0.025
River bed	0.032
Bare Ground/Scattered Brush/Weeds	0.045
Cottonwood	0.06
Scattered trees	0.08
Medium to Dense trees/Brush	0.1

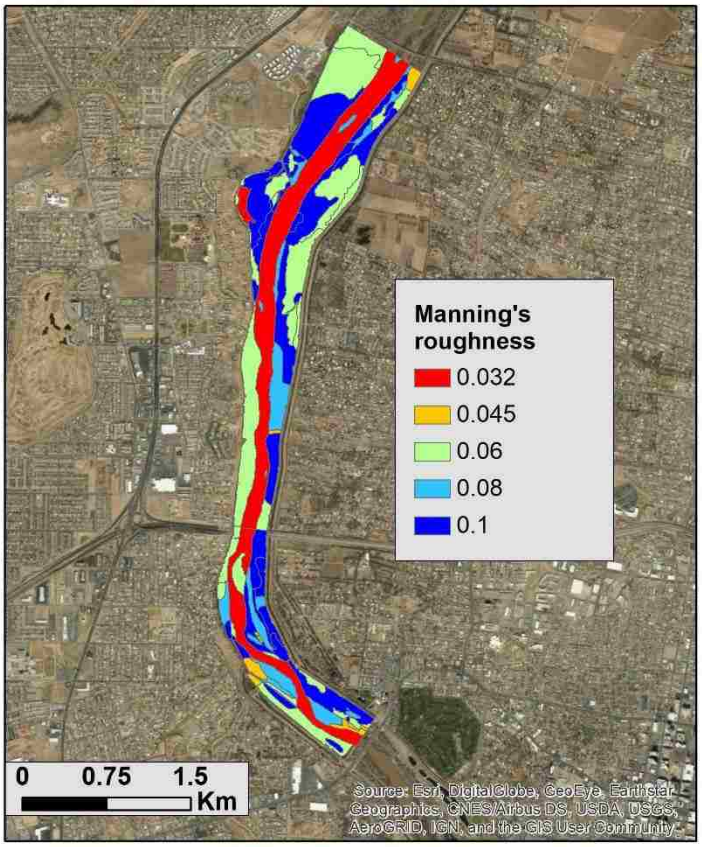

Figure 7: Default Manning's roughness values based on land cover for the study reach

b. Dynamic roughness

The algorithm proposed by Jarvela (2004) consists of several parameters. The parameters are vegetation height, LAI, Cdχ, χ, Uχ, U and h. The vegetation height and LAI were determined from LiDAR data. U and h were calculated internally from the model. The values of Cdχ, χ, and Uχ were assigned on the basis of previous studies. Uχ is the minimum reference velocity which is usually taken as 0.1 m/s (Fathi-Moghadam, 1996; Järvelä, 2002). The value of Cdχ and χ are unique for the particular species of vegetation. The value of Cdχ ranges from 0.43 to 0.69 and χ ranges from -0.57 to -0.38 (Järvelä, 2004). For this study, intermediate values for both parameters Cdχ (0.5) and χ (-0.45) were

applied. In order to check the sensitivity of this assumption, a range of values were simulated for 283 m^3/s of flow.

SRH-2DV model requires average value of height and LAI assigned based on land cover. Since, the land cover used in this study consists of 93 polygons representing land use type, the value of height and LAI determined from LiDAR in the format of a raster file was combined with the polygons. The values of raster cells lying inside the polygon were average to get the value for each polygon. Besides the value of LAI and height to calculate dynamic roughness, SRH-2DV also requires default roughness value. This default roughness value represents the roughness due to vegetation only. Model calculates the value of roughness due to vegetation where we have defined landcover as a vegetation. Because of this default roughness value for open/barren land and water were assigned as zero. When hydraulic condition or vegetation parameters lies outside the range of applicability for the specified method (Jarvela (2004)), then the model will assign the default roughness value. Manning's roughness values from the study of Adair (2016) were assigned for each polygon to define the default roughness values. Vegetation height, LAI, default roughness, type of the solver used for the calculation of dynamic roughness, parameters (U_{χ}, $C_{d\chi}$ and χ) and objects IDs which referred to the same ID assigned for the shapefile of land cover were prepared in .csv format. Because SRH-2DV model takes the information of vegetation parameters in the form of .csv file. A sample of a .csv file used for determination of roughness due to remote sensing derived vegetation parameters is included in **Appendix A.** It also needs shapefile of land cover created from ArcGIS having same object IDs mentioned in .csv file. In this study, *Jarvela (2004)* was selected as the

solver for the estimation of dynamic roughness values. The roughness values in SRH-2DV are partitioned into sediment grain roughness and vegetation roughness. Sand grain roughness values (0.032 for main stream and 0.025 for the floodplain) were assigned for the created 2D-mesh. Using the assigned solver, vegetation roughness was calculated, and the sediment grain roughness value was added to get the total roughness value, which was again used to calculate hydraulic parameters including depth, velocity, WSE, and Froude number.

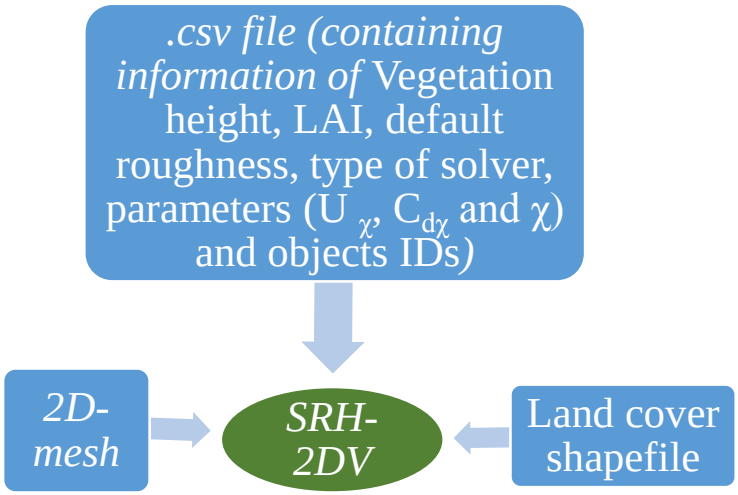

Figure 8: Inputs for SRH-2DV

5. RESULTS

5.1 Vegetation parameters

The results from the CHM and LAI mapping routines are shown in Figures 9 and 10. The results showed the maximum height for the study area is around 26.7 m (87.5 ft) and the maximum LAI is about 9.5.

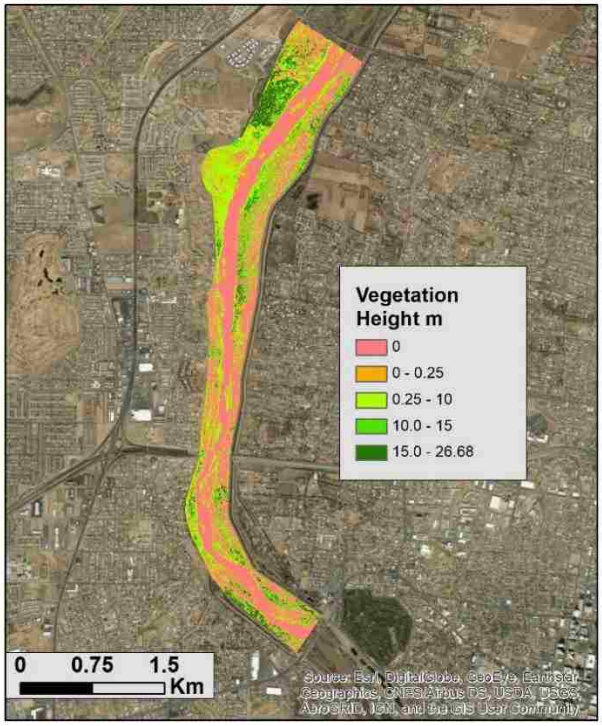

Figure 9: Canopy Height Model from LiDAR

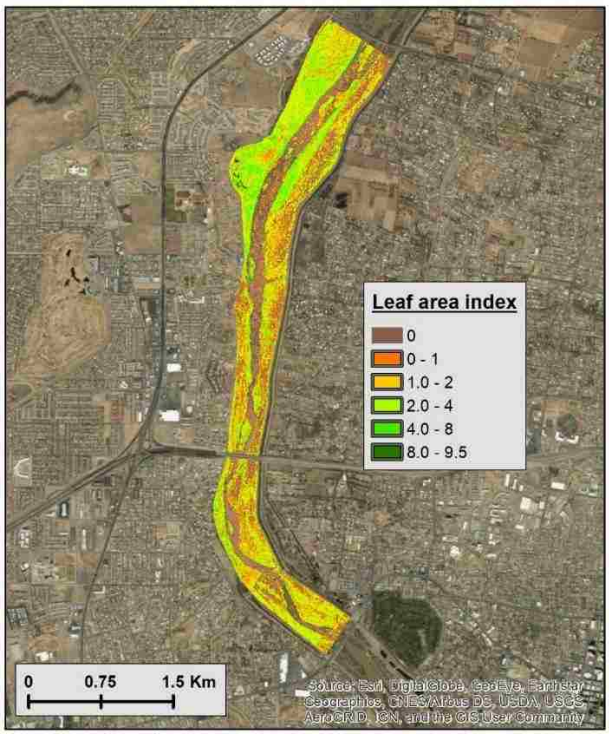

Figure 10: LAI from LiDAR

Since, the model required height and LAI assigned for the polygon created for vegetation types or land cover, the values from LiDAR data were averaged for each polygon. Figures 11 and 12 represents the mapping of average height and LAI for the land cover polygon which was used as the input for modified model.

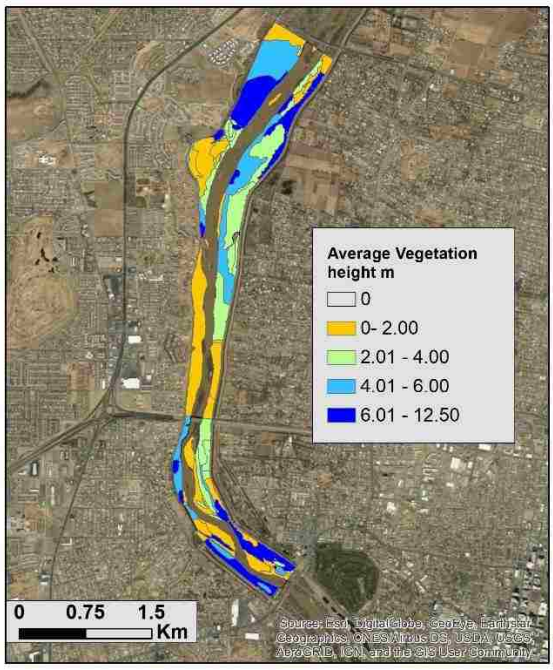

Figure 11: Average height for landcover polygon

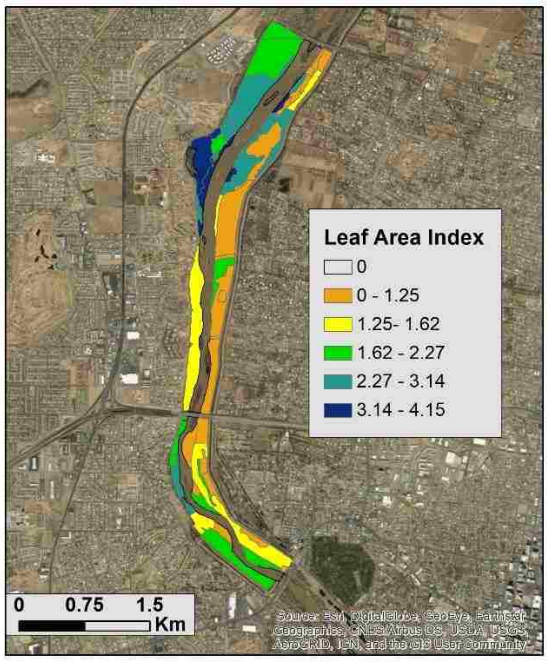

Figure 12: Average LAI for landcover polygon

The parameters of vegetation from the field were collected for six different types of vegetation which are listed in Table 2. The measured value of height and LAI are also shown in the table. The value of height and LAI for the particular type of vegetation species obtained from the LiDAR were compared with those collected from the field. From this observation, the parameters obtained from LiDAR were verified.

Table 2: Comparison of vegetation parameters from LiDAR with field data

		Measured in field		Average value for each vegetation type		Average value from LiDAR	
S. No	**Vegetation types**	**Height, m**	**LAI**	**Average Height, m**	**Average LAI**	**Average Height, m**	**Average LAI**
1	Monotypic Cotton wood	8.5	0.77	8.925	1.710	7.62	1.18
2	Monotypic Cotton wood	9.4	2.65				
3	Native/Exotic	8.6	1.49	6.400	1.517	6.096	1.34
4	(N/E) Cottonwood/ Salt Cedar	5.1	1.47				
5	(N/E) Cottonwood/ Salt Cedar	5.5	1.59				
6	Monotypic Salt Cedar	8.9	1.68	7.250	1.260	6.208	2.46
7	(Monotypic Salt Cedar	5.6	0.84				
8	Native Mixed	4.3	1.64	5.182	2.235	4.572	0.94
9	Native Mixed	6.1	2.83				
10	Cottonwood/Salt Cedar (Native / mixed)	6.0	1.23				
11	Cottonwood/Tree Willow	9.6	2.53	8.03	1.760	15	0.97
12	Cottonwood/Tree Willow	6.5	0.99				
13	Coyote Willow	2.6	0.56	2.25	0.865	5	0.61
14	Monotypic Coyote Willow	1.9	1.17				

5.2 Hydraulic parameters

From the range of modeled discharge under two roughness approaches, it was seen that there is significant effect of vegetation parameters on hydraulic roughness which eventually impacts the hydraulic parameters. The summary of dynamic Manning's roughness value calculated from the model for four different flow scenarios are shown in Table 3 categorized as maximum, minimum, and average value and separated based on land cover type. Also, the default roughness value, which was assigned for simulating the same flow scenarios, are included in the table. The result reveals an increase in average roughness value for each land cover type for all flows whereas the minimum value computed by model were closer to the default roughness. The mapping of dynamic roughness obtained using vegetation parameters for each flow are included in Appendix B.

Table 3: Summary of dynamic roughness value for four different flow scenarios

	Flows	**For 142 m^3/s (5,000 cfs)**			**For 198 m^3/s (7,000 cfs)**			**For 283 m^3/s (10,000 cfs)**			**For 425 m^3/s (15,000 cfs)**		
Land cover types	**Default value**	**Min**	**Max**	**Average**	**Min**	**Max**	**Average**	**Min**	**Max**	**Average**	**Min**	**Max**	**Average**
Sand dunes	0.025	0.025	0.025	0.025	0.025	0.025	0.025	0.025	0.025	0.025	0.025	0.025	0.025
River bed	0.032	0.032	0.032	0.032	0.032	0.032	0.032	0.032	0.032	0.032	0.032	0.032	0.032
Bare Ground / Scattered Brush/ Weeds	0.045	0.0470	0.087	0.067	0.045	0.112	0.074	0.047	0.136	0.08	0.046	0.133	0.080
Cotton wood	0.06	0.06	0.192	0.086	0.05	0.192	0.086	0.057	0.193	0.088	0.060	0.211	0.092
Scattered trees	0.08	0.078	0.156	0.1	0.062	0.177	0.11	0.072	0.180	0.114	0.071	0.207	0.118
Medium to Dense trees/Brush	0.1	0.066	0.181	0.096	0.077	0.201	0.102	0.073	0.217	0.102	0.065	0.223	0.107

Further, the Manning's roughness values (constant and dynamic) were compared (Figures 13 to 16) for four different flow scenarios. The difference maps were obtained by subtracting the value of constant roughness from the dynamic roughness values. The red and orange regions represent conditions where the dynamic roughness values were less than (negative value in map) than the constant. The blue shades represent areas where the dynamic roughness values were greater than (positive value in map) constant roughness.

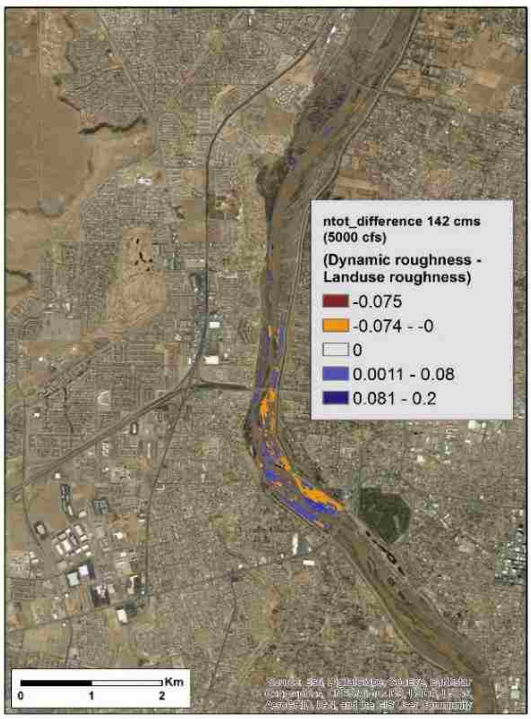

Figure 13: Change in roughness value for 142 m^3/s (5,000 cfs) between constant and dynamic roughness

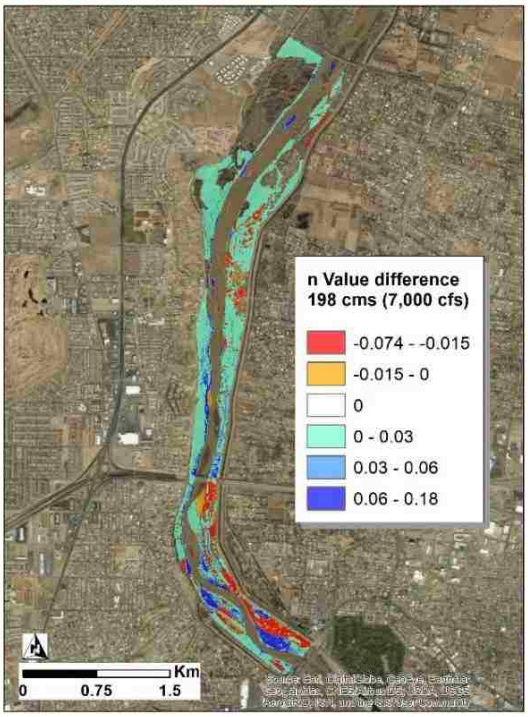

Figure 14: Change in roughness value for 198 m^3/s (7,000 cfs) between constant and dynamic roughness

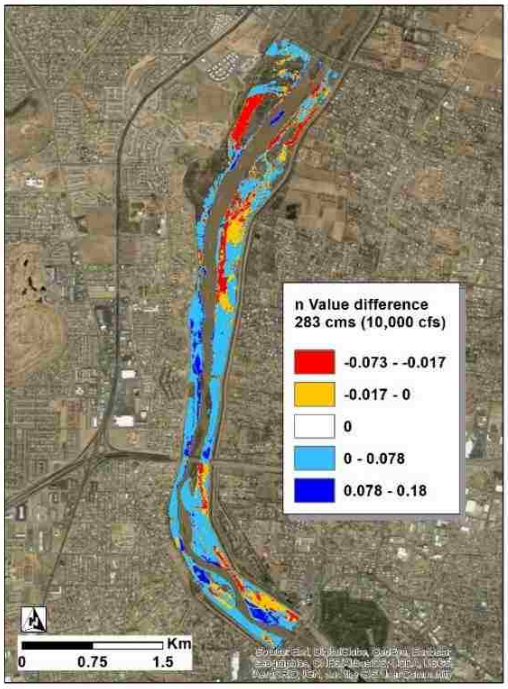

Figure 15: Change in roughness value for 283 m^3/s (10,000 cfs) between constant and dynamic roughness

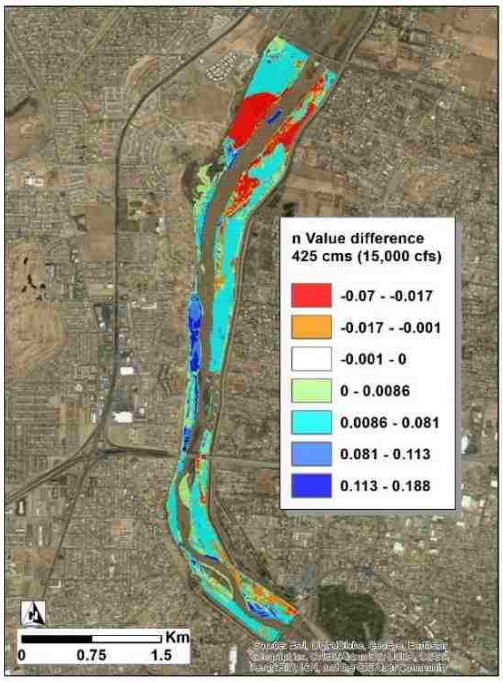

Figure 16: Change in roughness value for 425 m^3/s (15,000 cfs) between constant and dynamic roughness

To represent the full range of deviation between two roughness approaches, histograms were generated (Figure 17 to 20). The dotted line represents the mean value of change in roughness for the entire study area. Positive values mean the dynamic roughness is greater than the constant roughness.

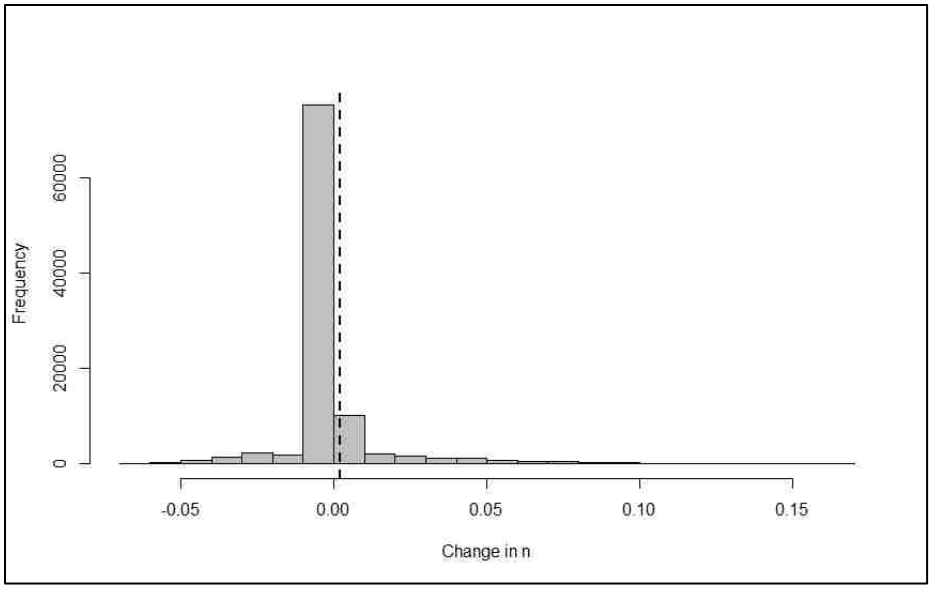

Figure 17: Histogram for change in Manning's *n* for 142 m^3/s (Dynamic roughness –constant roughness)

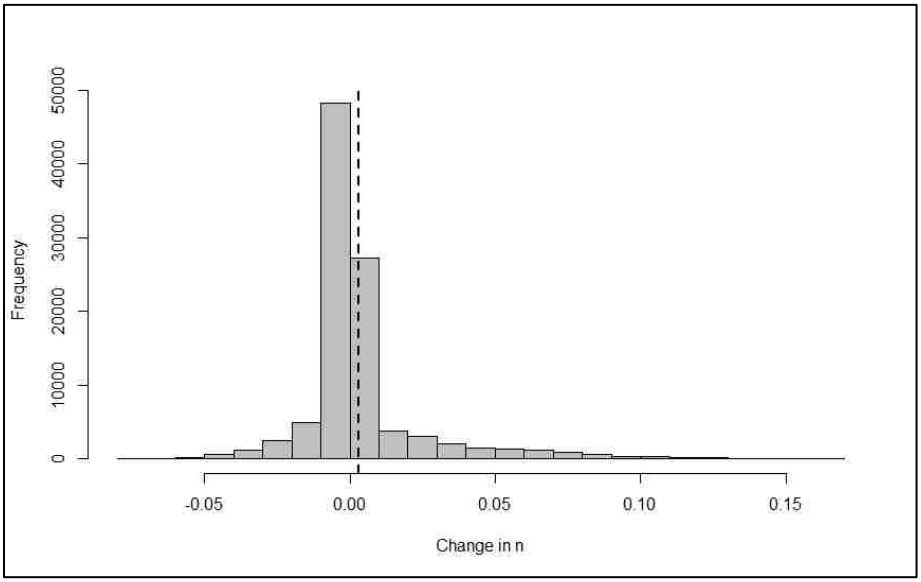

Figure 18: Histogram for change in Manning's n for 198 m^3/s (Dynamic roughness – Constant roughness)

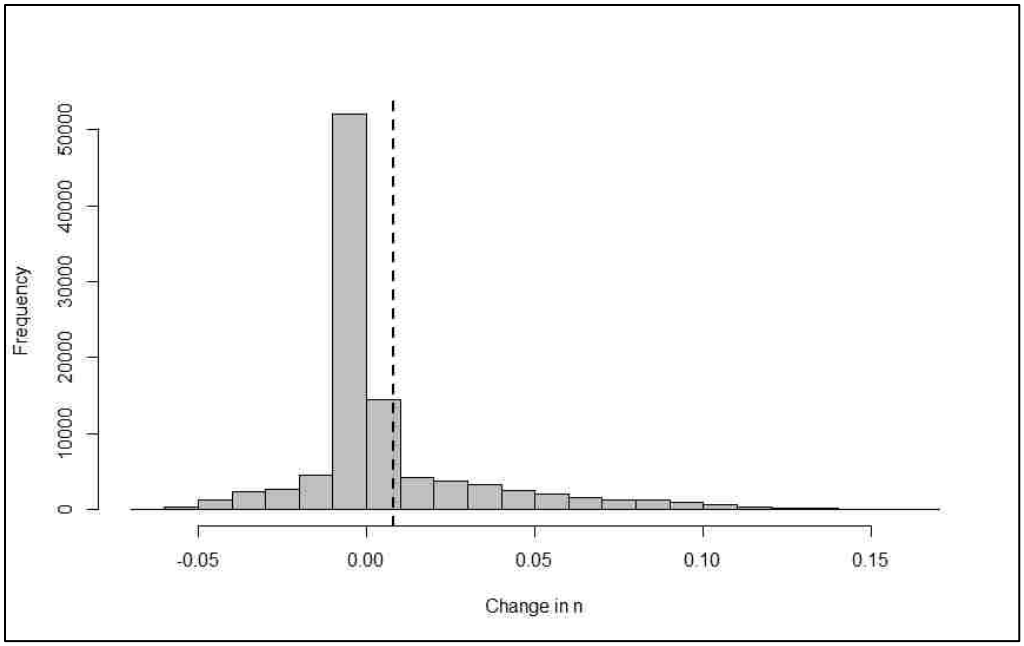

Figure 19: Histogram for change in Manning's n for 283 m^3/s (Dynamic roughness – Constant roughness)

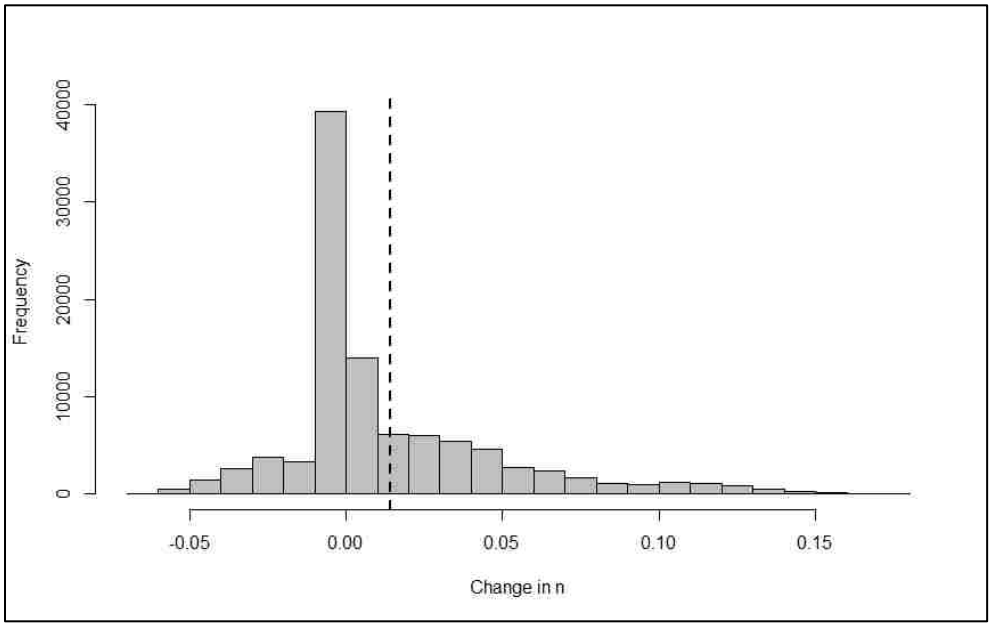

Figure 20: Histogram for change in Manning's n for 425 m^3/s (Dynamic roughness – Constant roughness)

Figures 21 and 22 represents the histograms for the comparison of depth and velocity for the number of wetted cells. The results are shown for 283m^3/s (10,000 cfs). The blue bar represents the value for dynamic roughness for the number of wetted cells and the orange bar represents the value from manually assigned roughness. This histogram represents only the number of cells having the similar values. To understand the actual spatial variability of hydraulic parameters, the mapping of change in depth and velocity for 283 m^3/s are shown in Figures 23 and 24. In these figure, blue shades represent the depth and velocity by the dynamic roughness approach were greater than the land cover approach. The histograms and mapping of hydraulic parameters for the other three flows are included in Appendix B.

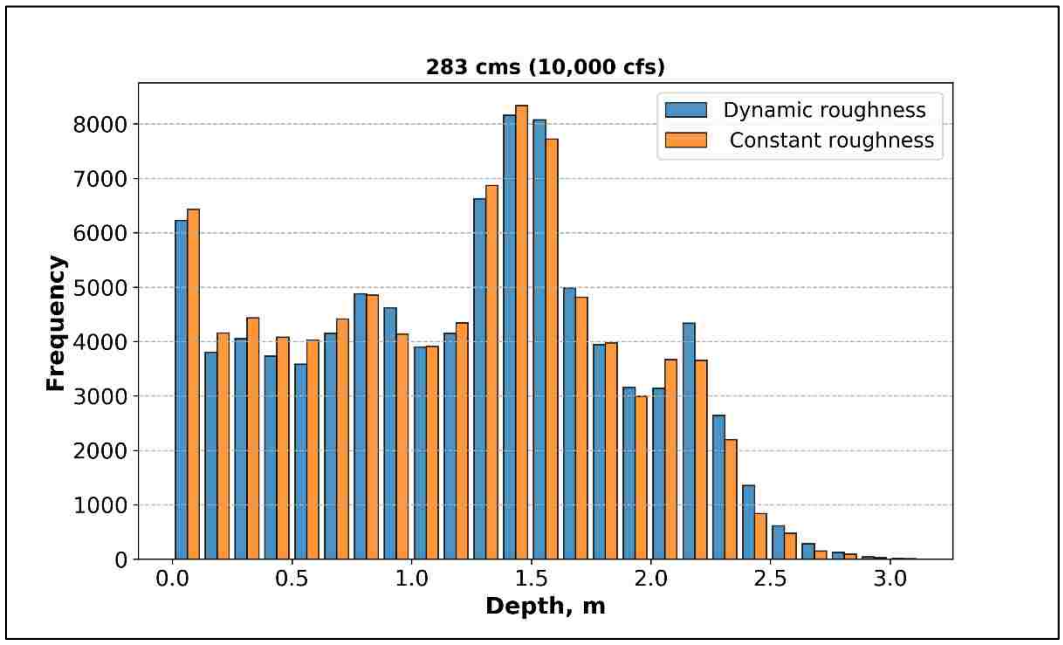

Figure 21: Depth for 283 m^3/s (10000 cfs)

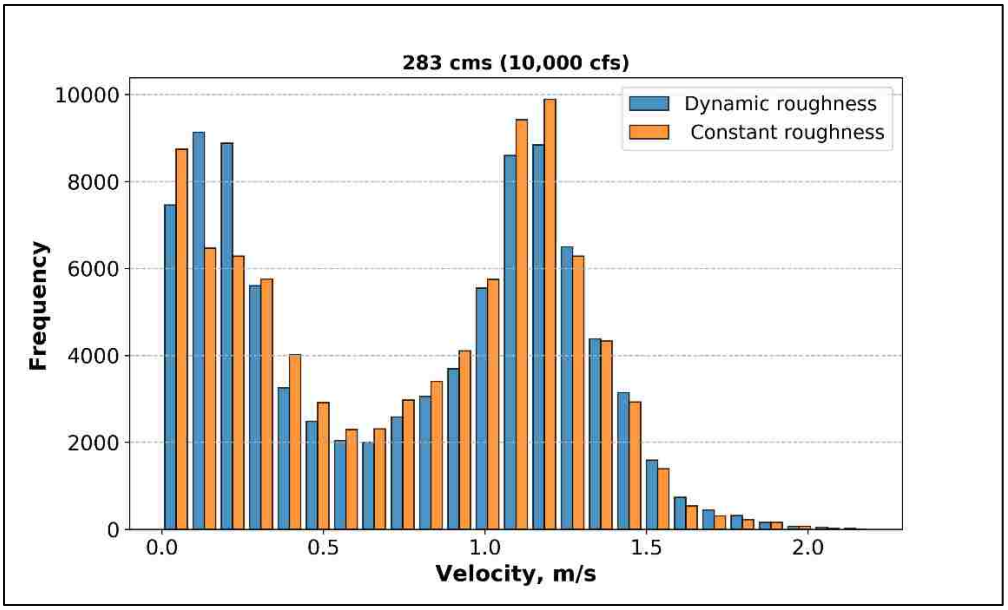

Figure 22: Velocity for 283 m^3/s (10000cfs)

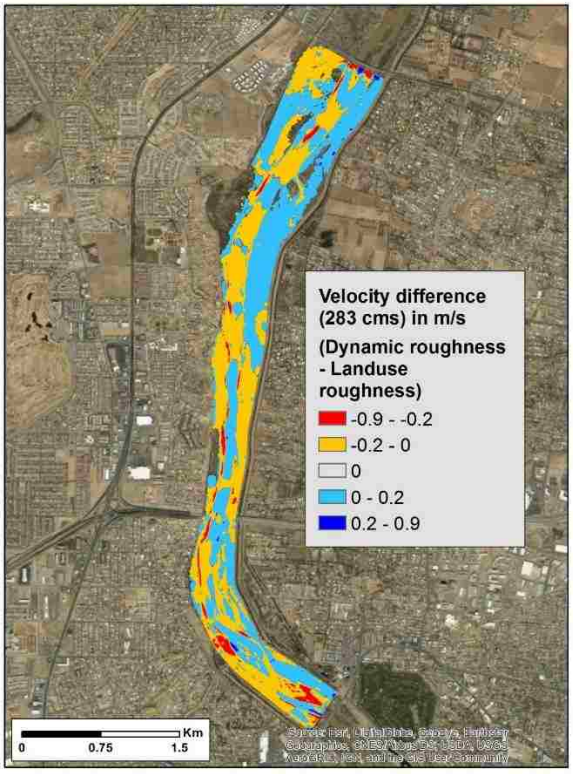

Figure 23: Mapping of change in velocity for 283 m^3/s (Velocity due to dynamic roughness – Velocity due to constant roughness)

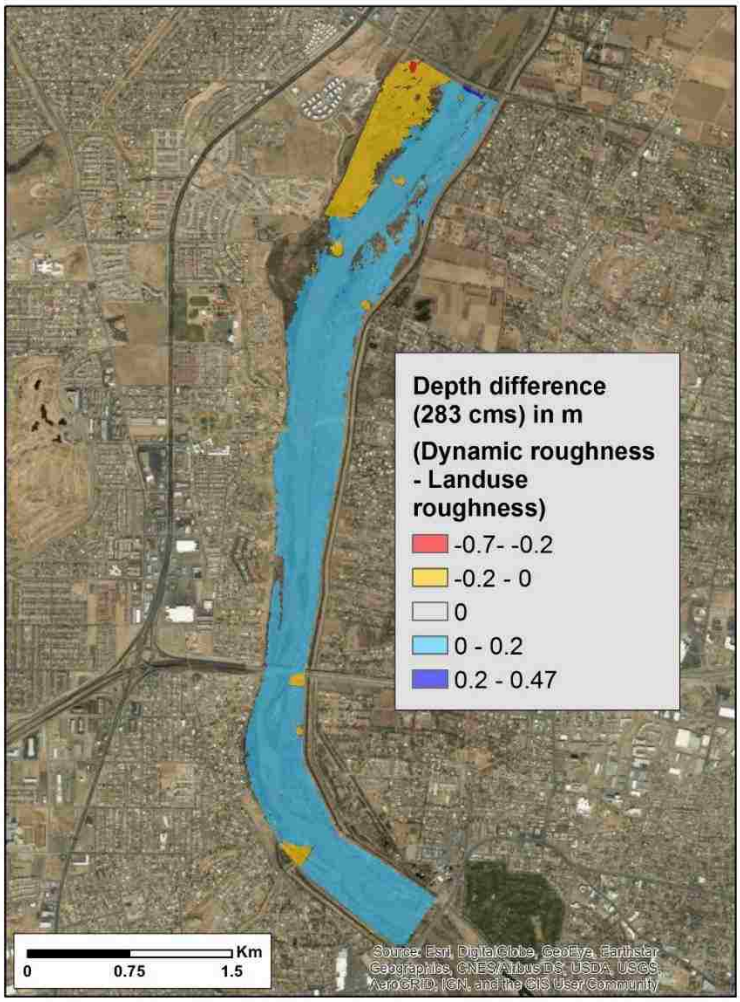

Figure 24: Mapping of change in depth for 283 m^3/s (depth due to dynamic roughness – depth due to constant roughness)

Table 4 represents the statistical analysis (mean, median and standard deviation) of velocity, depth, water surface elevation and roughness value for the constant and dynamic roughness approaches. The mean change in hydraulic parameters were found to be very small.

Table 4: Summary of statistical analysis of change in velocity, water depth, water surface elevation and roughness due to constant and dynamic roughness for different flows.

Jarvela (2004) Approach

Flow (m^3/s)	**Statistical analysis**	**Δ velocity (m/s)**	**Δ depth (m)**	**Δ WSE (m)**	**Δ n**
142	**Mean**	-0.010	0.014	0.014	0.002
	Median	-0.003	0.011	0.011	
	Standard deviation	0.072	0.024	0.023	0.016
198	**Mean**	-0.013	0.023	0.023	0.002
	Median	-0.003	0.019	0.019	
	Standard deviation	0.082	0.025	0.025	0.021
283	**Mean**	-0.017	0.040	0.040	0.008
	Median	-0.005	0.039	0.039	
	Standard deviation	0.097	0.037	0.037	0.027
425	**Mean**	-0.024	0.060	0.060	0.014
	Median	-0.012	0.059	0.059	
	Standard deviation	0.120	0.041	0.041	0.034

Also, the depth of water for 283 m^3/s was compared with the results obtained from a calibrated model for the same reach (Byrne, 2017). Calibrated model was simluated using D-Flow Flexible Mesh (D-Flow FM) software. Figures 25 and 26 show the differences in water depth. The difference was obtained by subtracting the result of calibrated model from the result obtained by constant and dynamic roughness. positive values mean the water depth due to dynamic roughness are greater than the depth from calibrated model.

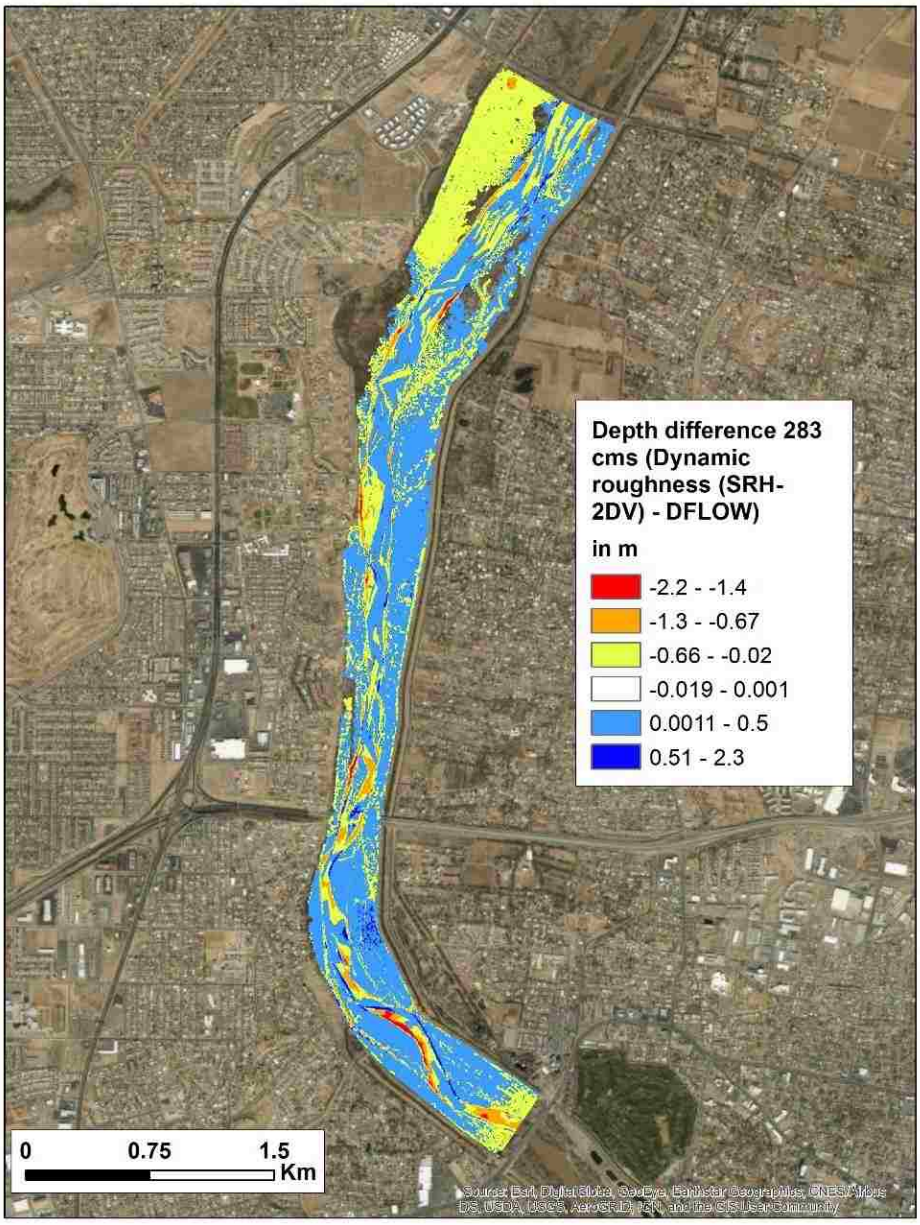

Figure 25: Depth difference for 283 m^3/s (Depth of dynamic roughness from SRH-2DV – Depth of constant roughness from DFlow)

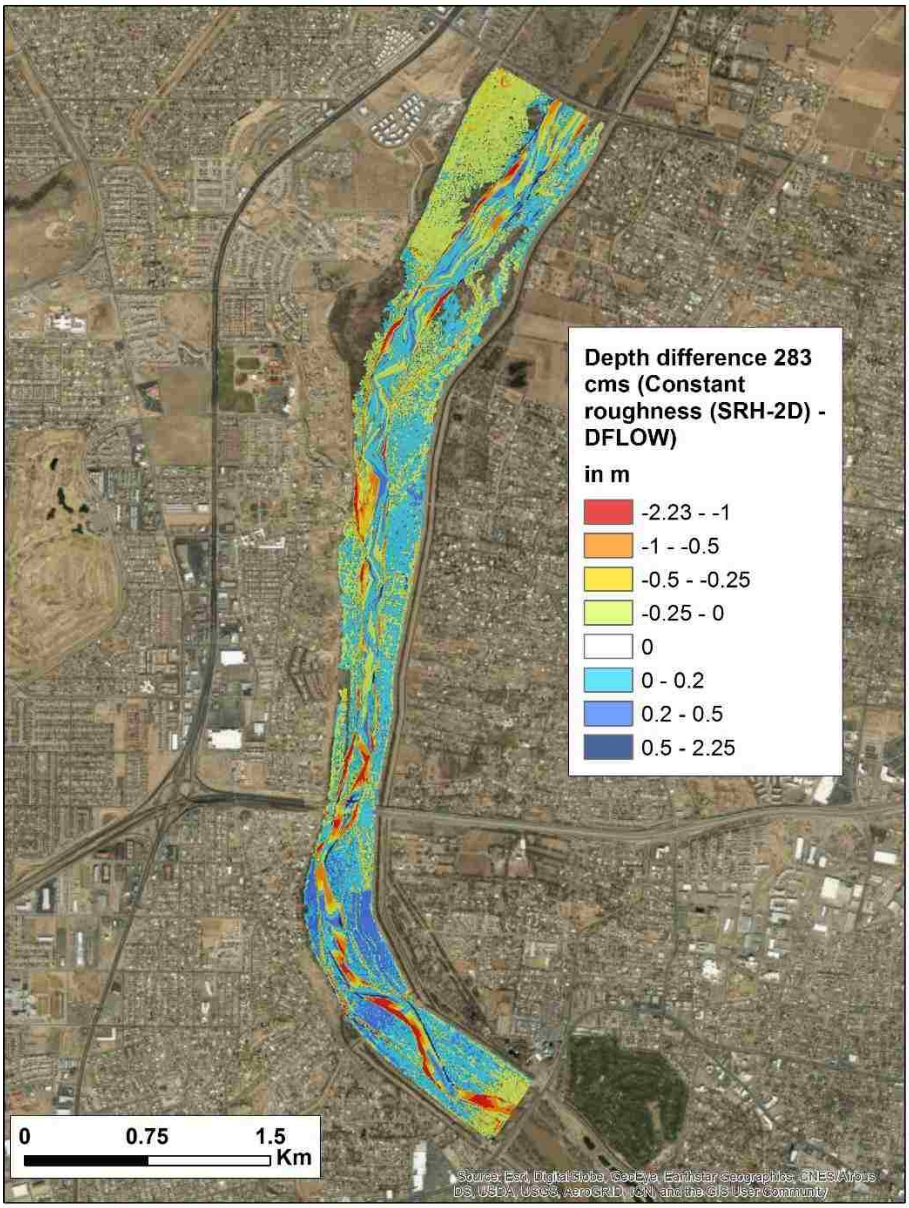

Figure 26: Depth difference for 283 m^3/s (Depth of constant roughness from SRH-2D – Depth of constant roughness from DFlow)

5.3 Sensitivity analysis

While following the approach of Jarvela (2004), certain parameters were assumed based on the previous studies and these parameters also need to be verified. The parameters like $C_{d\chi}$ and χ depends on the species of vegetation which were used based on the previous studies (Jarvela, 2002). These parameters were verified by decreasing and increasing the parameters by certain value within the range of values for those parameters. The model was simulated by keeping $C_{d\chi}$ constant and varying χ and vice versa for 283 m^3/s. The summary of statistical analysis for sensitivity analysis are shown in Table 5. The values in the table below show that while changing the value of those parameters, hydraulic parameters were differed by negligible amount. The roughness value seemed to be decreasing when the value of χ was increased or decreased. When the value of $\mathbf{C_{d\chi}}$ changed to 0.4, the roughness values decreased. However, the use of larger value for $C_{d\chi}$ (0.6 and 0.7), average dynamic roughness value increased causing a increase in the water level and a reduction in the velocity of flow. All the values were obtained by subtracting the results calculated from varied parameters from the results obtained from assumed standard parameters. So, the positive value indicates that the values of hydraulic parameters were decreased while changing the parameters.

Table 5: Summary of statistical analysis of sensitivity analysis

Constant Parameter	Varying Parameter	Statistical analysis	Δ velocity (m/s)	Δ depth (m)	Δ WSE (m)	Δ nv
Constant $C_{d\chi}$	χ = - 0.35	**Mean**	-0.001	0.003	0.003	0.0004
		Median	-0.001	0.002	0.002	0.000
		Standard deviation	0.005	0.003	0.003	0.005
	χ = - 0.55	**Mean**	-0.002	0.006	0.006	0.0008
		Median	-0.001	0.003	0.003	0.000
		Standard deviation	0.009	0.006	0.006	0.006
Constant χ	$C_{d\chi}$ = 0.4	**Mean**	-0.005	0.011	0.011	0.0024
		Median	-0.002	0.008	0.008	0
		Standard deviation	0.014	0.009	0.008	0.008
	$C_{d\chi}$ = 0.6	**Mean**	0.004	-0.009	-0.009	-0.002
		Median	0.001	-0.006	-0.006	0
		Standard deviation	0.012	0.007	0.007	0.009
	$C_{d\chi}$ = 0.7	**Mean**	0.006	-0.015	-0.016	-0.004
		Median	0.002	-0.010	-0.011	0
		Standard deviation	0.021	0.013	0.013	0.012

The dynamic roughness value, depth and velocity after altering the values of those parameters were analyzed using histogram. $C_{d\chi} = 0.5$ and $\chi = -0.45$ are value used in this study for all four flows. All the histograms are shown in Appendix B. Also, the spatial variability of hydraulic parameters due to change in parameters were mapped and shown in Appendix B.

6. DISCUSSION

6.1 Vegetation parameters

One of the objectives of this research was the mobilization of remote sensing data in prediction of vegetation parameters for the computation of hydraulic roughness of riparian vegetation. Figures 9 and 10 represent the height and LAI for the riparian vegetation of the study reach. 26.67 m (87.5 feet) and 9.5 were the maximum value of height and LAI respectively. The locations of old cottonwood trees were identified to verify the maximum height of vegetation and similar height was found from the field data. Beside cottonwood trees, the height of the vegetation for the other species were smaller compare to field data. The value of LAI doesn't only depend on the particular species but also depends on the season of the year of data collected. LAI from the field observation were more comparable to LiDAR. Some values of LAI from LiDAR were similar to field data. But for some specific areas where the value was above 4 from Also, the field data were collected at the month of October of the year 2017 i.e. leaf on condition whereas LiDAR data was taken in March and April, 2010 LiDAR were verified from previous studies.

Because of this reason, LAI was verified from the previous studies. The study of Cleverly et al. (2006) estimated LAI as an average of 4.5 and 3 for cottonwood and salt cedar respectively in 2003, for Rio Grande reach. They found the average LAI for cottonwood as maximum of 7 in the year 2001. Their study concludes that the value of LAI even for the same reach tends to fluctuate year to year. Another study of Hartwell et al. (2010) had found average of 9.31 and 3.99 value of LAI for cottonwood and willow at the confluence of Gila and Lower Colorado river. From these studies, the value of LAI was reasonable. The pixels basis value of LAI and height were converted into average value for the polygon of each vegetation mapping. These values were reduced to around 12.5 m (41 feet) and 4.5 for height and LAI respectively which are shown in Figures 11 and 12. These values represent the average value for entire area of each polygon which was used as input for model.

6.2 Hydraulic parameters

The results of hydrodynamic model displayed that the vegetation parameters have a significant effect on estimation of hydraulic roughness for different flows. The statistical analysis of change in constant and dynamic roughness, implied that the overall Manning's roughness values were more when estimated from vegetation parameters compared to constant roughness for all simulated flows. The change in Manning's roughness value for four different flow (142 m^3/s, 198 m^3/s, 283 m^3/s and 425 m^3/s) are shown in Figures 13 to 16 for the study reach. The study of Abu-Aly et al. (2014) also found the higher roughness causing the increase in inundation extend due to increase in depth of water and reduction of velocity for dynamic roughness. In their study, the method of Casas et al. (2010) was used which utilizes the vegetation height for determination of dynamic roughness.

Histograms plotted for these changes showed the difference in roughness value were relatively small for most of the flow area (close to zero) for all flows though some of region indicates the higher changes of 0.18. The default maximum possible value of roughness due to vegetation was assigned as 0.2 in SRH-2DV model. If the range of calculated value exceeds this allocated value, then the model will assign 0.2 as a vegetation induced roughness. However, the maximum value for constant roughness was roughness 0.1 (for medium to dense tress/brush). This might be one possible reason for the over prediction of dynamic Manning's n value for some key areas. Whereas for some areas having more constant roughness compare to dynamic can be the use of unnecessarily high value for some areas like area covered with cottonwood trees and use of smaller value for Coyote willow.

Furthermore, statistical analysis and histogram plots demonstrate that the difference in velocity for different flows are very small (< 1.7 centimeter/second in average). Also, the change in water depth is small (<4 cm in average). The value of standard deviation for each of the parameters for different flows shows the value close to zero representing smaller deviation of values from mean value. Due to increase in roughness, the depth of water was increased while the velocity was decreased. The other significant identification due to change in roughness value was the inundation extend. The area of inundation has also deferred due to change in roughness value. The higher value of changes in water depth due to change in roughness value can be observed in spatial mapping. The mapping of change in these parameters are shown in Figures 23 and 24 for 283 m^3/s. The depth of water for 283 m^3/s were compared with the result from calibrated model from previous study and there was greater change in depth and inundation extends. The results

showed that the depth of water was changed greater within the channel, so it is obvious to have greater change in floodplain. Also, the resolution of mesh used by calibrated model was finer compared to SRH-2D model.

To see the inundation extent on flood plain, model was simulated for 4 different flows. There was not significant flooding over floodplain due to 142 m^3/s and 198 m^3/s whereas in case of 425 m^3/s, almost all area of flood plain was inundated. The results of 283 m^3/s were interesting. Because of that, variation in hydraulic parameters due to 283 m^3/s were only discussed over here. However, the results of other flows are included in Appendix.

One more thing that needs to clarify if the flow used in this study represent the flow of MRG. The flow of MRG is controlled by water release from Cochiti dam. Dam release maximum of 142 to 170 m^3/s from the reservoir (Richard & Julien, 2003). Also, the model was simulated for steady state condition, which also shows that the amount of flow which were used may occur for very small time but steady flow for that big flow may not be possible. However, the increasing risk of wildfire and extreme rainfall events likely to increase the rate of runoff and soil erosion (Gould et al., 2016). Storm water runoff discharging from North diversion channel into MRG at Albuquerque is one of the possible event causing peak flow.

6.3 Sensitivity analysis

While following the approach of Jarvela (2004), certain parameters were selected randomly on the basis of previous study. The previous study also doesn't represent the similar type of vegetation distribution. So, it led to necessity of performing the sensitivity analysis to observe the effect in varying those parameters. In this study, model required

inputs height, LAI varies with time and season of the year, $C_{d\chi}$ and χ depends on the species of vegetation and other hydraulic parameters like water depth was calculated internally by the model. Since, LAI and height were derived from LiDAR and considered as fixed value for this study, only the variable that can be altered are the value of $C_{d\chi}$ and χ. The limited studies were found which has derived the value of $C_{d\chi}$ and χ for different species. Though, the exact value of these parameters were not found for the species along the riparian zone of Rio Grande. The models were simulated varying one parameter and keeping other constant for the flow of 283 m^3/s. The histogram plots for the change in velocity, depth and roughness shows relatively minor changes. Due to increment and decrement of χ, there was very minor changes in roughness values as well as water depth and velocity. The value of roughness was slightly higher with small rise in water level decreasing the velocity. The result was same when $C_{d\chi}$ is 0.4, whereas, when $C_{d\chi}$ is increased to 0.6 and 0.7, the roughness value was decreased. These results signify that these parameters need to be selected carefully. Similarly, other varying parameters height and LAI of vegetation were simulated for 10% increment and decrement. the results revealed that height and LAI are sensitive in inundation. Due to increase in the height of vegetation, the average depth of water for 283 m^3/s decreased, decreasing the inundation extend. The inundation extends or depth of water on the study reach are shown in Appendix B. In addition, the decrement in height of vegetation conveyed the opposite relation compared to height increment. However, increasing the value of LAI revealed the drastic change in hydraulic parameter. From this result also, it shows that the LAI has a significant effect supporting the hypothesis of Jalonen et al. (2013).

6.4 Existing uncertainties

The existence of uncertainty is one of the major issue of the models. In this study, LiDAR data were used for determination of vegetation parameters. Due to noise of LiDAR points because of ground surface, reflection due to water surface and atmosphere, proper knowledge is required for correcting the data. In addition, the height of the vegetation computed from this study did not indicate the single height for the tree i.e. height value was assigned for circumference of a tree crown (for example cottonwood trees) ignoring the lower vegetation (shrubs, meadows) or bare ground covered by the canopy. This increases uncertainty in determining true height and LAI that actually effects the flow.

other factor that likely increases the uncertainty is the representation of terrain. To represent the channel bathymetry, the cross-section data collected by BOR were used in this study. But those cross-sections were collected at larger distance greater than 150 m. Also, the pattern of river (MRG) includes the number of prominent islands and sand bars. The data taken at that distance is not sufficient to represent those islands. Because of this, it will affect the volume of water that the cross-section can convey altering the inundation of floodplain. The effect of cross-section data was seen while comparing the result with previously run model (from DFLOW-FM). It was seen that there were remarkable changes in inundation depth in floodplain due to greater change in water depth in the main channel. Similarly, some of the parameters required for implementation of Jarvela (2004) approach were based on the previous study which increases the uncertainties. Models were simulated by changing those parameters only for the purpose of understanding their effect on determining hydraulic parameters.

7. CONCLUSION

This study has explored the techniques implemented widely in the study of forest to estimate vegetation parameters using remote sensing data, for the computation of hydraulic roughness due to vegetation. Moreover, LAI which was used to represent the density of vegetation and was determined using the empirical formula (Beer Lambert law). The value of LAI was estimated for only one season. LAI won't have that much effect in determination of hydraulic roughness due to taller vegetation like cottonwood trees. But for the shorter leafy vegetation, LAI estimation will have major effect on estimation of hydraulic roughness. Because of this, accuracy of flood inundation or level depends on the accuracy of predicted LAI. The accuracy of LAI can be improved by collecting the LiDAR and field observation data for the same season (leaf-on) of a year. Also, more field data are required for verifying the results of LiDAR data.

Two-dimensional hydrodynamic model was used to accomplish the second objective of this study. The hydraulic parameters such as velocity, depth was compared for dynamic and constant roughness. The comparison reflected the minor changes in hydraulic parameters and also there was change in the inundation pattern due to use of different roughness condition (constant and dynamic). Even though the comparison reflects the similar results, further study is essential to identify the better method of representing the hydraulic roughness due to vegetation and the importance of hydraulic roughness due to vegetation for different flow conditions. Also, calibration of model is recommended to identify the accurate method for representing vegetation induced roughness. Since the inundation extend of flood plain also depends on the precision of channel bathymetry, we

should be careful in representing the correct geometry of channel in addition to the estimation of hydraulic roughness.

Despite having uncertainties while using remote sensing data, the use of remote sensing data provides a large labor saving from field-based techniques. Thus, this study concluded that these techniques hold much potential and additional research should be performed to reduce uncertainties and verify the approach. From the findings, the overall change in parameters for two roughness conditions were small which signifies that the both roughness value can be used for large scale projects like flood control. However, significant changes in some key areas for two roughness condition reflects that the roughness value has substantial effect while working on smaller scale projects like bank erosion, habitat restoration, channel shifting, etc.

8. APPENDICES

APPENDIX A. METHODS OVERVIEW

Processing of LiDAR points for determining height and LAI:

1. CHM (Determining vegetation height):

LiDAR points are classified into several returns such as first, intermediate and last returns. First returns is the returns from top of vegetation, buildings, electric cables and so on whereas as the last return represents the return from the ground surface. Here CHM is difference of DSM and DTM. DTM and DSM can be extracted using different tools, but I have used ArcMap 10.5. Raw LiDAR data were available in .las file format for the study area. The points were already classified as ground and non-ground points. Following steps can be used to determine CHM:

i) In order to calculate the statistics of. las data and convert it into. lasd layer that is readable by ArcMap, LAS Dataset was created and raw data was added in LAS Dataset. Then. lasd layer was created after adding raw data and that layer was added in ArcMap.

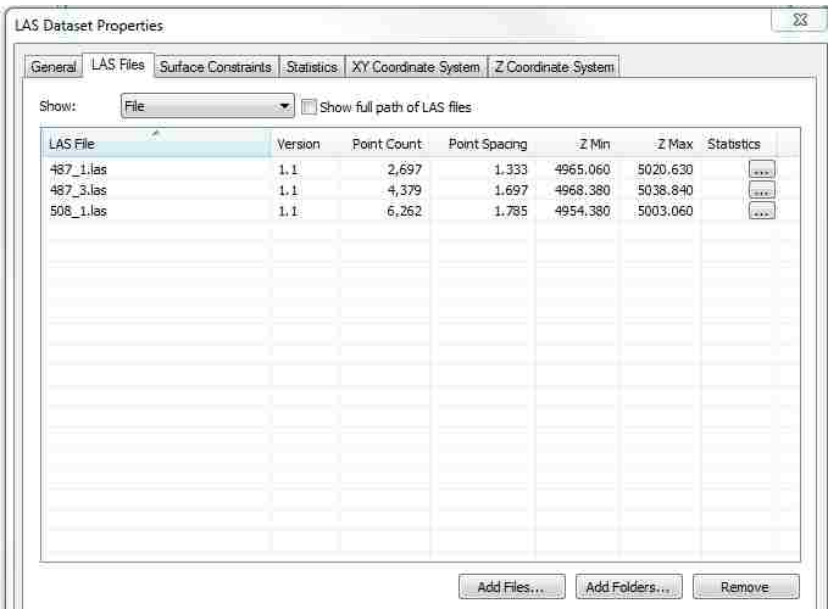

Figure a

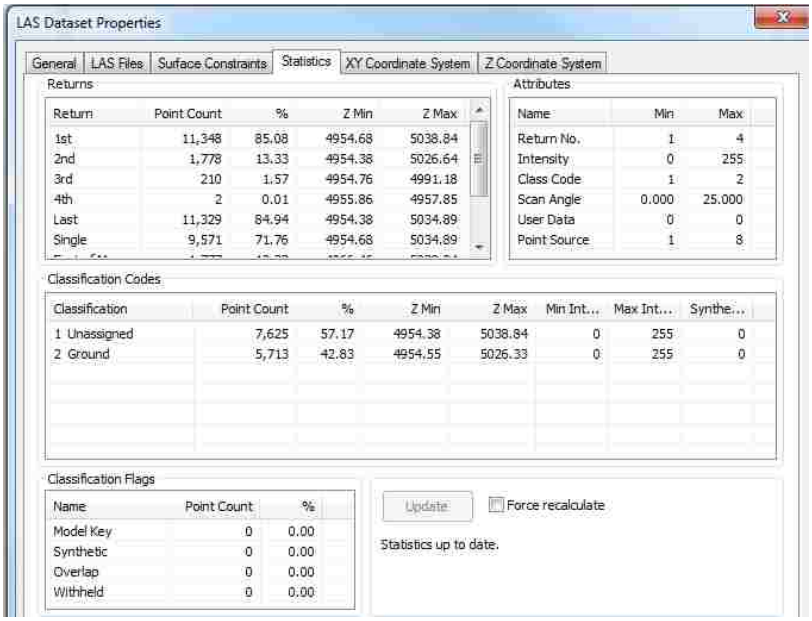

Figure b

Figure 27: a) Adding raw data in LAS Dataset and b) Statistics of points

ii) After adding. lasd layer in ArcMap, to create DTM, only last return was activated and using those points, raster was created. The raster created from those points

represent the DTM. Cell assignment was chosen as average that means, the value for each cell of raster will be assigned with average value of points in that cell. The cell size was selected as 1 meter. Usually, cell size is estimated on the basis of spacing and number of points.

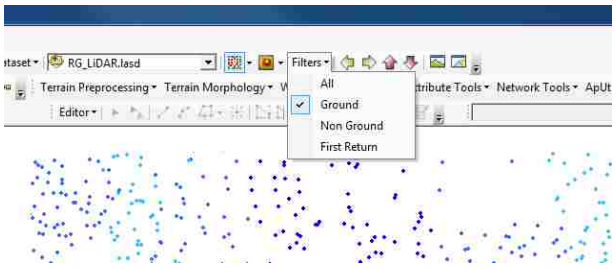

Figure a

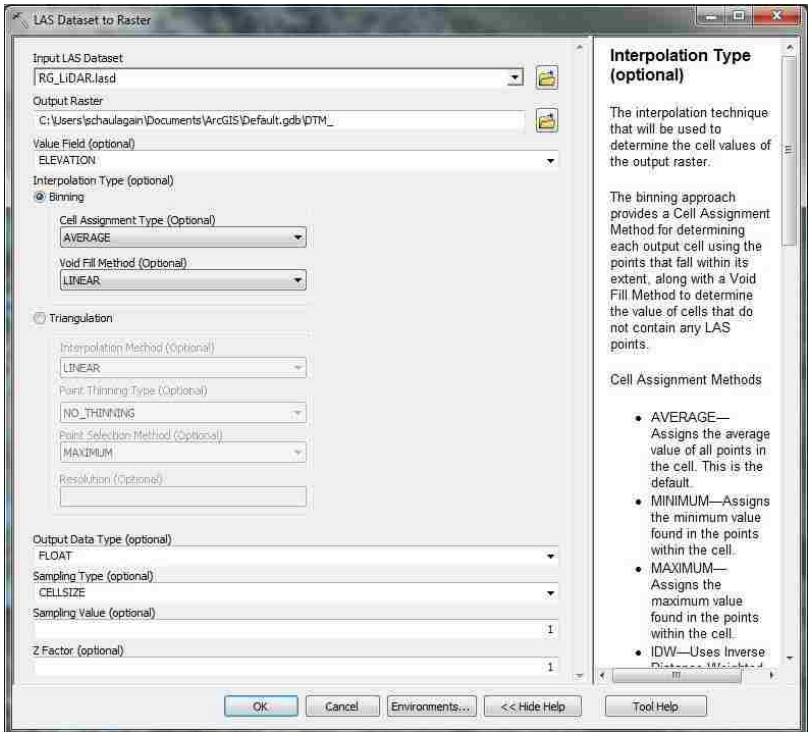

Figure b

Figure 28: a) Activating ground points (last returns) and b) creating DTM

iii) Similarly, to create DSM, first return was activated. For this, cell assignment was chosen as Maximum since we are creating surface model. The cell size was chosen as 1 meter.

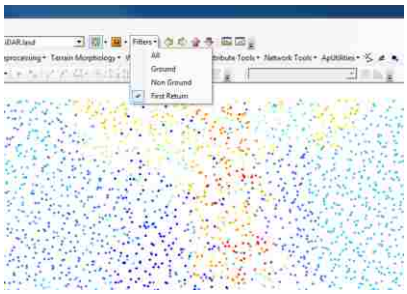

Figure a

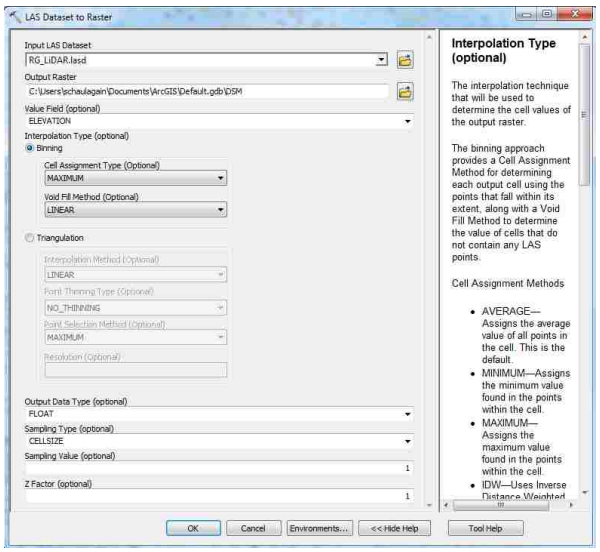

Figure b

Figure 29: a) Activating first returns and b) creating DSM

iv) After creating DSM and DTM, using raster calculator, the difference between DTM and DSM was determined which is the height of vegetation.

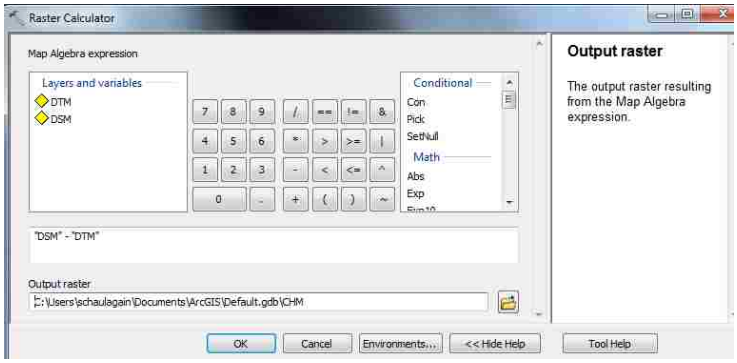

Figure a

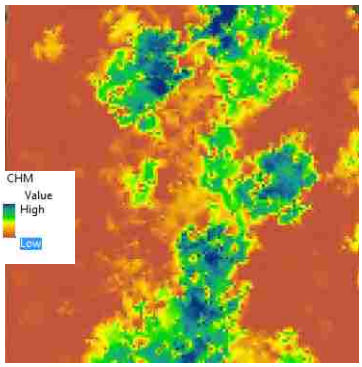

Figure b

Figure 30: a) Raster calculator to create CHM and b) Example of CHM

Before creating DTM and DSM, we have to remove the outliers if exists which might be due to birds, reflection from water, power lines, towers, etc. In order to prevent from erroneous value due to outliers, data should be checked.

LAStools was used to view and remove outliers. Following codes were used in command prompt of windows in order to run lasview and lasheight tool to view the points and remove outliers:

lasview -i <give the name of directory of input file>

lasheight -i <give the name of directory of input file> -drop_below <give the value of height for which points are to be dropped> -drop_above < give the value of height above which points are to be dropped> -o.las

LAI

To find LAI using modified Beer Lambert law, the ratio of ground points to total points is required. For this, following simple steps were followed:

1. Using LAS Point Statistics as raster geoprocessing tool of ArcMap, ground points were counted. In this case, ground points were activated i.e last returns. This step created raster counting the ground point for the specified cell size of raster. In this study, 1 meter was used as cell size.

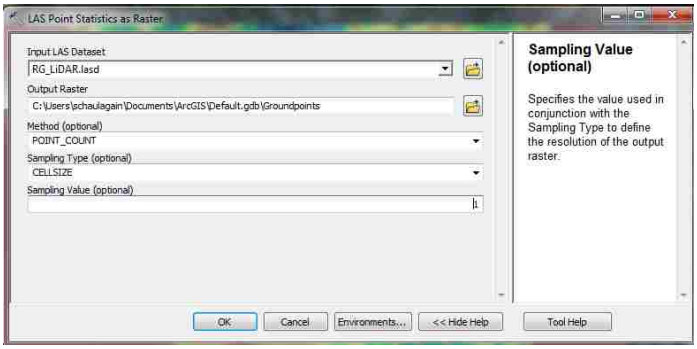

Figure 31: Ground points

2. First step was repeated to count the points but in this case all returns was activated.

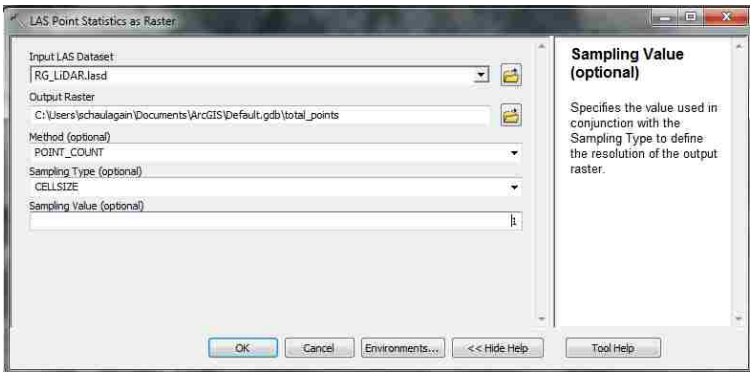

Figure 32: Total points

3. After that, ratio of raster from first and second steps were calculated which was used in modified Beer Lambert law to get LAI.

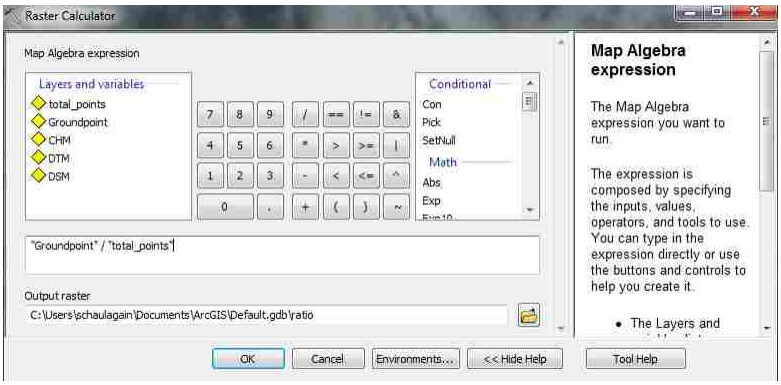

Figure 33: Raster calculator to calculate ratio of grounds to total points

Content of .csv file used to contain the information of height, LAI and the information connecting shapefile of vegetation map.

OBJECTID	ABBREV	VEGTYPE	METHOD	AVGHGT_FT	AVGLAI	AVGSD_FT	M_FT2	Cdx	X	Ux_FT_S	cD	KSIE	VEGMODE	DEFAULT_nv
1	SC6S	Montano Bridge, west side. Remapped after June 2003 Montano Fire. Former Graham property.	Jarvela_2004	3.85901	1.88097	n/a	n/a	0.5	-0.45	0.328	1	n/a	growing	0.029
2	OW	Open Water	Static_No Veg	n/a	n/a	n/a	n/a	n/a	n/a	n/a	n/a	n/a	n/a	0
3	C2	Typed from aerial IR photos and distant view in field. Former Graham property.	Jarvela_2004	16.6365	2.33502	n/a	n/a	0.5	-0.45	0.328	1	n/a	growing	0.035
4	RO/CW3	island in river spanning Montano bridge, mapped from west bank; MH 4/23/03 split poly "a" is south of bridge	Jarvela_2004	3.26321	2.23802	n/a	n/a	0.5	-0.45	0.328	1	n/a	growing	0.055
5	RO/NMO-RO3	Montano Bridge, east side.	Jarvela_2004	2.13607	1.21318	n/a	n/a	0.5	-0.45	0.328	1	n/a	growing	0.055

		Remapped after June 2003 Montano Fire.												
6	OP	Montano Bridge, east side. Remapped after June 2003 Montano Fire. (As of May 2004, woody materials have been removed.)	Jarvela_2004	3.09506	0.532682	n/a	n/a	0.5	-0.45	0.328	1	n/a	growing	0.02
7	C/CW-RO1	Cottonwood/Coyote willow	Jarvela_2004	9.27067	0.862784	n/a	n/a	0.5	-0.45	0.328	1	n/a	growing	0.075
8	C/CW3	sparse overstory and understory with grasses	Jarvela_2004	3.83354	0.477446	n/a	n/a	0.5	-0.45	0.328	1	n/a	growing	0.055
9	C/RO1	Typed from aerial IR photos and discussion with others who know property. Former Graham property.	Jarvela_2004	41.0397	2.87836	n/a	n/a	0.5	-0.45	0.328	1	n/a	growing	0.073
10	C2	closed canopy	Jarvela_2004	26.5029	1.39674	n/a	n/a	0.5	-0.45	0.328	1	n/a	growing	0.035

11	C/SC-RO1	Native Mixed	Jarvela_2004	11.6105	2.18596	n/a	n/a	0.5	-0.45	0.328	1	n/a	growing	0.075
12	CW5	Cyote willow	Jarvela_2004	1.82391	0.270452	n/a	n/a	0.5	-0.45	0.328	1	n/a	growing	0.075
13	C4	open canopy	Jarvela_2004	4.83916	0.583936	n/a	n/a	0.5	-0.45	0.328	1	n/a	growing	0.036
14	C/RO1	Ntive/exotic	Jarvela_2004	22.0351	1.71921	n/a	n/a	0.5	-0.45	0.328	1	n/a	growing	0.074
15	CW6	Island in Rio Grande -- visually determined from E bank	Jarvela_2004	4.82469	2.68183	n/a	n/a	0.5	-0.45	0.328	1	n/a	growing	0.05
16	C/RO-SC1	native/exotic	Jarvela_2004	20.9045	3.41716	n/a	n/a	0.5	-0.45	0.328	1	n/a	growing	0.073
17	C/SC3S	native/saltcedar	Jarvela_2004	7.13574	1.10322	n/a	n/a	0.5	-0.45	0.328	1	n/a	growing	0.055
18	C/RO1	native/exotic	Jarvela_2004	18.8013	1.97194	n/a	n/a	0.5	-0.45	0.328	1	n/a	growing	0.071
19	TW/CW3	CW surrounds pond w/ some cattails (too small to plot separately).	Jarvela_2004	12.1871	2.22093	n/a	n/a	0.5	-0.45	0.328	1	n/a	growing	0.055
20	CW5	Shrub wetland	Jarvela_2004	11.5923	3.91396	n/a	n/a	0.5	-0.45	0.328	1	n/a	growing	0.074

21	MH6	Cattail and CW < 5 ft tall; C & RO < 3 ft tall. Much of cattail is dead. Water regime altered in early 2003. May get wetter in summer.	Jarvela_2004	7.13685	2.45589	n/a	n/a	0.5	-0.45	0.328	1	n/a	growing	0.036
22	C/RO-SC1S	native/exotic	Jarvela_2004	34.4709	2.84805	n/a	n/a	0.5	-0.45	0.328	1	n/a	growing	0.074
23	C2	Scattered trees -- very open ""savannah"" -- grass sparse throughout	Jarvela_2004	7.71985	1.16245	n/a	n/a	0.5	-0.45	0.328	1	n/a	growing	0.035
24	RO/CW3	Narrow strip of marsh within stand.	Jarvela_2004	11.5209	3.75116	n/a	n/a	0.5	-0.45	0.328	1	n/a	growing	0.053
25	C/SC-RO1	native/exotic	Jarvela_2004	20.6669	3.40991	n/a	n/a	0.5	-0.45	0.328	1	n/a	growing	0.074
26	CW5F	Height variable, but just tall enough to be suitable WIFL habitat. Although patch is narrow, it abuts wetland.	Jarvela_2004	10.4096	3.76899	n/a	n/a	0.5	-0.45	0.328	1	n/a	growing	0.074

27	CW5	Shrub wetland. Beaver lodge.	Jarvela_2004	7.86141	2.64893	n/a	n/a	0.5	-0.45	0.328	1	n/a	growing	0.074
28	C2	Closed canopy - but no understory (except leafless dead and down)	Jarvela_2004	26.4581	2.36857	n/a	n/a	0.5	-0.45	0.328	1	n/a	growing	0.035
29	CW5	Shrub wetland.	Jarvela_2004	12.7077	4.2961	n/a	n/a	0.5	-0.45	0.328	1	n/a	growing	0.074
30	C2	Cottonwood	Jarvela_2004	16.2044	3.06905	n/a	n/a	0.5	-0.45	0.328	1	n/a	growing	0.035
31	MH5	Cattail marsh with some small open water areas.	Jarvela_2004	2.10924	3.4556	n/a	n/a	0.5	-0.45	0.328	1	n/a	growing	0.074
32	MH6	Cattail marsh; largely dead because surface water flow has been cut off by berm & channel.	Jarvela_2004	3.1844	1.78489	n/a	n/a	0.5	-0.45	0.328	1	n/a	growing	0.035
33	C/R01	native/exotic	Jarvela_2004	10.3036	3.53782	n/a	n/a	0.5	-0.45	0.328	1	n/a	growing	0.075
34	MH5-OW	Open water = 50%; vegetation = 50%.	Static_NoVeg	n/a	n/a	n/a	n/a	n/a	n/a	n/a	n/a	n/a	n/a	0

35	C/SC-CW5	Native Mixed	Jarvela_2004	11.5366	3.98632	n/a	n/a	0.5	-0.45	0.328	1	n/a	growing	0.074
36	OW	Open water (pond)	Static_No Veg	n/a	n/a	n/a	n/a	n/a	n/a	n/a	n/a	n/a	n/a	0
37	C2	cottonwood	Jarvela_2004	5.47864	2.68799	n/a	n/a	0.5	-0.45	0.328	1	n/a	growing	0.036
38	CW5F	Shrub wetland. Dense CW; just tall enough for suitable WIFL habitat; small patch; wet soils.	Jarvela_2004	11.0286	3.78014	n/a	n/a	0.5	-0.45	0.328	1	n/a	growing	0.075
39	RO-CW5F	Shrub wetland. Dense vegetation, suitable WIFL habitat; wet soil; abuts marsh.	Jarvela_2004	11.89	4.11928	n/a	n/a	0.5	-0.45	0.328	1	n/a	growing	0.069
40	C/RO1F	Dense but is not potentially suitable WIFL habitat -- too dry	Jarvela_2004	22.9206	4.12286	n/a	n/a	0.5	-0.45	0.328	1	n/a	growing	0.074
41	C4	Closed canopy; No appreciable understory	Jarvela_2004	13.0309	1.00198	n/a	n/a	0.5	-0.45	0.328	1	n/a	growing	0.035

42	RO/CW 3S	none	Jarvela_2004	6.30244	1.49212	n/a	n/a	0.5	-0.45	0.328	1	n/a	growing	0.053
43	C/RO-CW1	native/exotic	Jarvela_2004	34.7418	3.97988	n/a	n/a	0.5	-0.45	0.328	1	n/a	growing	0.07
44	CW5	Cyote willow	Jarvela_2004	0.666823	0.339451	n/a	n/a	0.5	-0.45	0.328	1	n/a	growing	0.074
45	C2	Closed Canopy	Jarvela_2004	9.10652	1.59699	n/a	n/a	0.5	-0.45	0.328	1	n/a	growing	0.035
46	C2	cottonwood	Jarvela_2004	5.2135	1.50408	n/a	n/a	0.5	-0.45	0.328	1	n/a	growing	0.032
47	CW-RO5	Island in Rio Grande (seen from east shore)	Jarvela_2004	3.29642	2.88027	n/a	n/a	0.5	-0.45	0.328	1	n/a	growing	0.048
48	OP	openland	Jarvela_2004	1.28915	0.301533	n/a	n/a	0.5	-0.45	0.328	1	n/a	growing	0.021
49	C4	Closed canopy; No appreciable understory	Jarvela_2004	12.6652	1.22104	n/a	n/a	0.5	-0.45	0.328	1	n/a	growing	0.035
50	C/RO-CW1F	Desne; but not potentially suitable WIFL habitat. Too dry.	Jarvela_2004	8.44367	1.60681	n/a	n/a	0.5	-0.45	0.328	1	n/a	growing	0.059
51	OP		Jarvela_2004	0.798294	0.516143	n/a	n/a	0.5	-0.45	0.328	1	n/a	growing	0.022

52	C/RO-SC1		Jarvela_2004	3.26053	0.936237	n/a	n/a	0.5	-0.45	0.328	1	n/a	growing	0.07
53	RO/RO3	Island with tall vegetation	Jarvela_2004	18.6804	4.0145	n/a	n/a	0.5	-0.45	0.328	1	n/a	growing	0.053
54	C2	cottonwood	Jarvela_2004	3.66286	0.935586	n/a	n/a	0.5	-0.45	0.328	1	n/a	growing	0.032
55	C2	cottonwood	Jarvela_2004	15.7742	2.16051	n/a	n/a	0.5	-0.45	0.328	1	n/a	growing	0.032
56	OW	water	Static_NoVeg	n/a	n/a	n/a	n/a	n/a	n/a	n/a	n/a	n/a	n/a	0
57	C/RO-MB-SC1	native/exotic	Jarvela_2004	9.60584	1.11418	n/a	n/a	0.5	-0.45	0.328	1	n/a	growing	0.075
58	SC6	salt cedar	Jarvela_2004	2.20789	1.04841	n/a	n/a	0.5	-0.45	0.328	1	n/a	growing	0.035
59	C/RO-SC1	native/exotic	Jarvela_2004	12.1925	1.25646	n/a	n/a	0.5	-0.45	0.328	1	n/a	growing	0.074
60	C/RO-SC3	old signol fire	Jarvela_2004	11.3172	1.38051	n/a	n/a	0.5	-0.45	0.328	1	n/a	growing	0.055
61	RO5	Russian olive	Jarvela_2004	3.81915	1.38519	n/a	n/a	0.5	-0.45	0.328	1	n/a	growing	0.067
62	SE/MB-TH3	old burn, lots of old c limbs and trees	Jarvela_2004	19.4365	2.34735	n/a	n/a	0.5	-0.45	0.328	1	n/a	growing	0.048
63	SE-MB4	crow roost, upland drainage off	Jarvela_2004	24.7456	2.17393	n/a	n/a	0.5	-0.45	0.328	1	n/a	growing	0.035

		bluff (small channel and trash)												
64	CW5	high water channel	Jarvela_2004	16.4384	1.72161	n/a	n/a	0.5	-0.45	0.328	1	n/a	growing	0.074
65	SC3	salt cedar	Jarvela_2004	10.2304	0.967101	n/a	n/a	0.5	-0.45	0.328	1	n/a	growing	0.055
66	SC-RO-C5S	older pole plantation, several piezometers throughout	Jarvela_2004	6.41574	1.15248	n/a	n/a	0.5	-0.45	0.328	1	n/a	growing	0.075
67	C/RO1	native/exotic	Jarvela_2004	22.3814	2.5359	n/a	n/a	0.5	-0.45	0.328	1	n/a	growing	0.074
68	SC6	sandy bar at river edge, highwater channel, inundation	Jarvela_2004	5.18577	2.86206	n/a	n/a	0.5	-0.45	0.328	1	n/a	growing	0.032
69	OP	Open land	Jarvela_2004	1.25391	0.825993	n/a	n/a	0.5	-0.45	0.328	1	n/a	growing	0.02
70	C/RO-SC1	native/exotic	Jarvela_2004	21.5773	1.7636	n/a	n/a	0.5	-0.45	0.328	1	n/a	growing	0.073
71	C/CW3	Yerba mansa present	Jarvela_2004	10.0373	1.88737	n/a	n/a	0.5	-0.45	0.328	1	n/a	growing	0.056
72	SC-RO5	native/exotic	Jarvela_2004	8.58774	3.14434	n/a	n/a	0.5	-0.45	0.328	1	n/a	growing	0.075

73	C/RO1S	burn with tall standing dead material, some regreening, sparse overstory and understory	Jarvela_2004	13.7223	2.30153	n/a	n/a	0.5	-0.45	0.328	1	n/a	growing	0.067
74	CW6	Cyote willow	Jarvela_2004	8.47812	3.06653	n/a	n/a	0.5	-0.45	0.328	1	n/a	growing	0.035
75	RO5	Russian olive	Jarvela_2004	1.71592	0.96351	n/a	n/a	0.5	-0.45	0.328	1	n/a	growing	0.051
76	OP	2 parts to the polygon, burned, cleared, some c and tw poles; poly split by MWH on 4/18/03-No photo file to copy	Jarvela_2004	3.70281	1.47401	n/a	n/a	0.5	-0.45	0.328	1	n/a	growing	0.021
77	C/RO-SE1	native/exotic	Jarvela_2004	20.2903	1.61787	n/a	n/a	0.5	-0.45	0.328	1	n/a	growing	0.072
78	SC4	salt cedar	Jarvela_2004	2.7189	0.859947	n/a	n/a	0.5	-0.45	0.328	1	n/a	growing	0.036
79	OP	2 parts to the polygon, burned, cleared, some c and tw poles; poly split by MWH	Jarvela_2004	1.92561	1.60971	n/a	n/a	0.5	-0.45	0.328	1	n/a	growing	0.02

		on 4/18/03-No photo file to copy												
80	C/RO-MB3	native/exotic	Jarvela_2004	24.342	1.71903	n/a	n/a	0.5	-0.45	0.328	1	n/a	growing	0.055
81	C-SE2	Thick understory, but mostly dead	Jarvela_2004	26.2862	2.00687	n/a	n/a	0.5	-0.45	0.328	1	n/a	growing	0.03
82	RO5	russian olive	Jarvela_2004	16.4793	1.47349	n/a	n/a	0.5	-0.45	0.328	1	n/a	growing	0.074
83	C4	Cyote willow	Jarvela_2004	2.95156	0.573162	n/a	n/a	0.5	-0.45	0.328	1	n/a	growing	0.035
84	SE/RO-CW5	native/exotic	Jarvela_2004	4.30774	1.70604	n/a	n/a	0.5	-0.45	0.328	1	n/a	growing	0.055
85	OP	openland	Jarvela_2004	4.08124	1.05212	n/a	n/a	0.5	-0.45	0.328	1	n/a	growing	0.029
86	C/RO3S	native/exotic	Jarvela_2004	10.8433	1.6664	n/a	n/a	0.5	-0.45	0.328	1	n/a	growing	0.056
87	OP	open	Jarvela_2004	3.98816	1.55254	n/a	n/a	0.5	-0.45	0.328	1	n/a	growing	0.023
88	C-SE2	cleared understory-restoration site	Jarvela_2004	19.522	1.70708	n/a	n/a	0.5	-0.45	0.328	1	n/a	growing	0.035
89	C2	restoration site cleared understory in summer 2002	Jarvela_2004	8.64125	0.888635	n/a	n/a	0.5	-0.45	0.328	1	n/a	growing	0.035

90	OP	open area with pole plantings (c and tw)	Jarvela_2004	17.932	2.05111	n/a	n/a	0.5	-0.45	0.328	1	n/a	growing	0.02
91	OP	open	Jarvela_2004	3.76309	0.512997	n/a	n/a	0.5	-0.45	0.328	1	n/a	growing	0.02
92	RO5S	russian olive	Jarvela_2004	18.7909	2.29943	n/a	n/a	0.5	-0.45	0.328	1	n/a	growing	0.072
93	OP	Cleared area near Central Bridge	Jarvela_2004	9.67125	1.80095	n/a	n/a	0.5	-0.45	0.328	1	n/a	growing	0.02

APPEXDIX B. HYDRAULIC PARAMETERS

Unit conversion

1 miles = 1.609 Km

1 foot = 0.3048 m

1 cfs = 0.0283 m^3/s

Mapping of dynamic hydraulic roughness for individual flows:

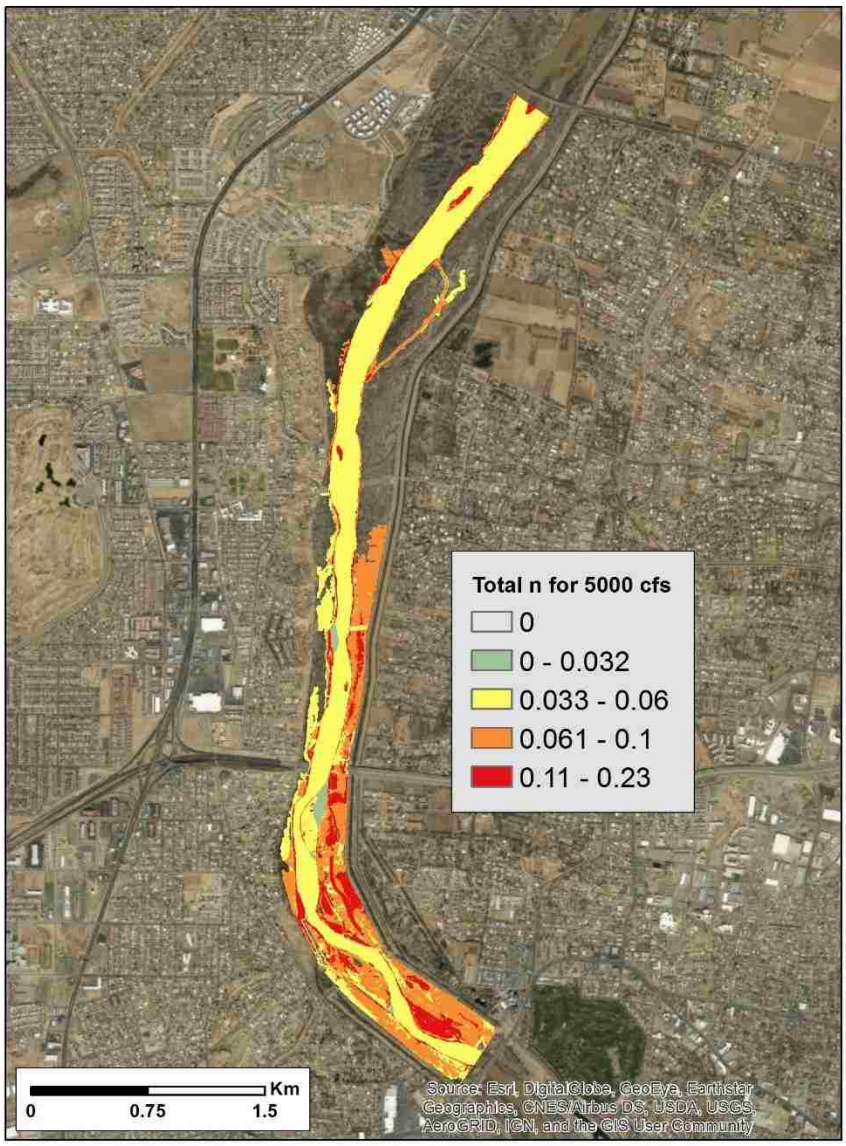

Figure a

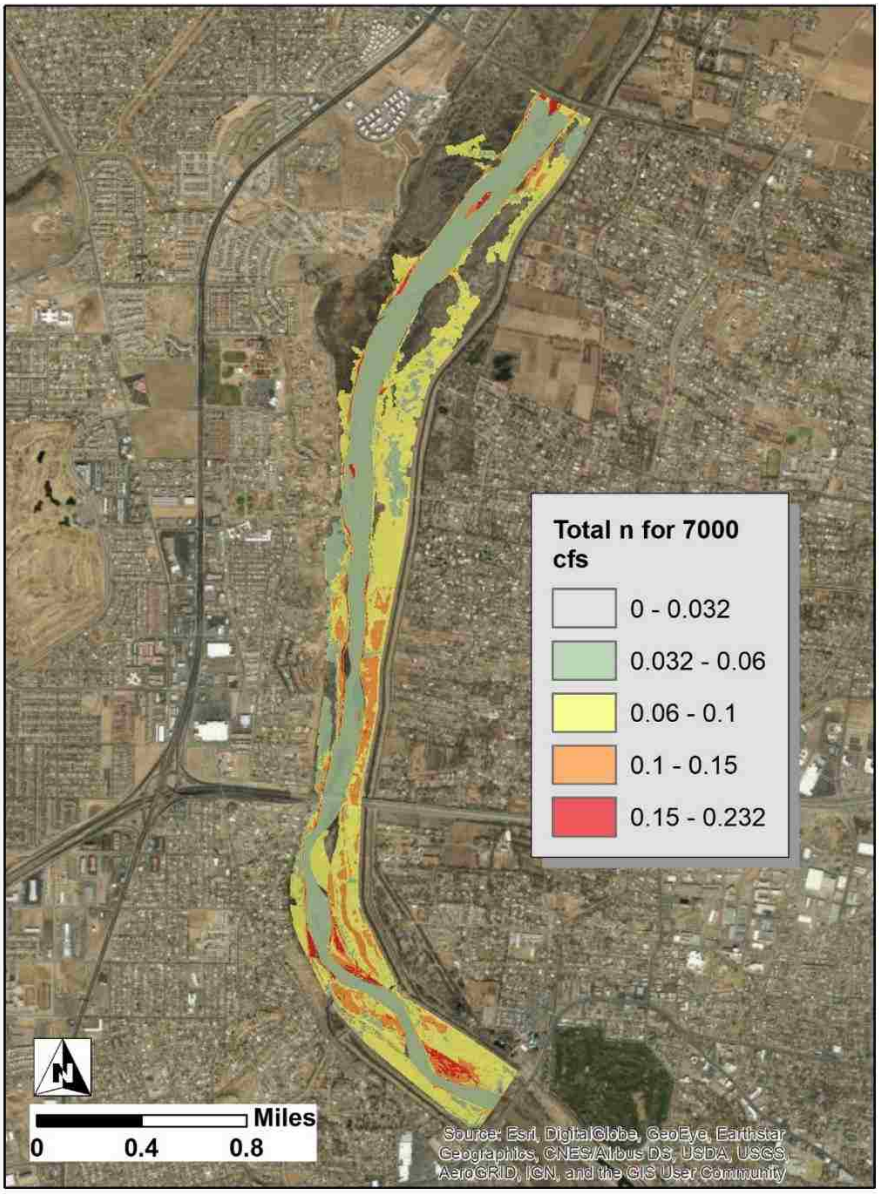

Figure b

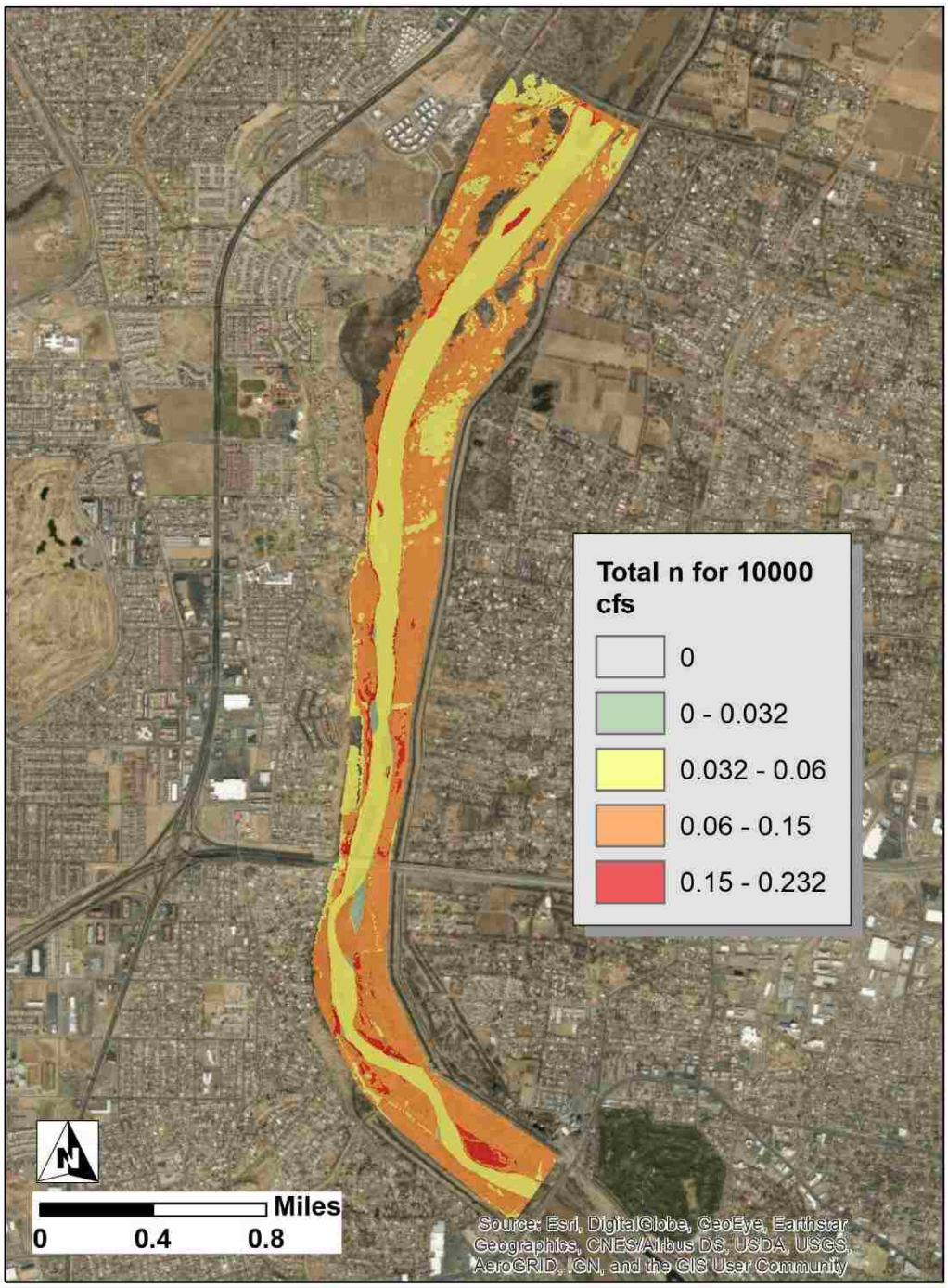

Figure c

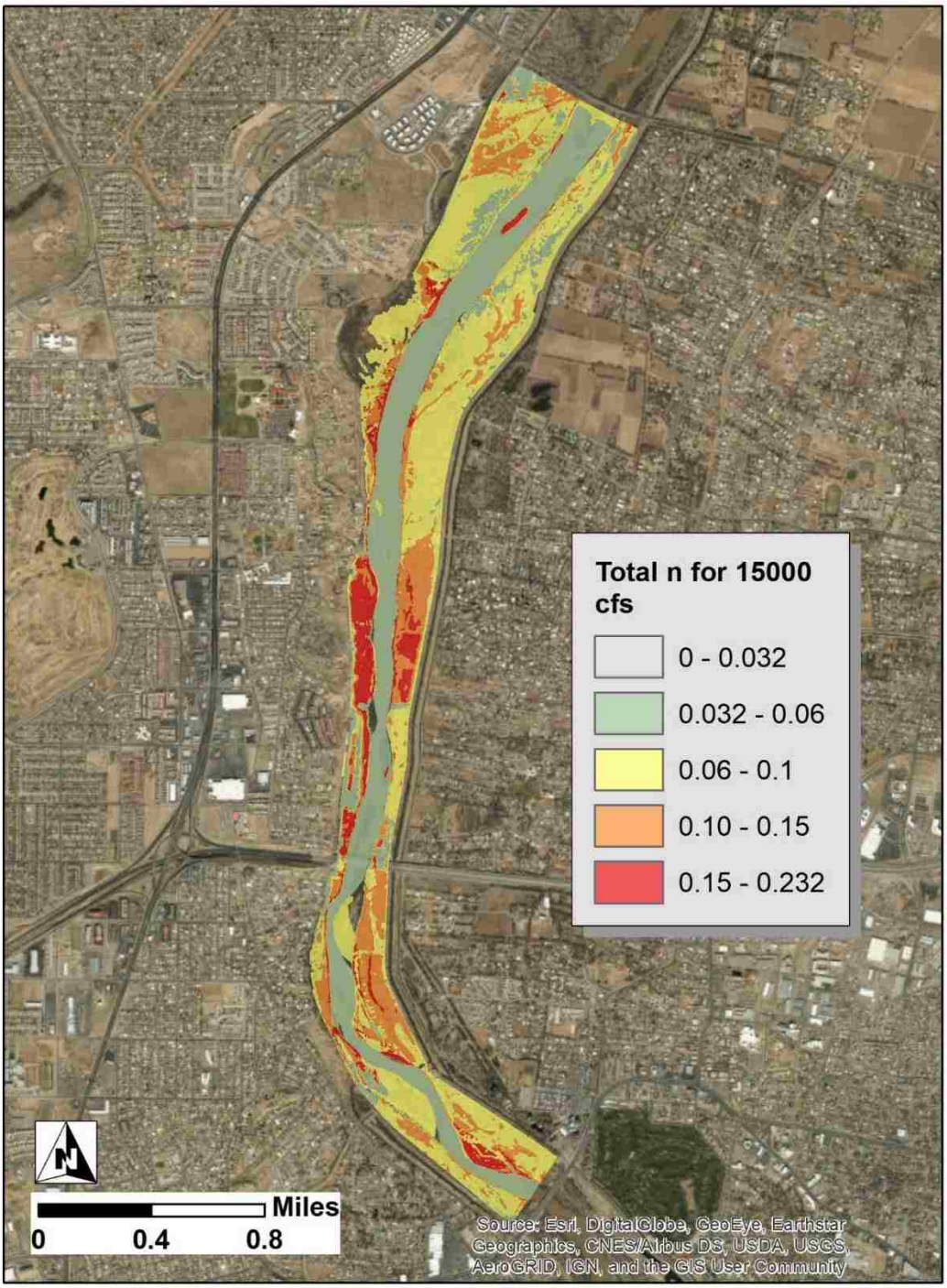

Figure d

Figure 34: Dynamic roughness for a) 142 m^3/s b) 198 m^3/s c) 283 m^3/s and d) 425 m^3/s

Mapping for the change in hydraulic parameters for 142 m^3/s (5000 cfs), 198 m^3/s (7000 cfs) and 425 m^3/s (15000 cfs)

The difference was obtained by subtracting the value due to land cover roughness from value obtained from dynamic roughness)

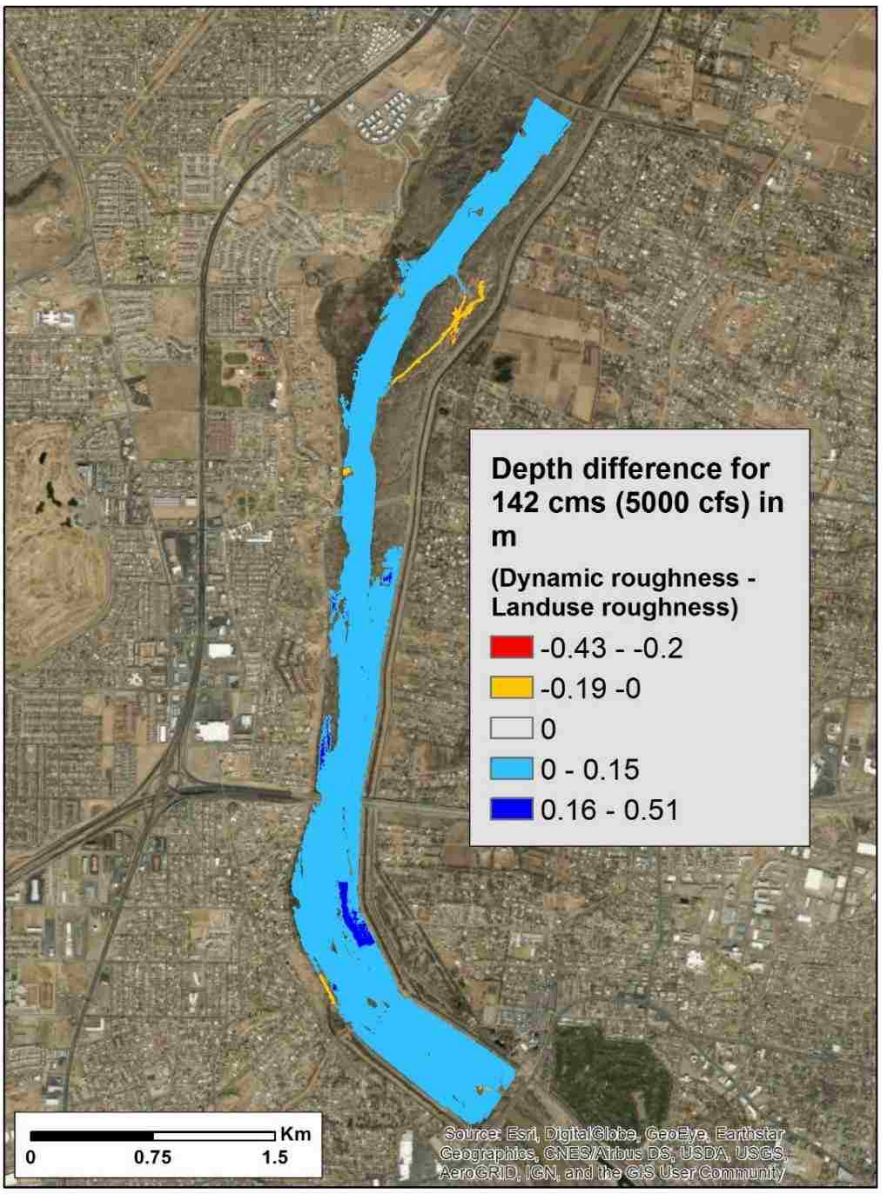

Figure a

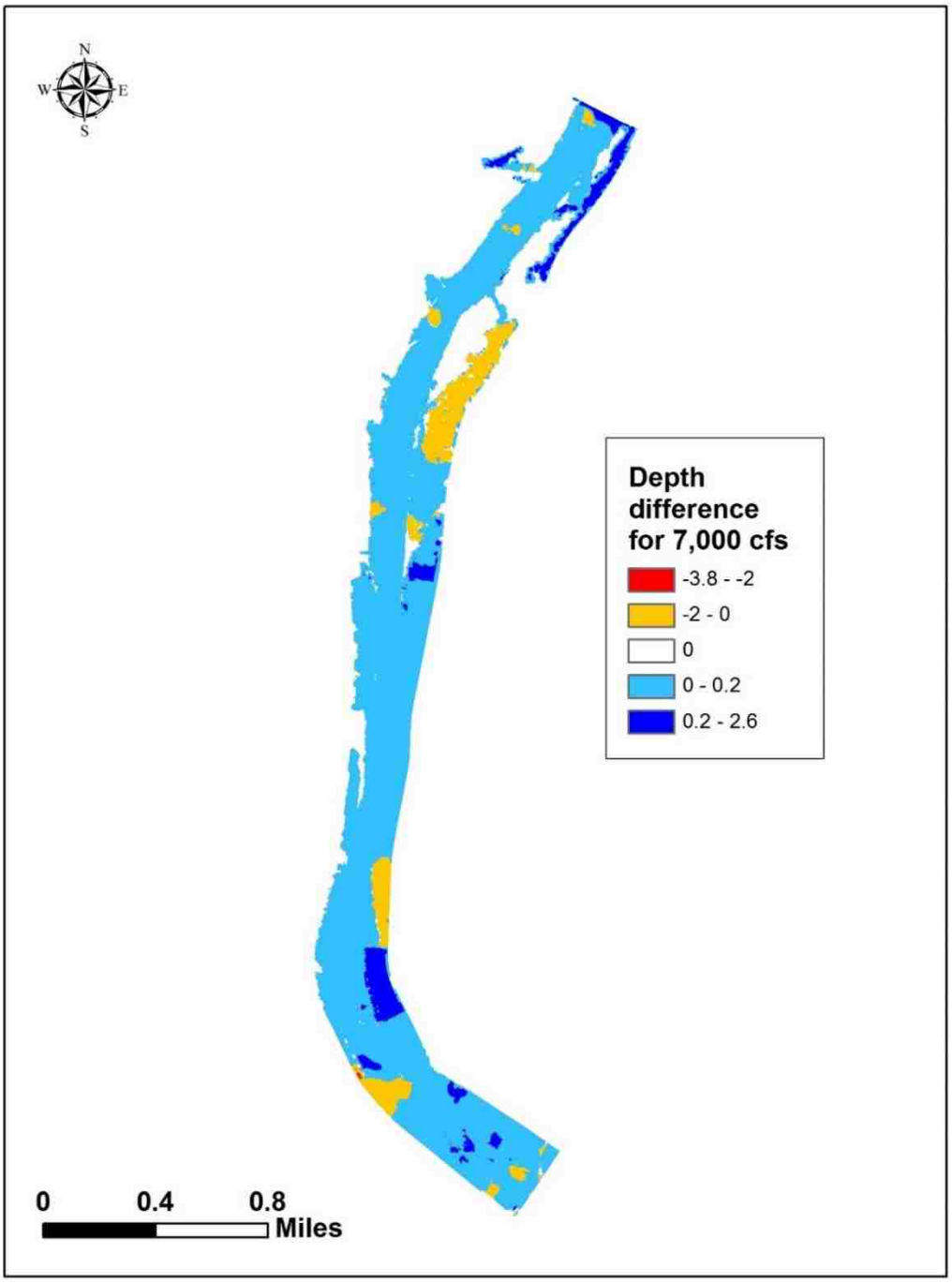

Figure b

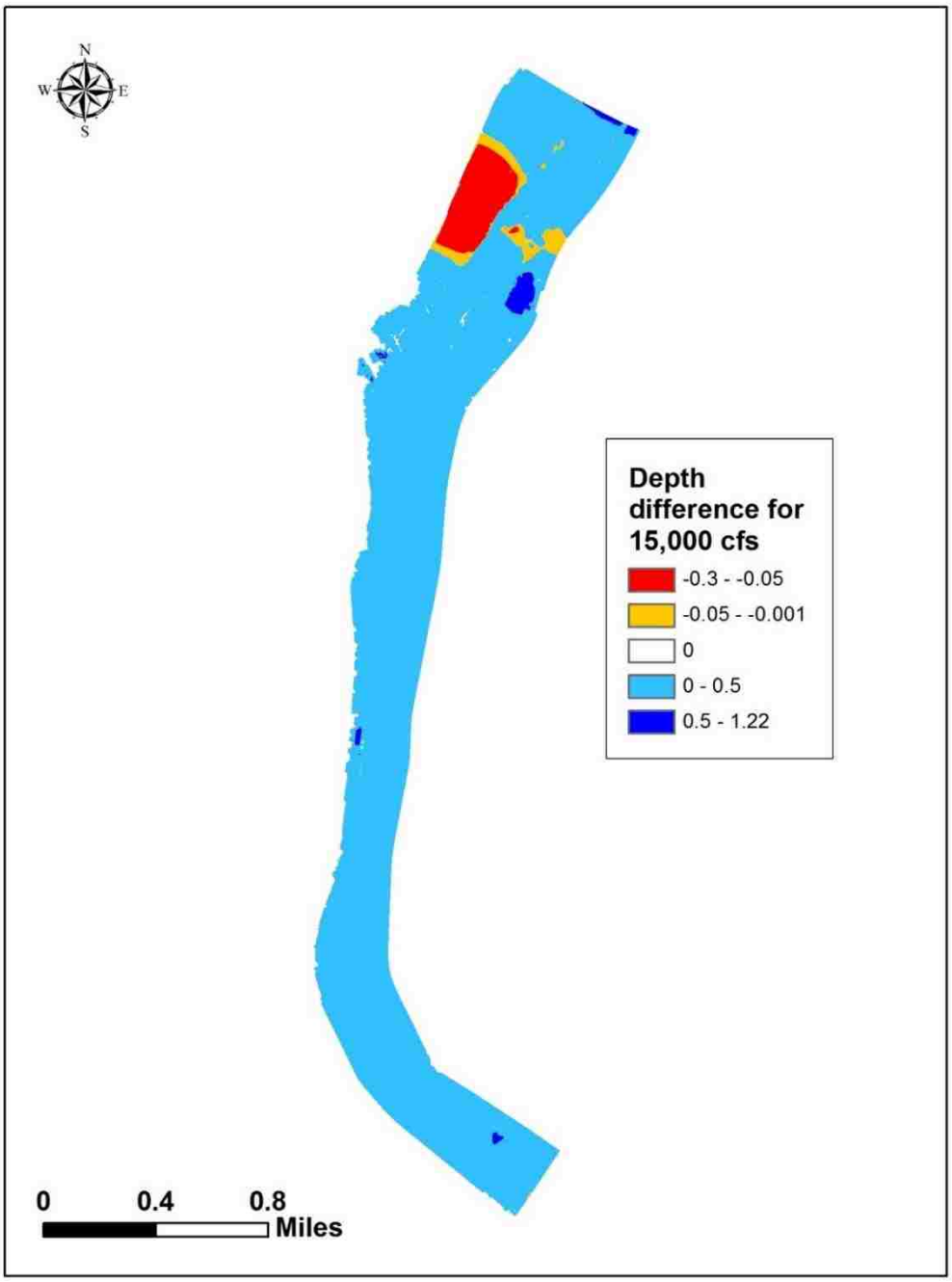

Figure c

Figure 35: Depth differences due to dynamic and constant roughness for a) 142 m^3/s b) 198m^3/s and c) 425 m^3/s

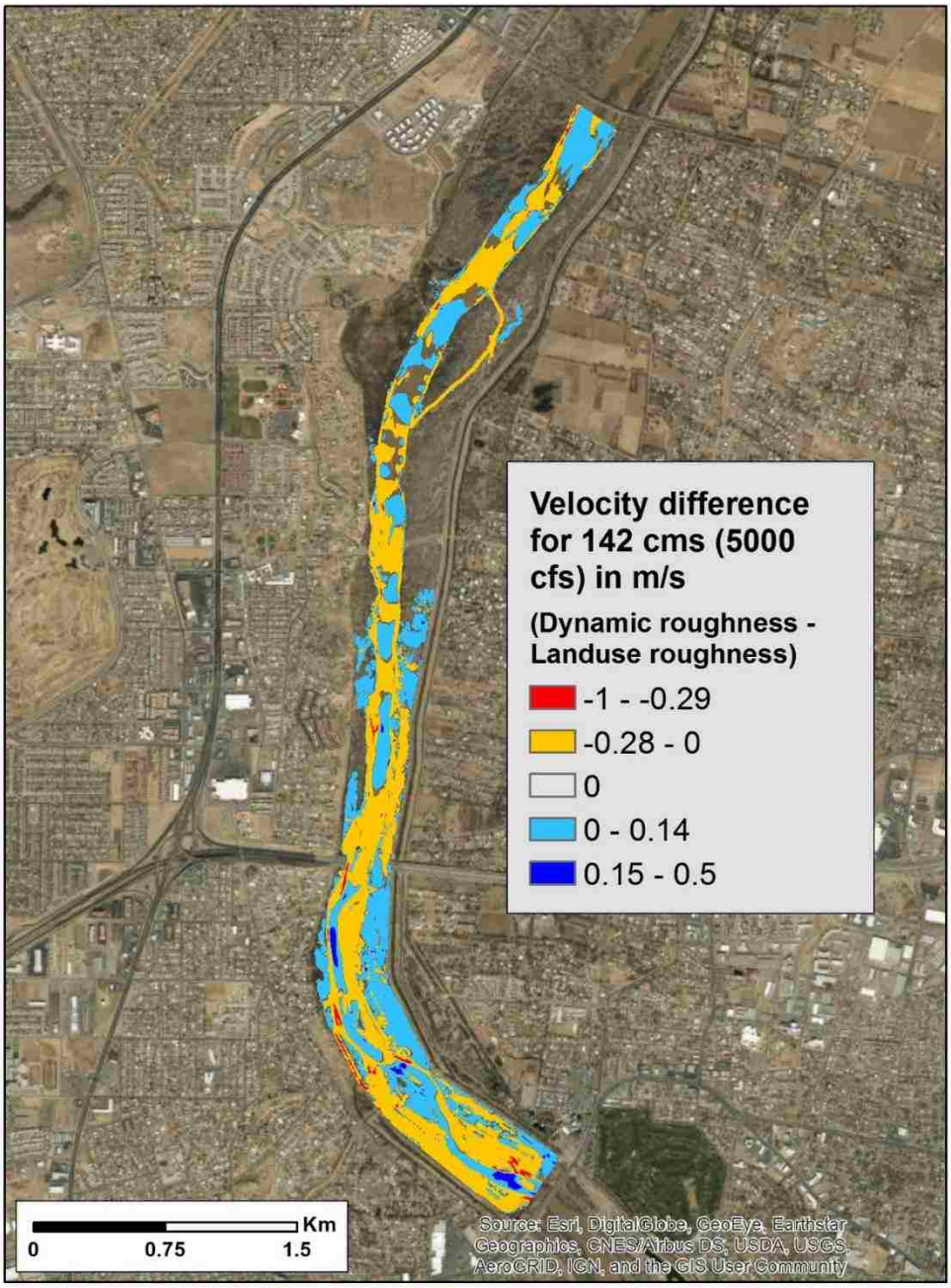

Figure a

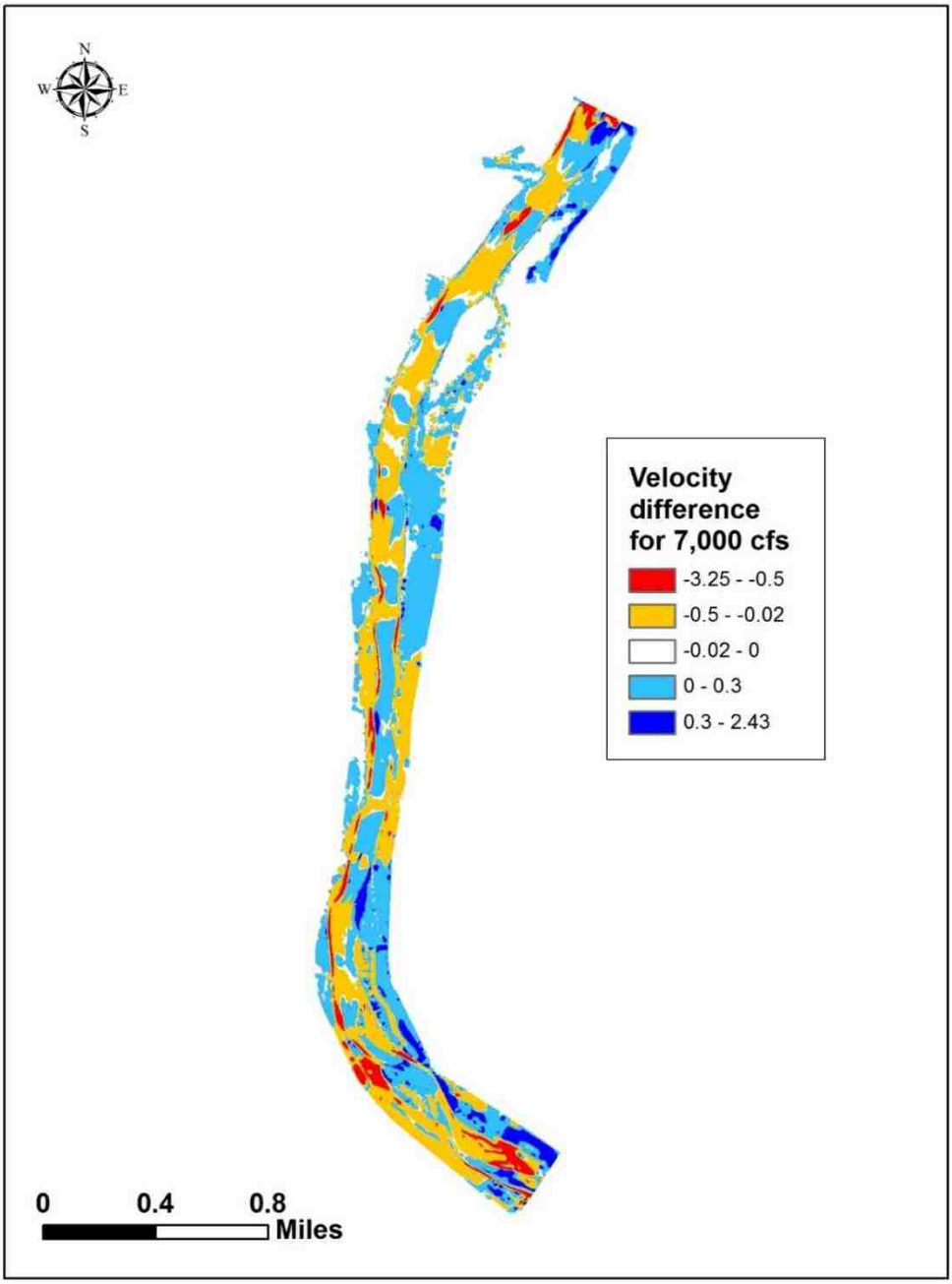

Figure b

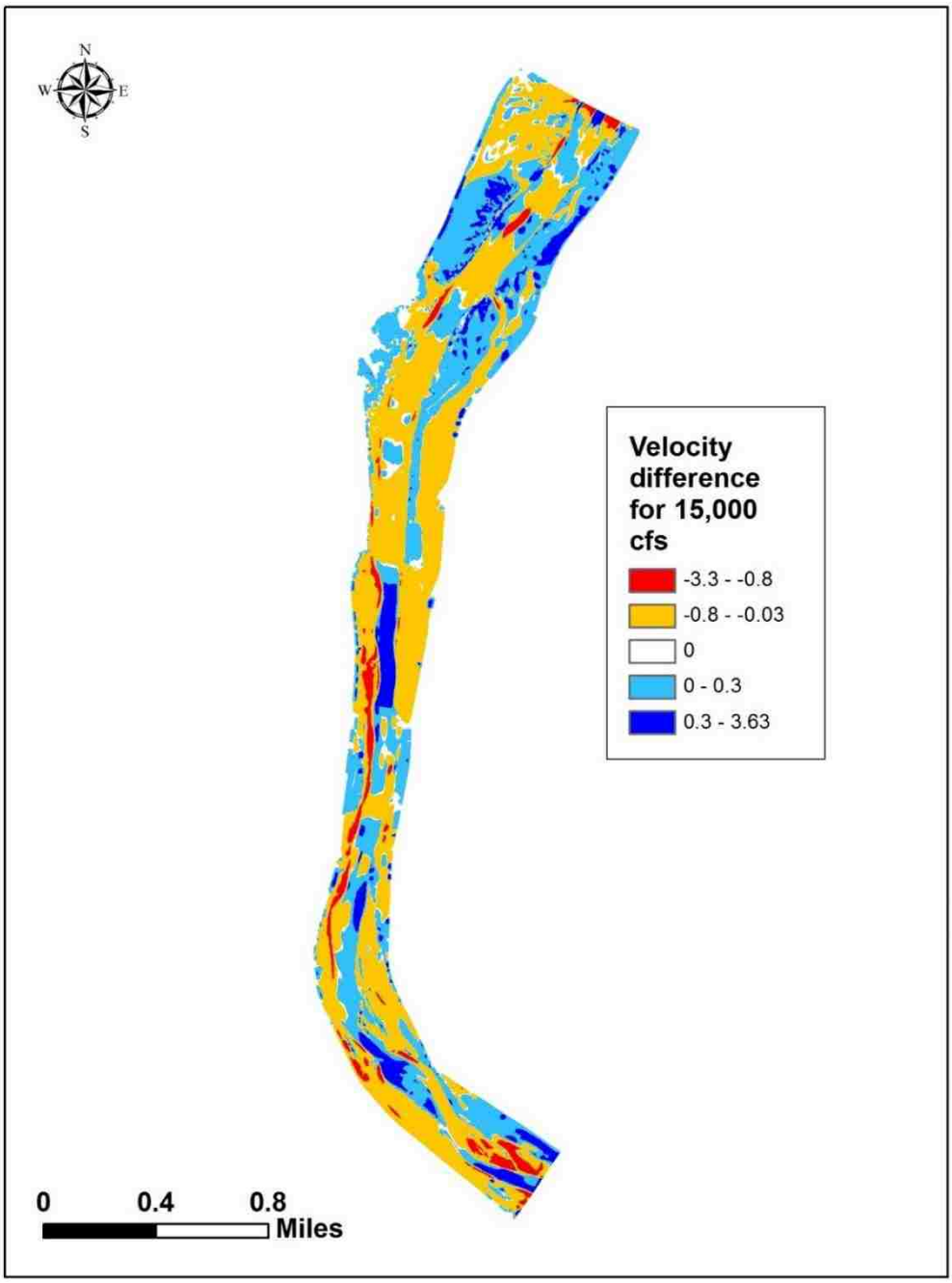

Figure c

Figure 36: Velocity differences due to dynamic and constant roughness for a) 142 m^3/s b) 198m^3/s and c) 425 m^3/s

Histograms of velocity and depth for different flows

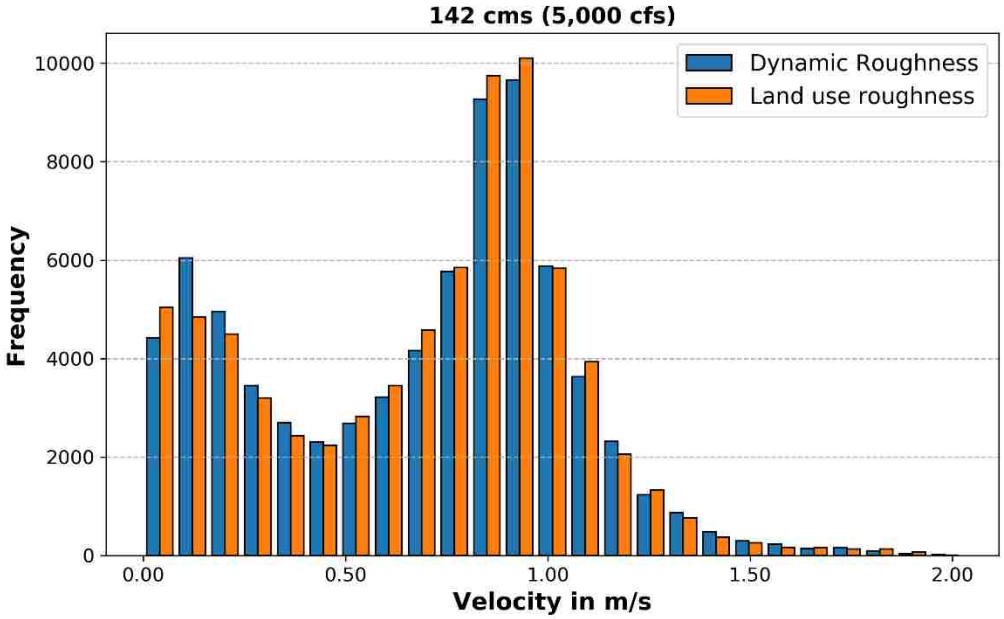

Figure a

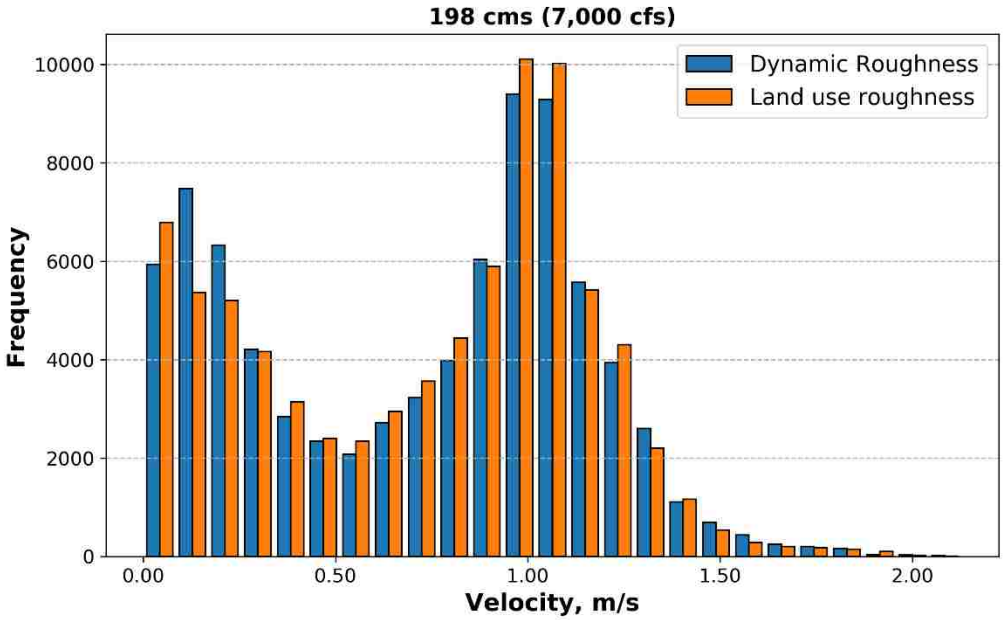

Figure b

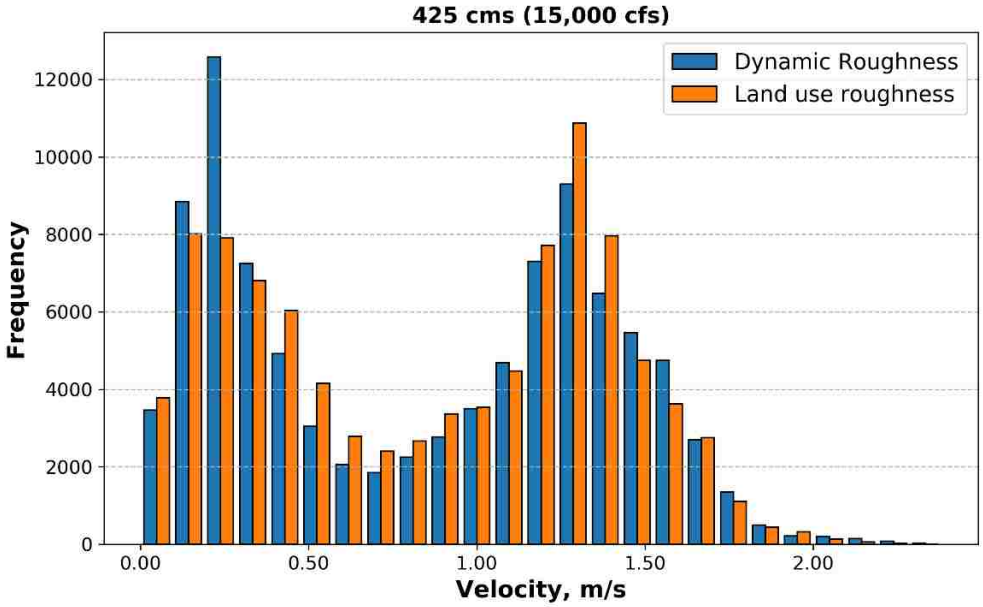

Figure c

Figure 37: Velocity due to dynamic and constant roughness for a) 142 m^3/s b) 198m^3/s and c) 425 m^3/s

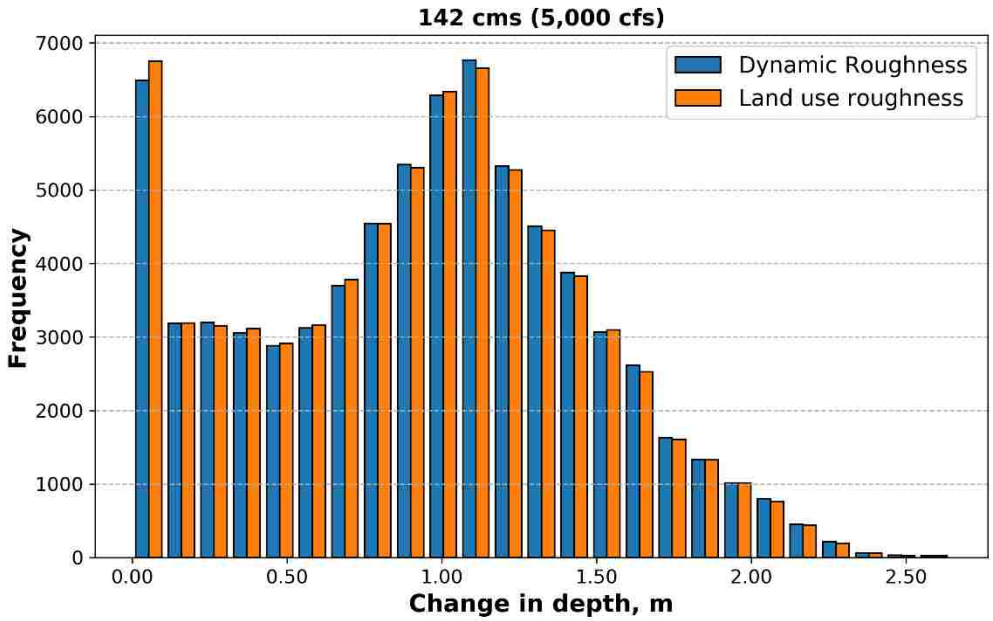

Figure a

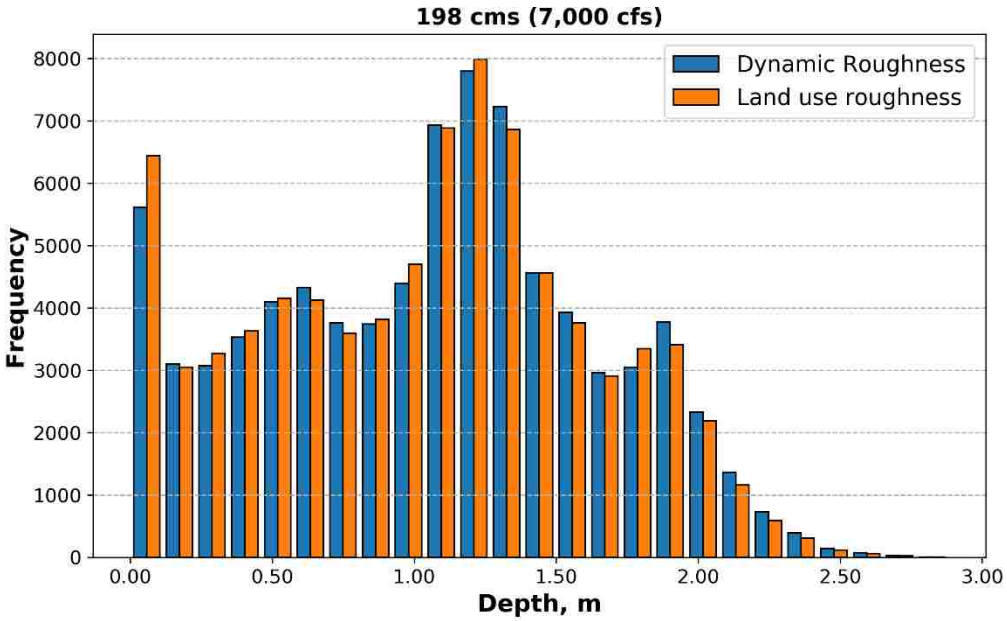

Figure b

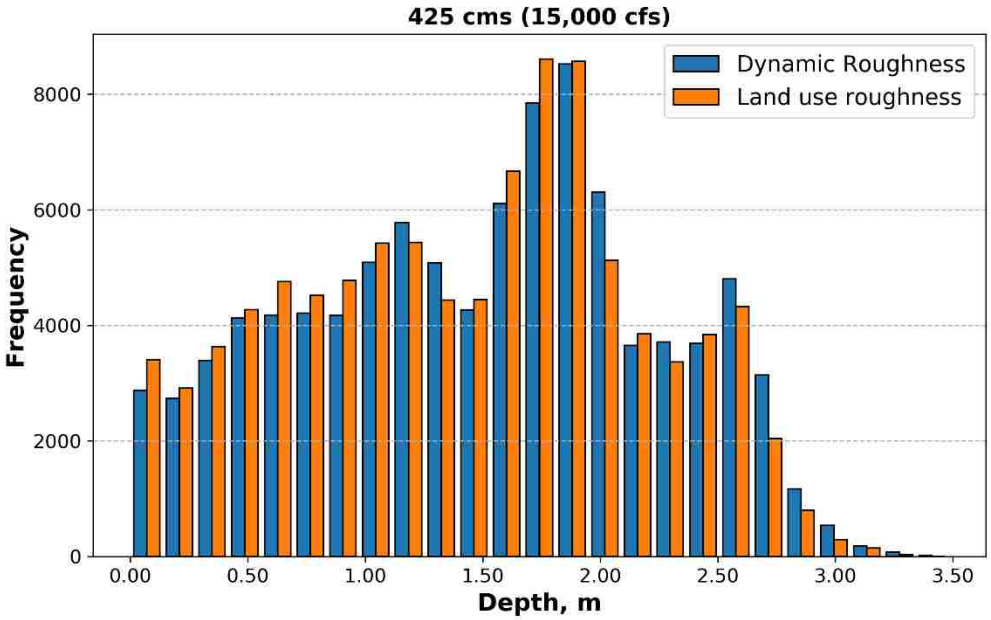

Figure c

Figure 38: Depth due to dynamic and constant roughness for a) 142 m^3/s b) 198m^3/s and c) 425 m^3/s

Mapping of hydraulic parameters for sensitivity analysis

The differnce was calculated by substracting the hydraulic parameters from varying parameters by assumed standard value of parameter. All depth are in feet and velocity in feet/seconds for sensitivity analysis.

Figure a

Figure b

Figure c

Figure d

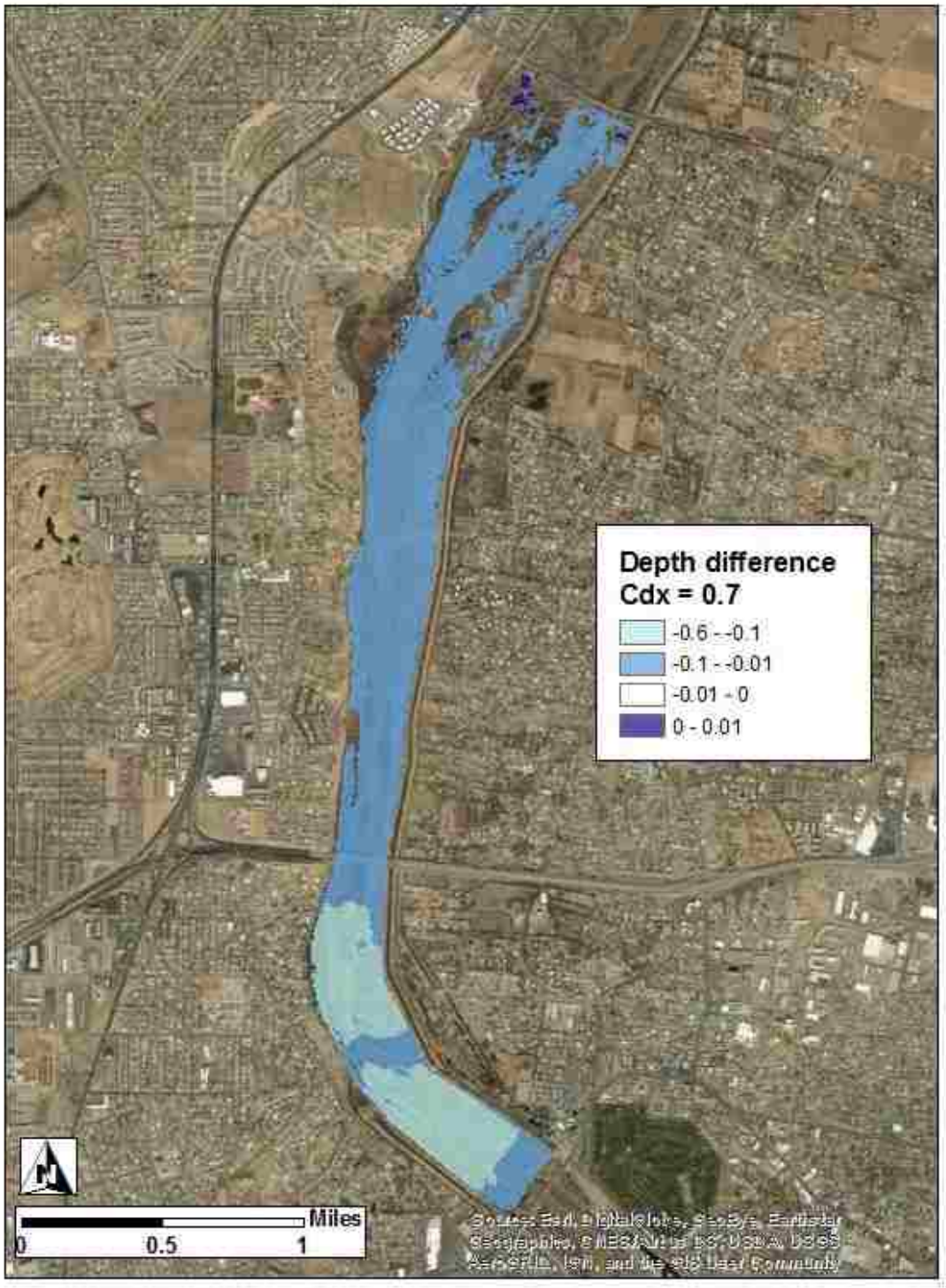

Figure e

Figure 39: Depth differences from sensitivity analysis

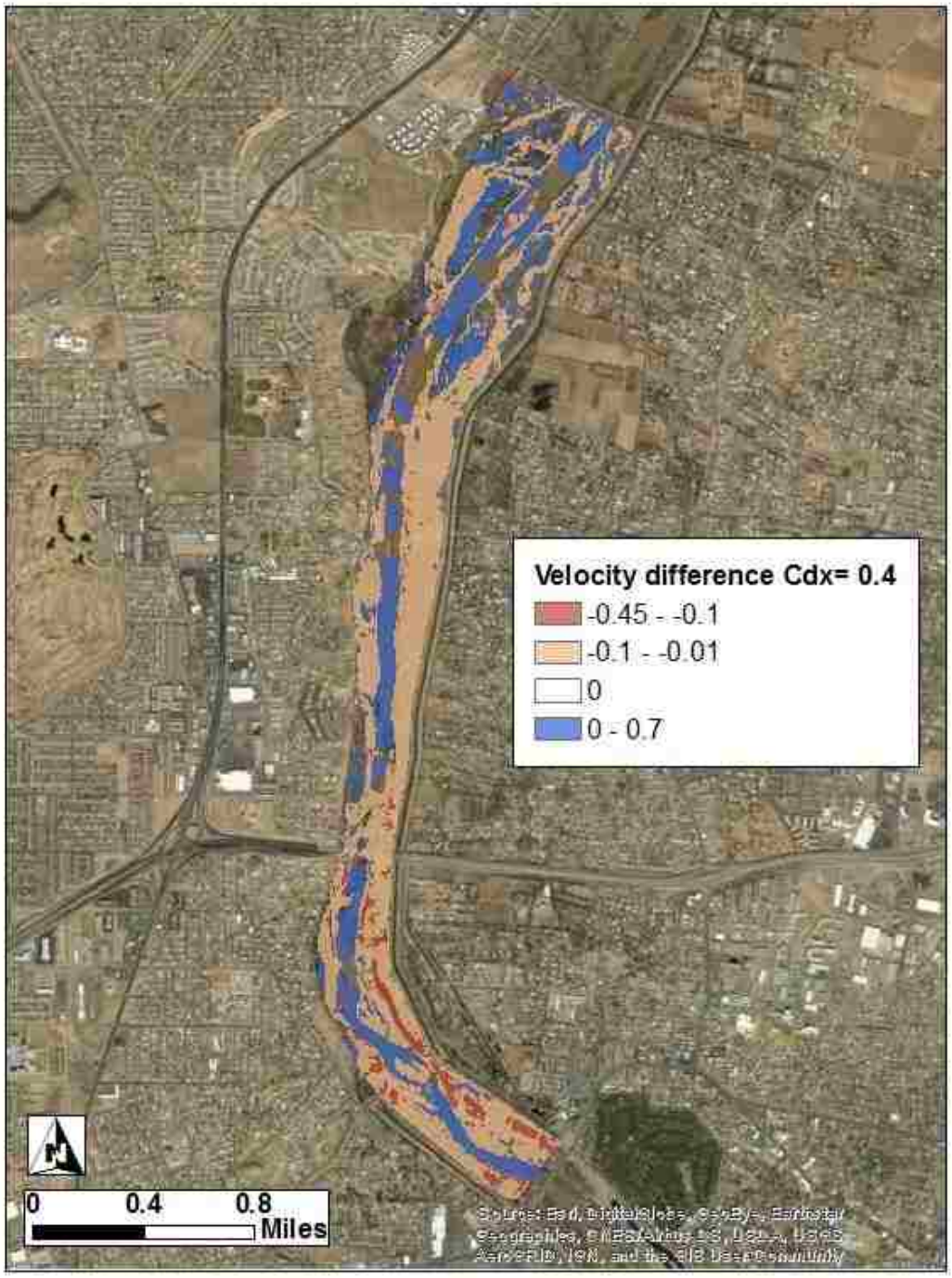

Figure a

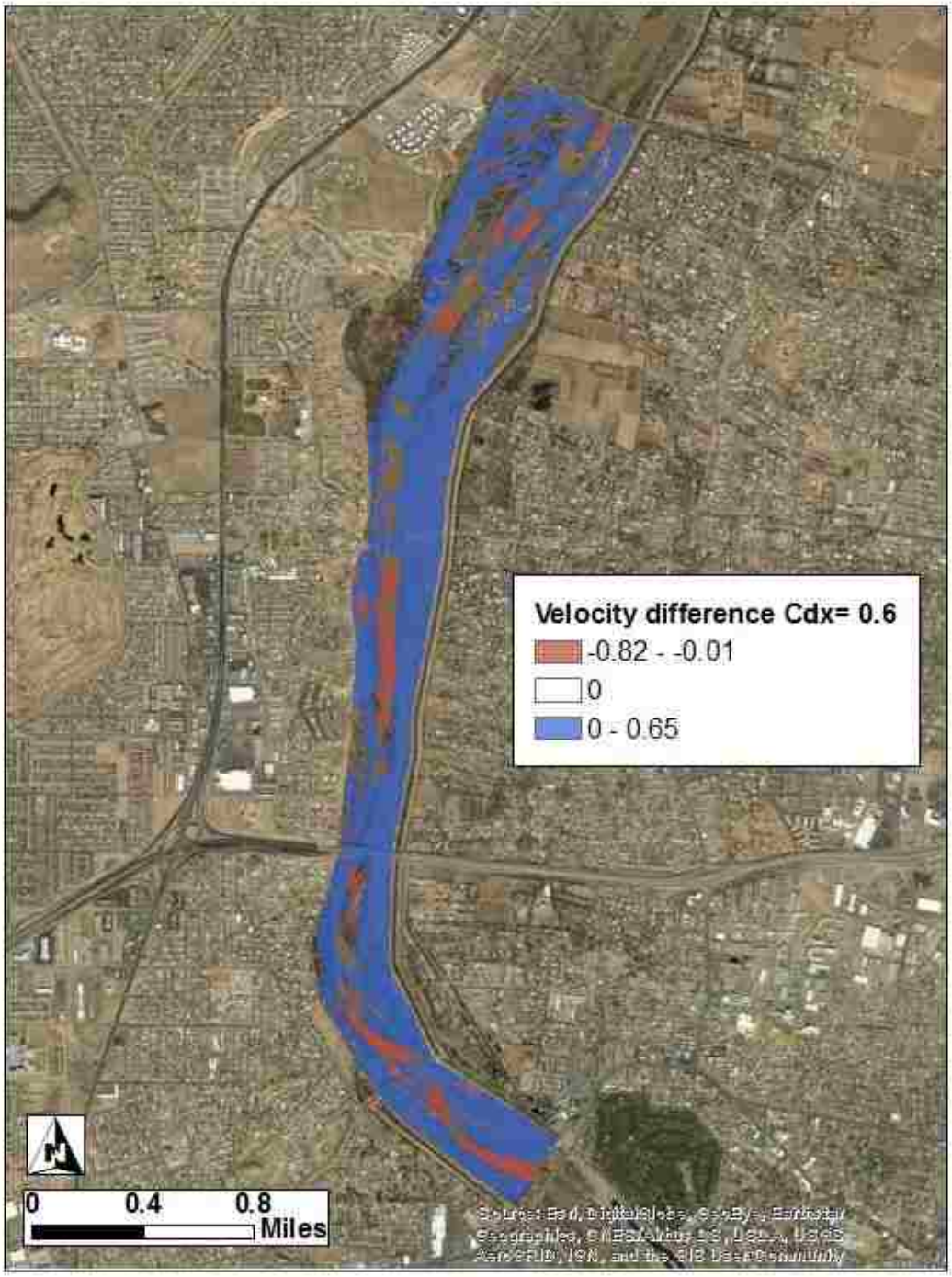

Figure b

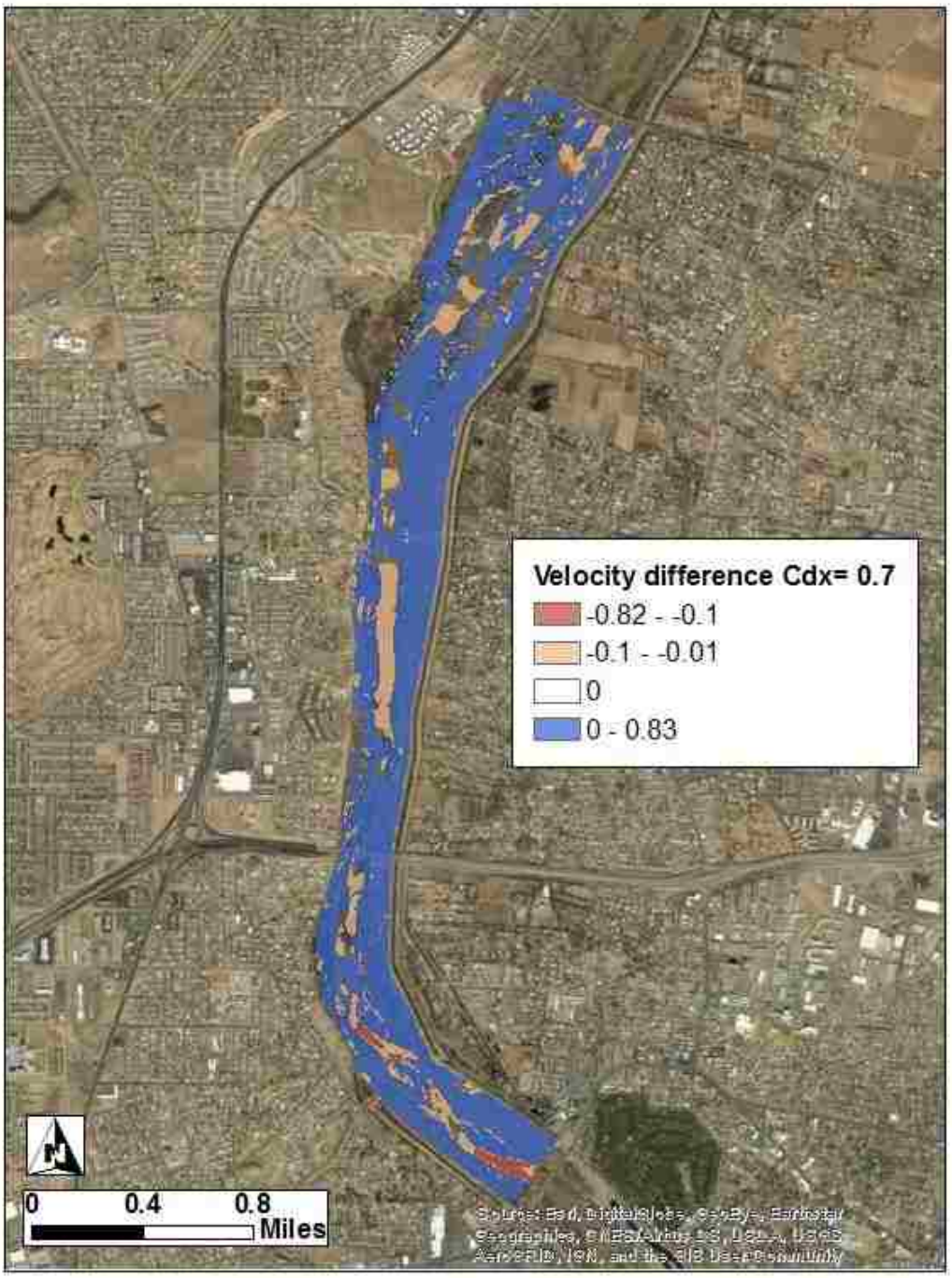

Figure c

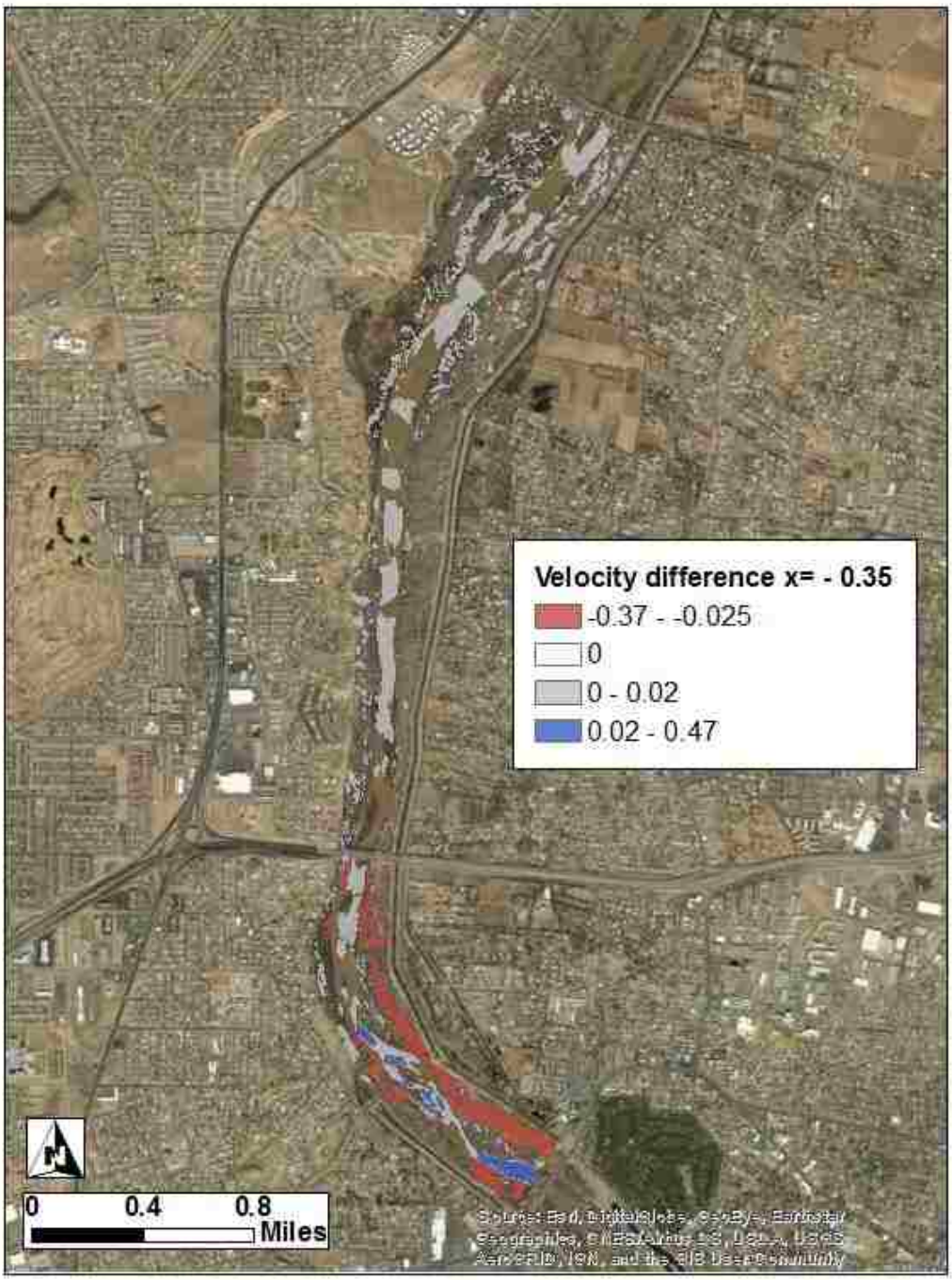

Figure d

Figure e

Figure 40: Velocity differences due to sensitivity analysis

Mapping of dynamic hydraulic roughness due to varying parameters

Mapping of differnce in hydraulic roughness which was obtained by subtracting dynamic hydraulic roughness calculated due to varying parameters from assumed standard parameters.

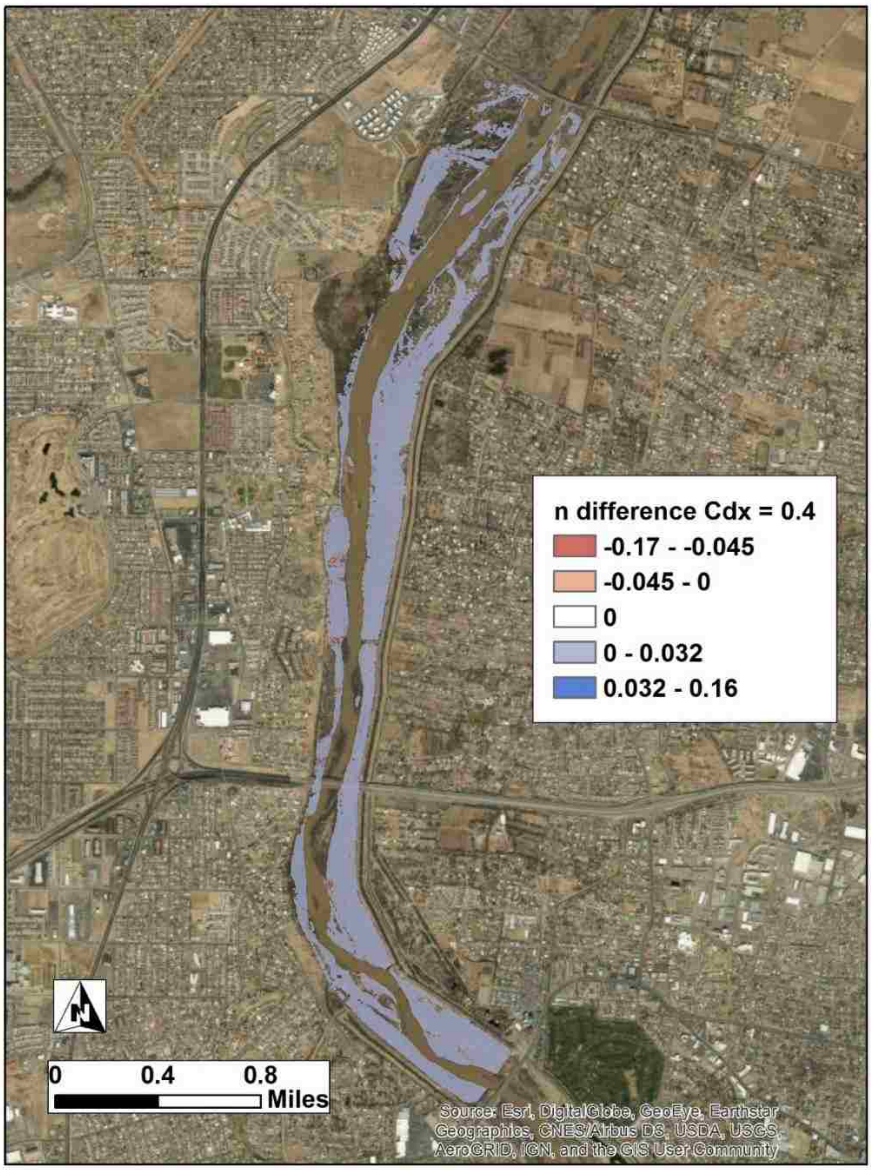

Figure a

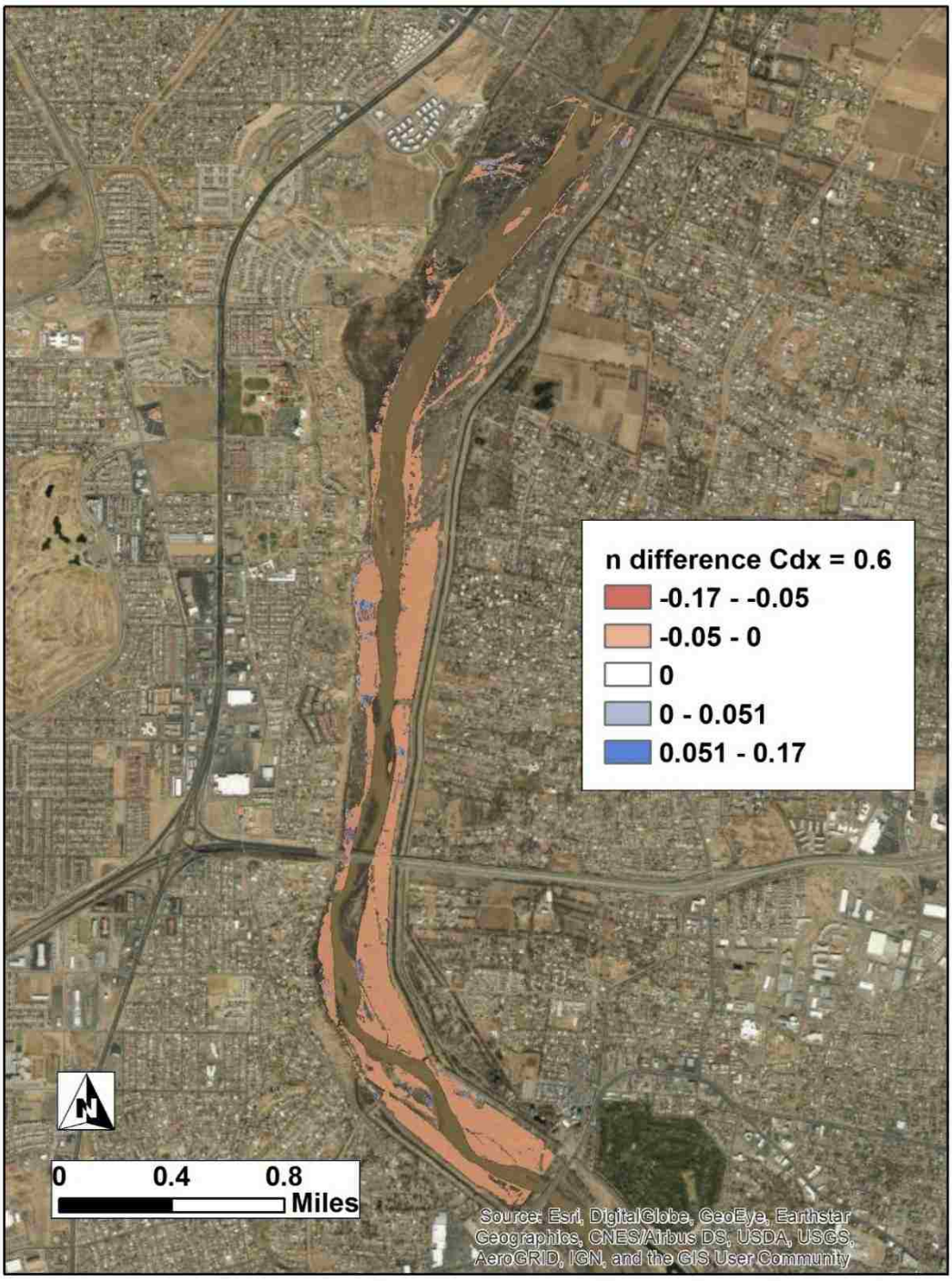

Figure b

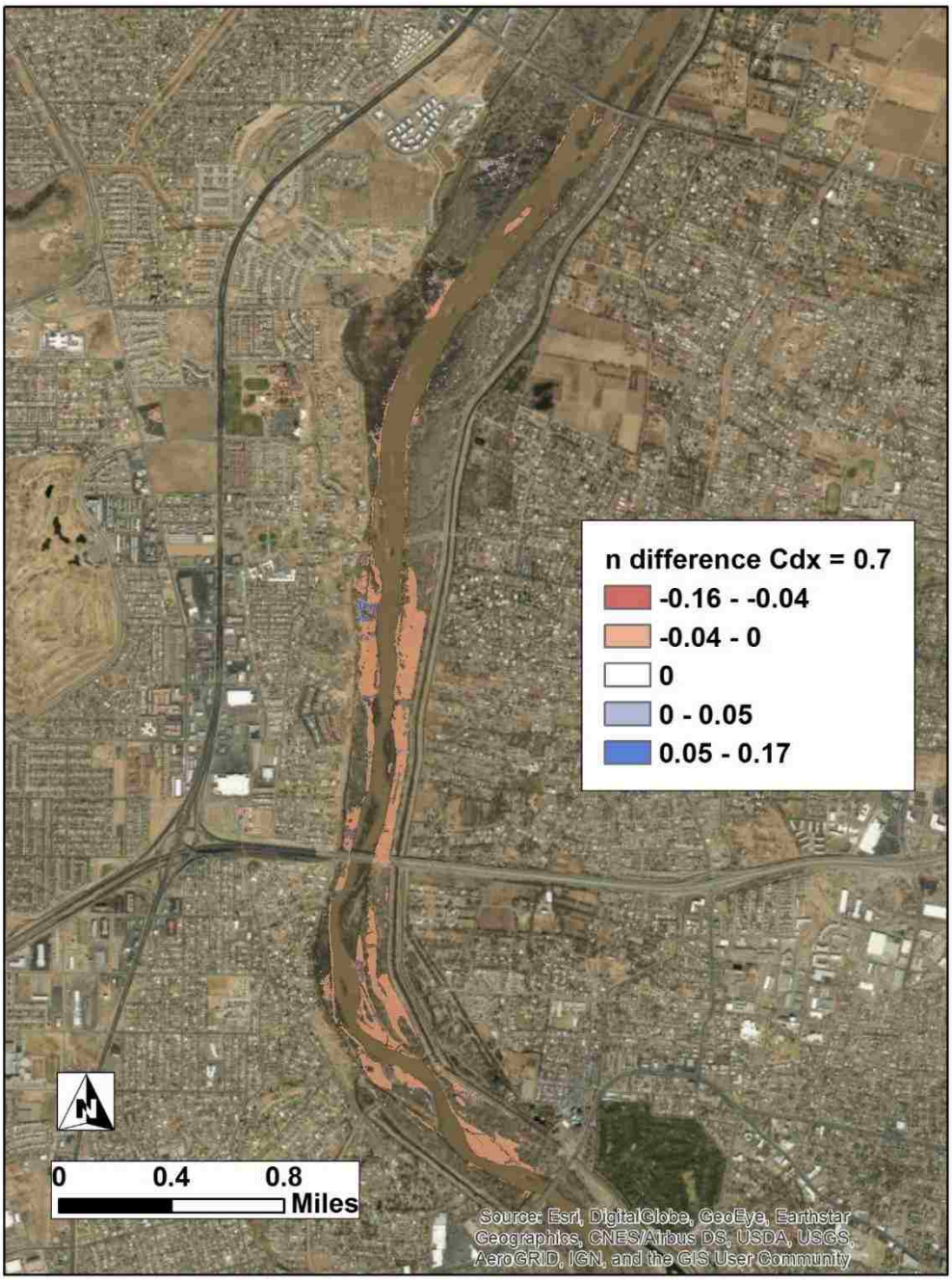

Figure c

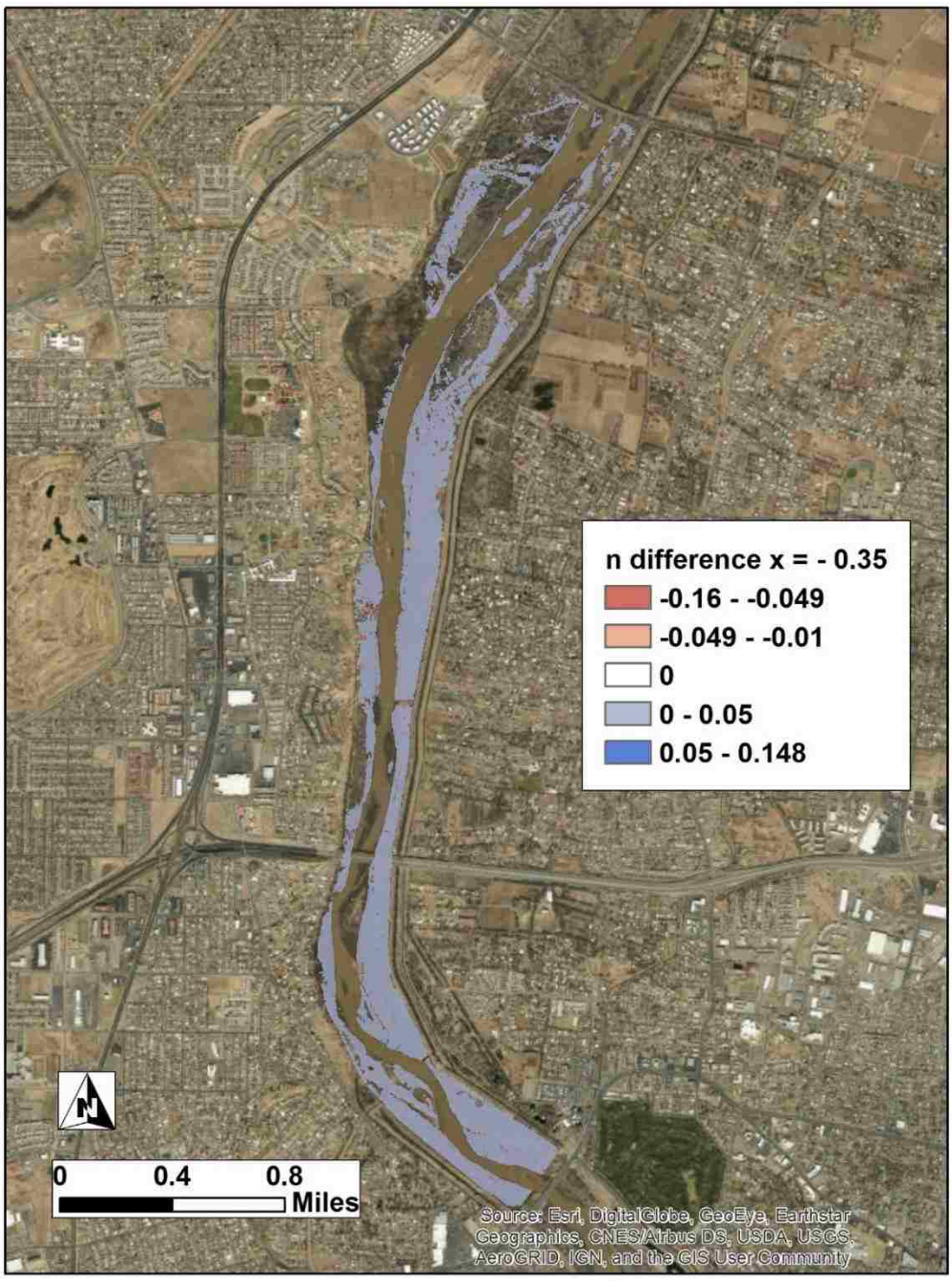

Figure d

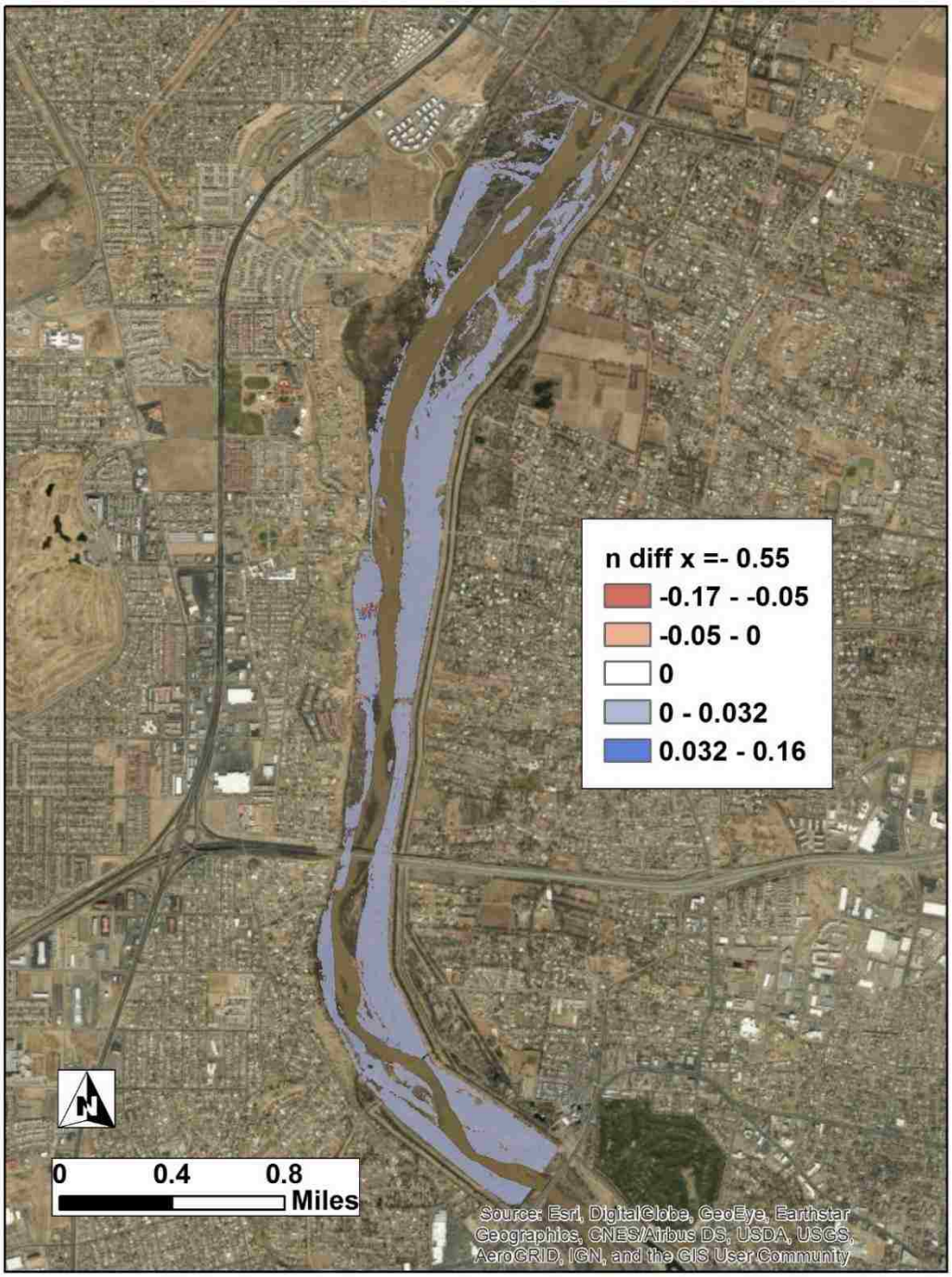

Figure e

Figure 41: Manning's n differences due to sensitivity analysis

Histograms for sensitivity analysis

The difference was calculated by substracting the hydraulic parameters from varying parameters by assumed standard value of parameter.

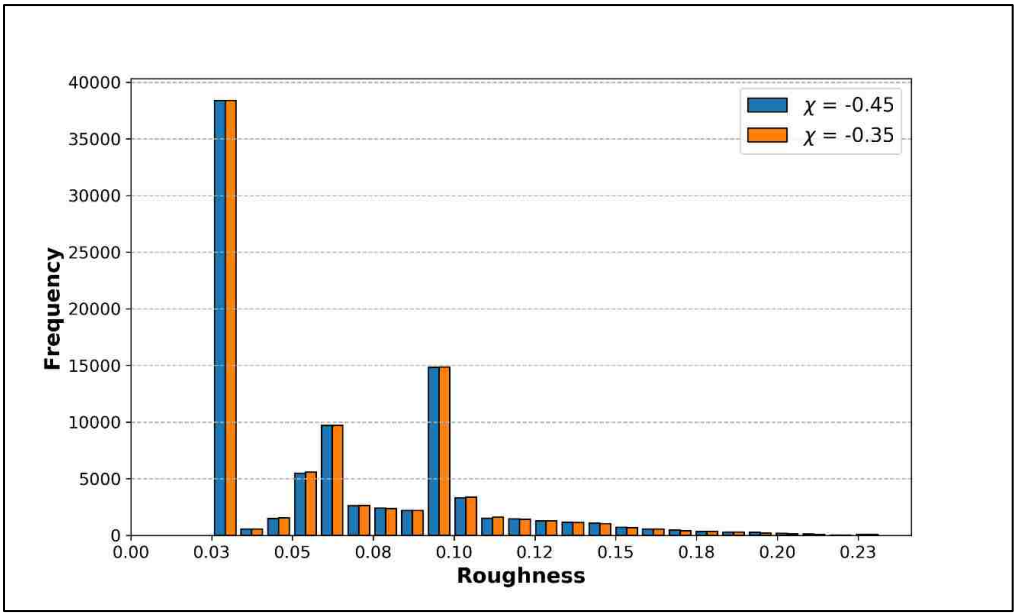

Figure a: n value for $\chi = -0.35$

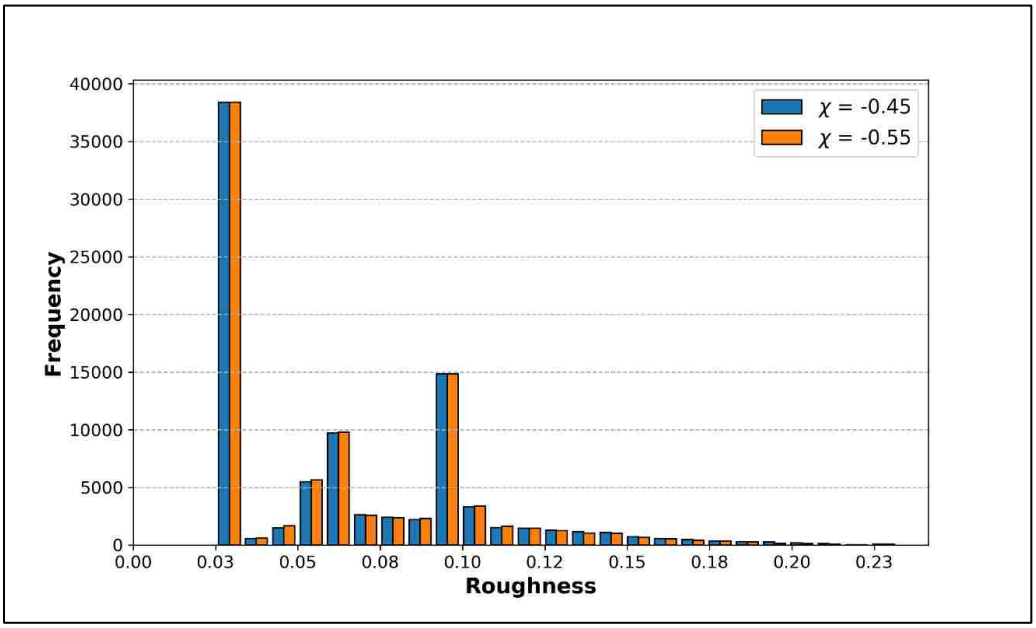

Figure b: n value for $\chi = -0.55$

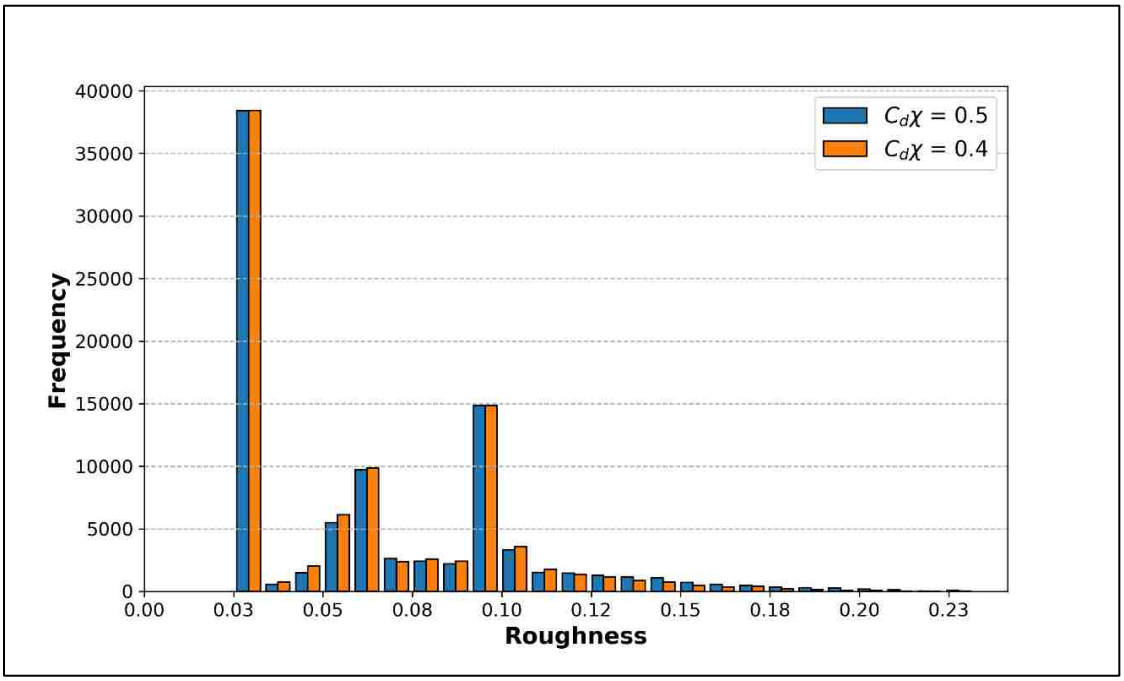

Figure c: n value for $C_{d\chi} = 0.4$

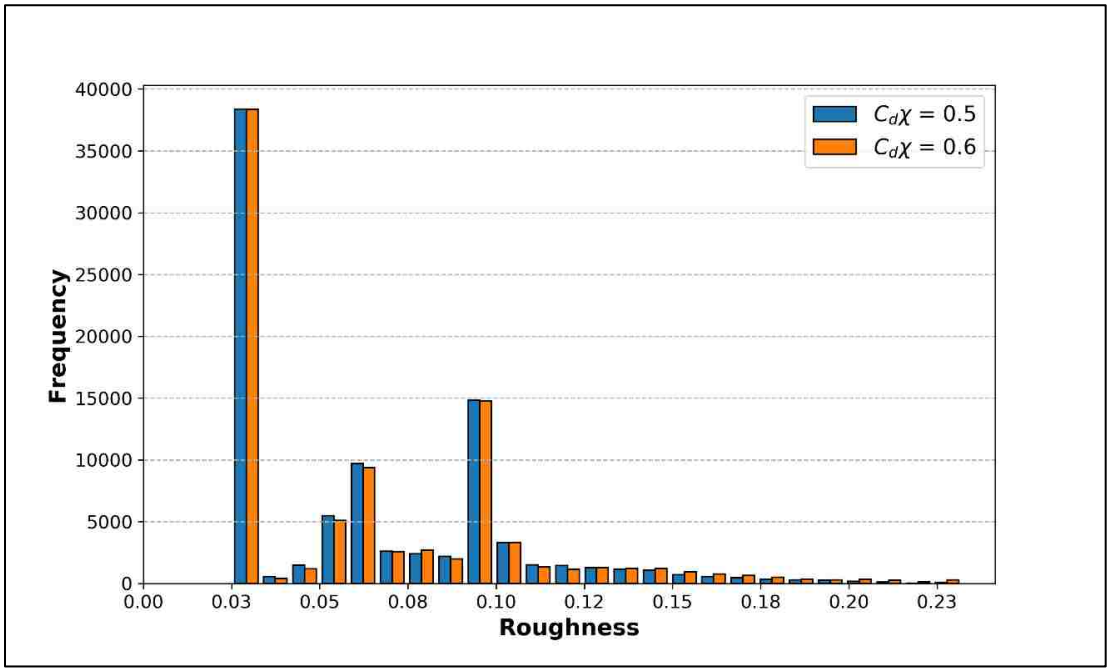

Figure d: n value for $C_{d\chi} = 0.6$

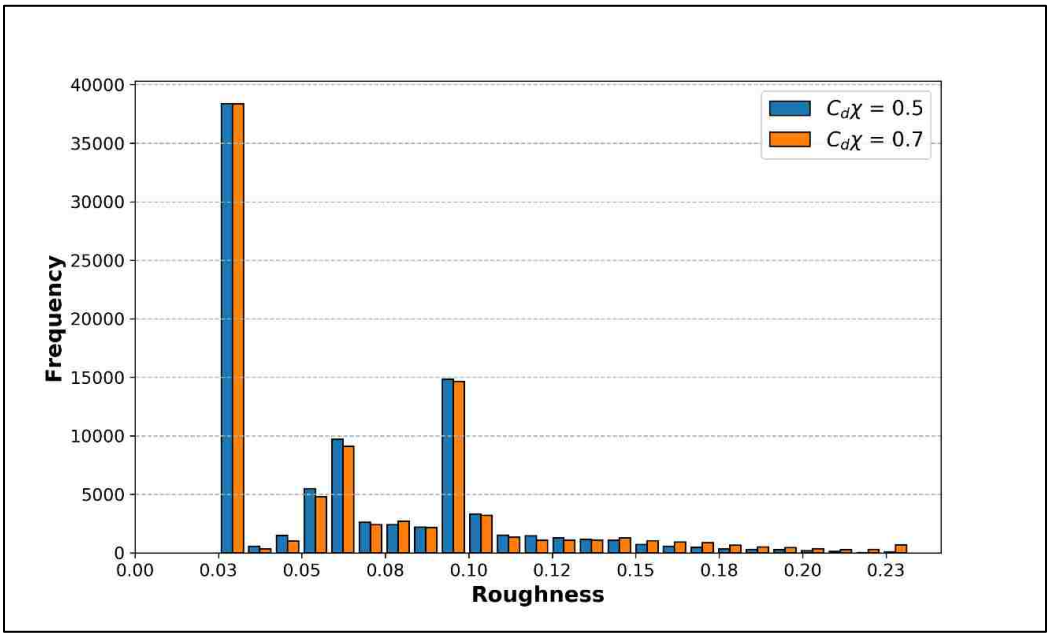

Figure e: n value for $C_{d\chi}$ = 0.7

Figure 42: Histogram for Manning's roughness n for sensitivity analysis

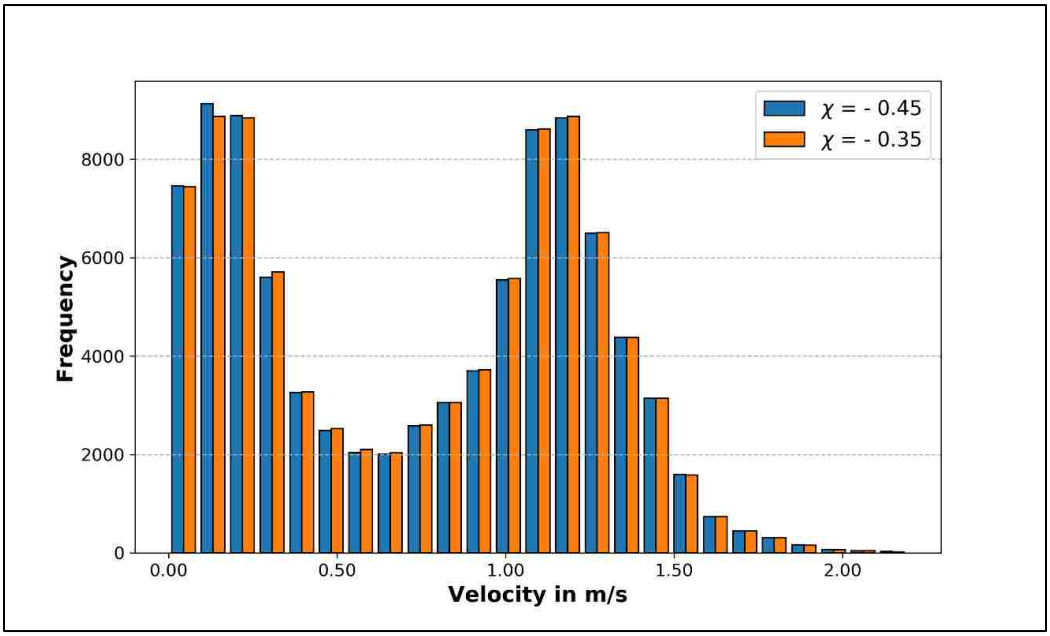

Figure a: Velocity for χ = -0.35

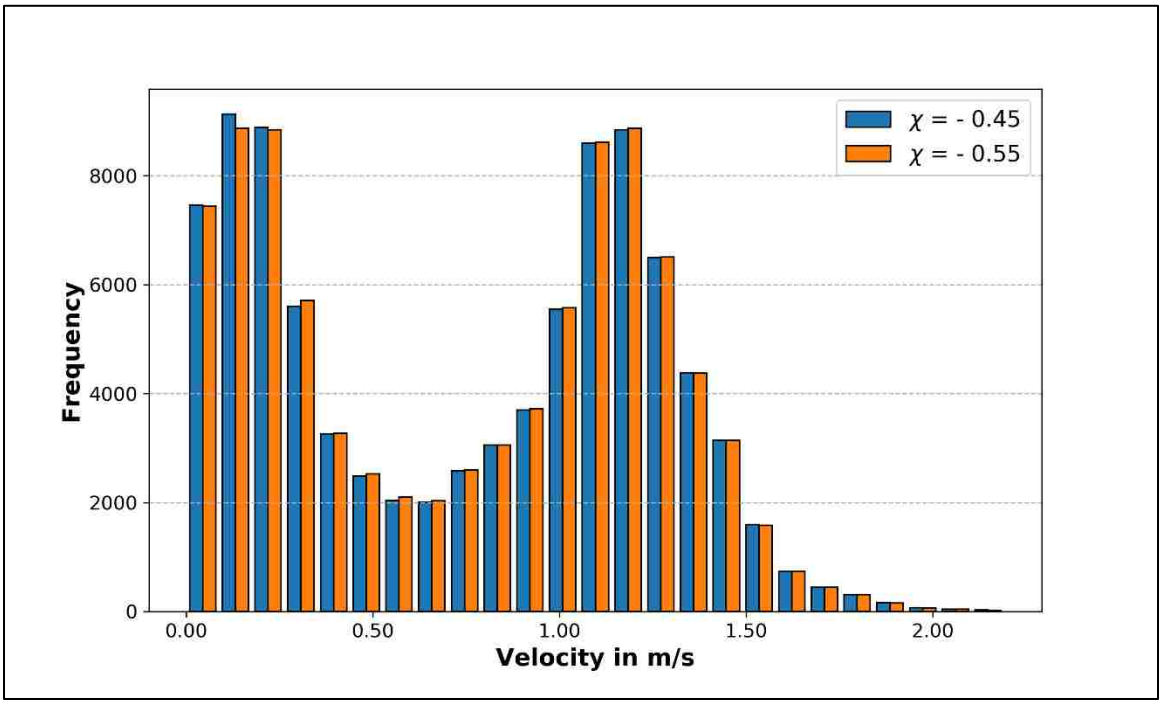

Figure b: Velocity for χ = -0.55

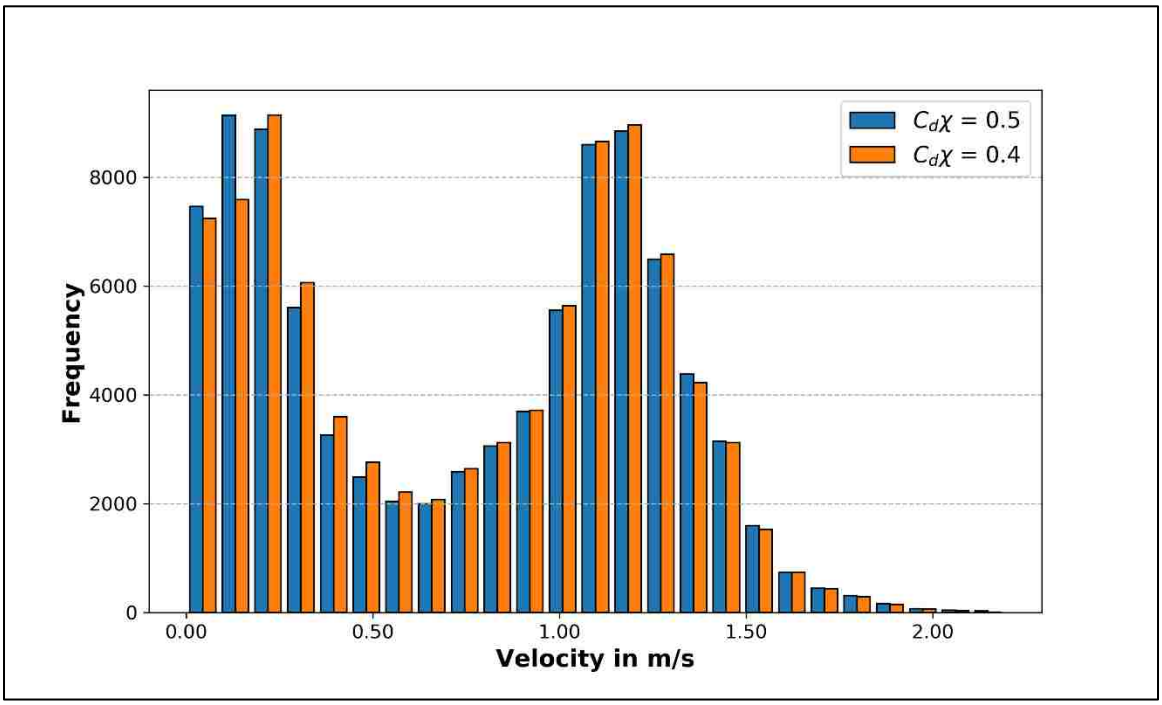

Figure c: Velocity value for Cdχ = 0.4

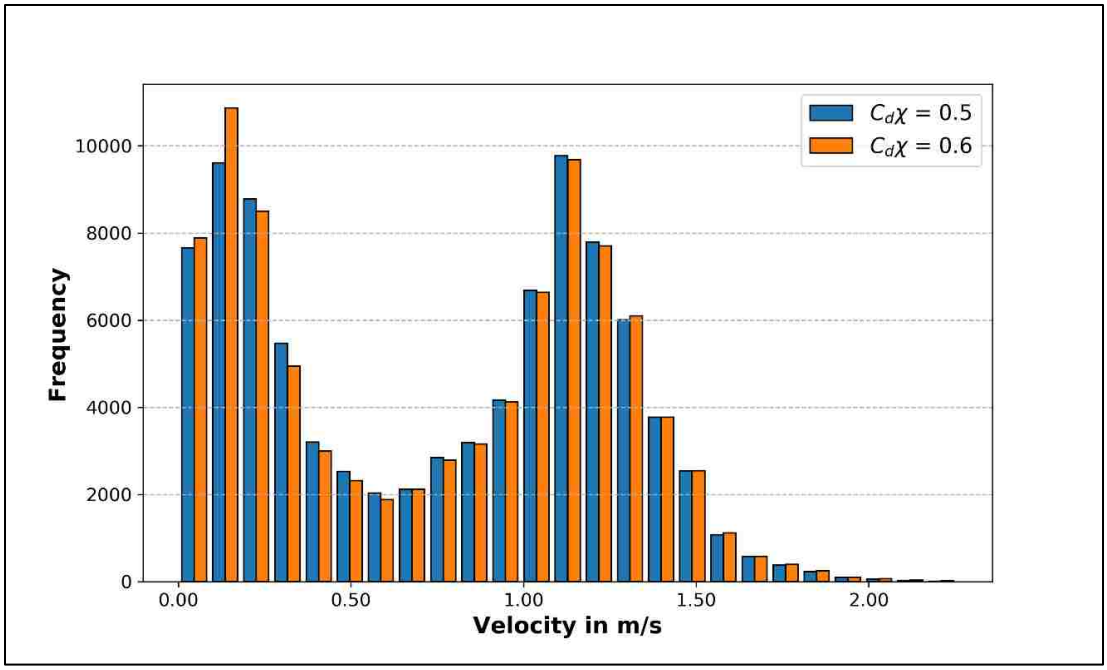

Figure d: Velocity value for Cdχ = 0.6

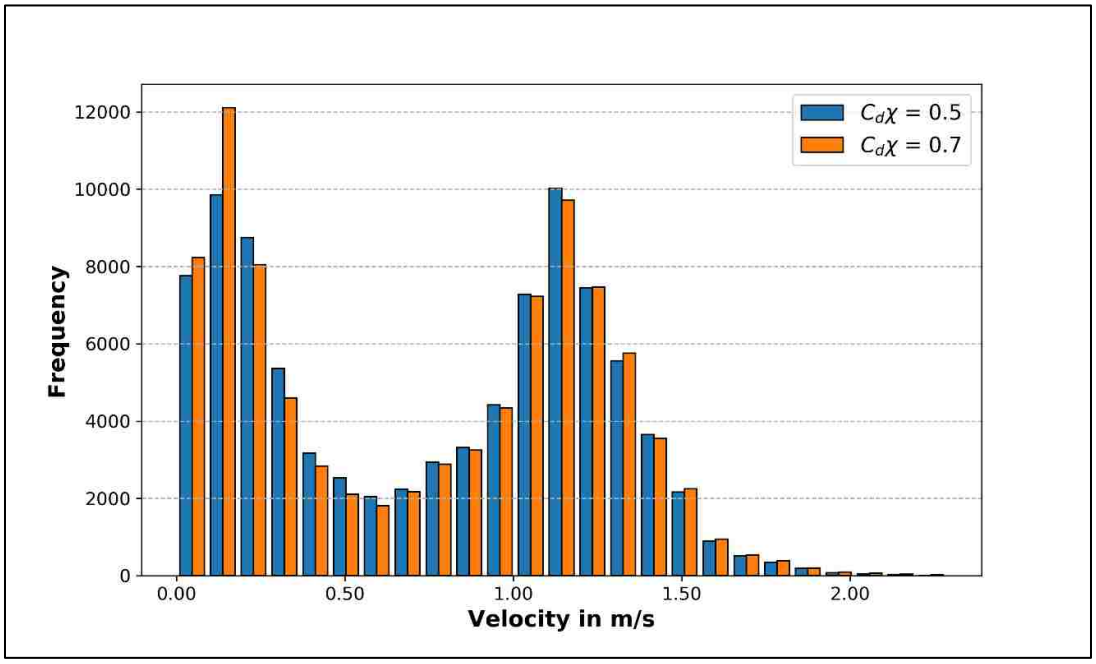

Figure e: Velocity value for Cdχ = 0.7

Figure 43: Histogram for Manning's roughness n for sensitivity analysis

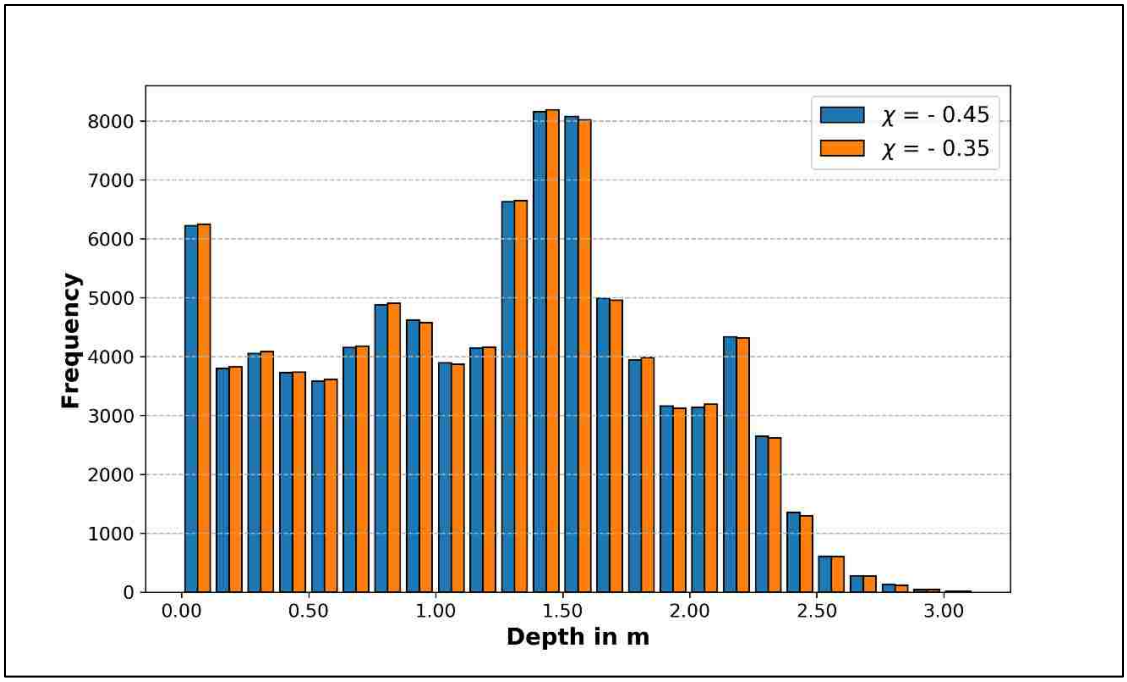

Figure a: Depth value for χ = -0.35

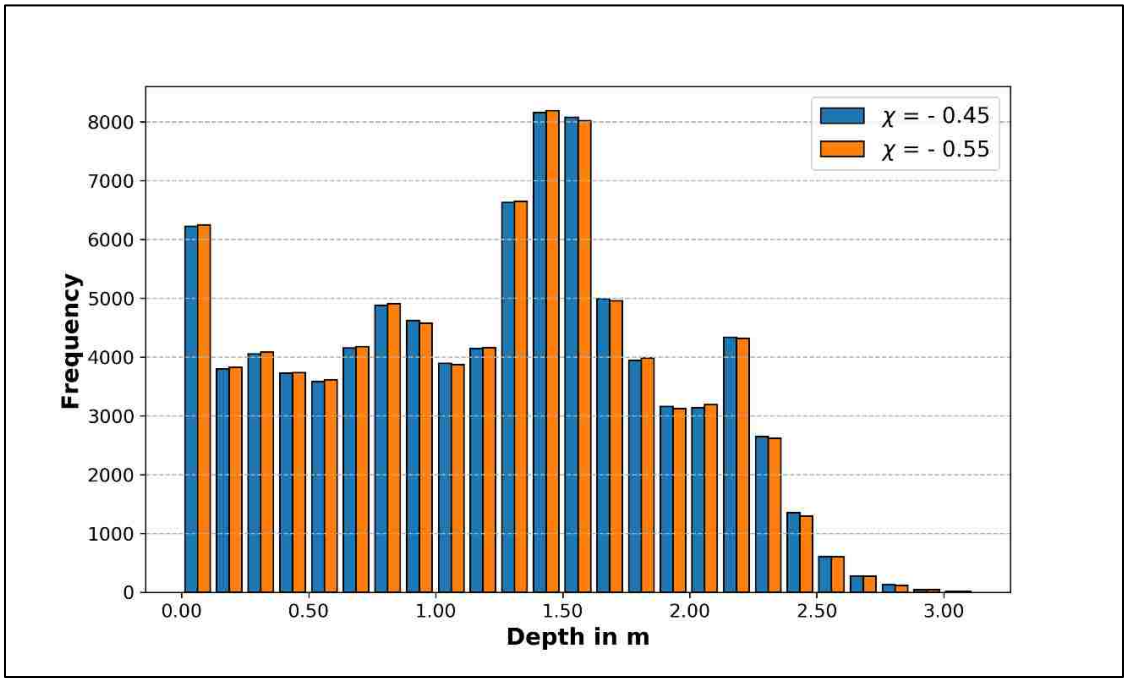

Figure b: Depth value for χ = -0.55

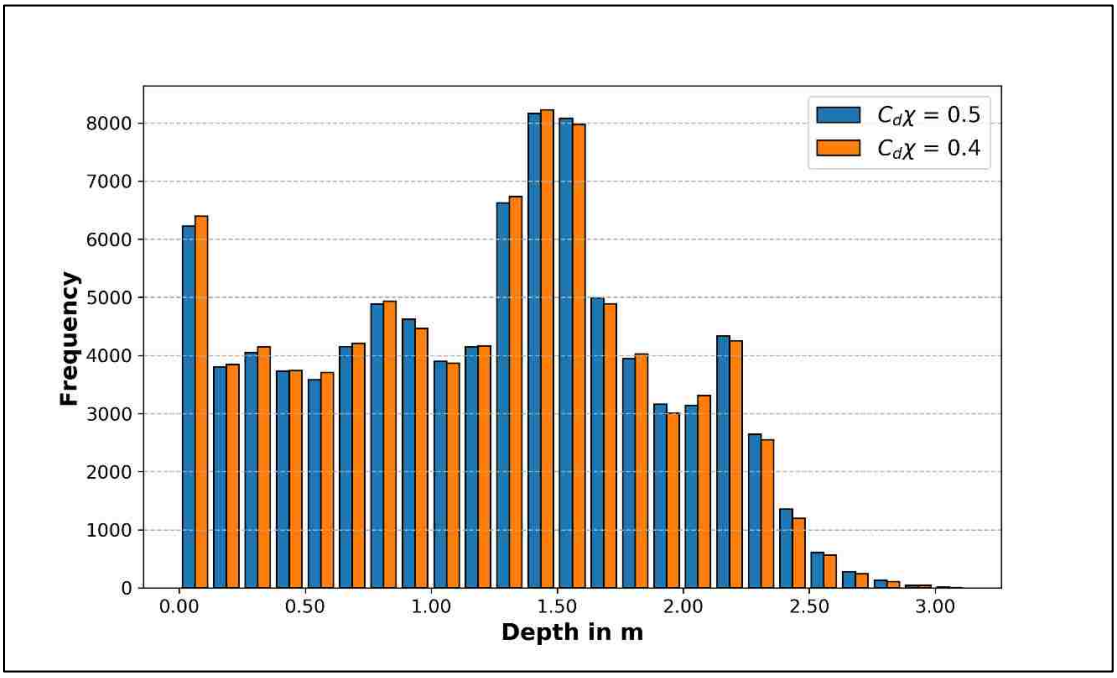

Figure c: Depth value for Cdχ = 0.4

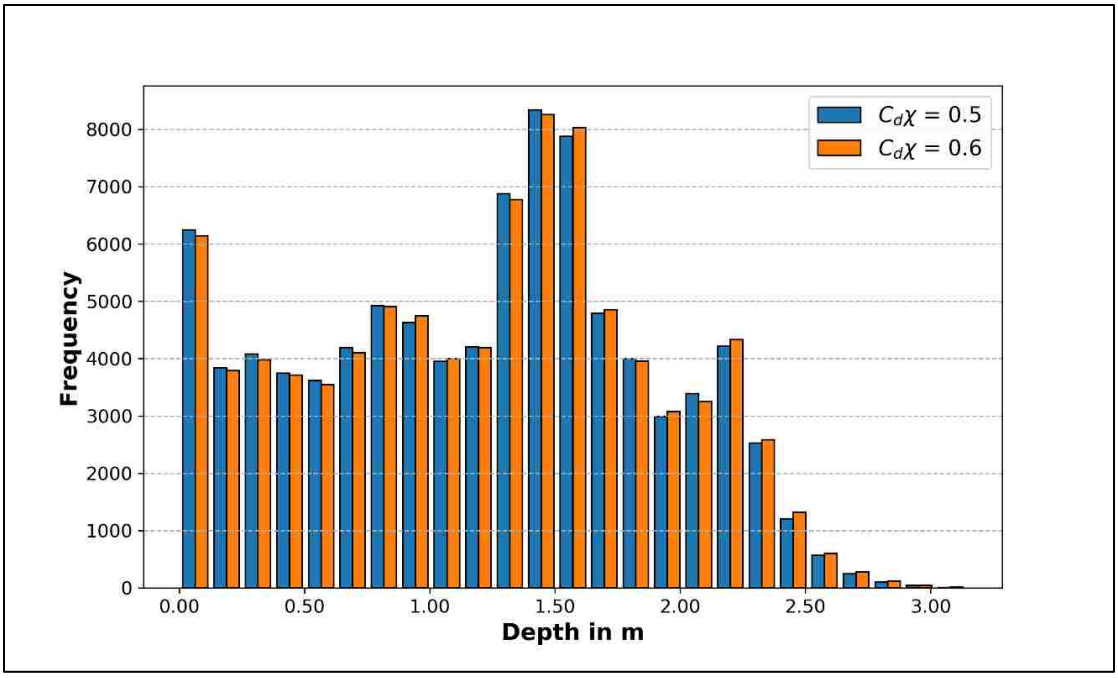

Figure d: Depth value for Cdχ = 0.6

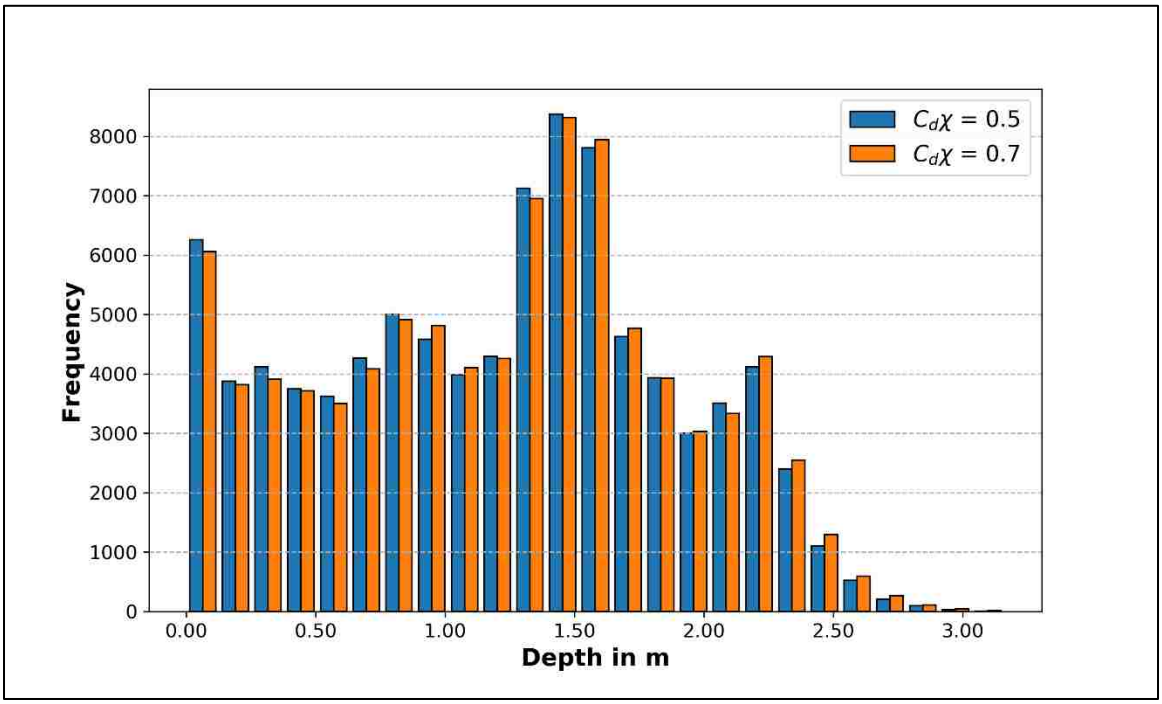

Figure e: Depth value for Cdχ = 0.7

Figure 44: Histogram for Manning's roughness n for sensitivity analysis

APPENDIX C. PICTURES OF FIELD

Photo 1: Site 1, Monotypic Cottonwood (sparse) (Close view, looking East)

Photo 2: Site 1, Monotypic Cottonwood (sparse) (looking East)

Photo 3: LAI measurement

Photo 3: Site 2, Monotypic Coyote Willows (looking North)

Photo 4: Site 2, Monotypic Coyote Willows (Sparse, looking west)

Photo 5: Site 4, Monotypic Cotton Wood (Dense, looking east)

Photo 6: Site 5, Native and Exotic (Dense, looking west)

Photo 7: Site 6, Native and Exotic (sparse, looking west)

Photo 8: Site 7, Monotypic Salt Cedar (Sparse, looing west)

Photo 9: Site 8, Monotypic Salt Cedar (Dense, looking west)

Photo 10: Site 9, Native Mixed (Sparse, looking south)

Photo 11: Site 10, Native Mixed (dense, looking west)

Photo 12: Site 11, Monotypic Coyote Willow (dense, looking east)

Photo 13: Tree diameter measurement

Photo 14: Measurement of tree height

Photo 15: Site 12, Cottonwood / Tree willow

Photo 16: Site 13, Cottonwood / Tree willow

Photo 17: Site 14, Native mixed

9. REFERENCES

Abu-Aly, T. R., Pasternack, G. B., Wyrick, J. R., Barker, R., Massa, D., & Johnson, T. (2014). Effects of LiDAR-derived, spatially distributed vegetation roughness on two-dimensional hydraulics in a gravel-cobble river at flows of 0.2 to 20 times bankfull. *Geomorphology*, *206*, 468–482. https://doi.org/10.1016/j.geomorph.2013.10.017

Adair, J. (2016). *Reconstructing the historical Albuquerque reach of the Middle Rio Grande to evaluate the influence of river engineering on floodplain inundation*.

Afzalimehr, H., & Dey, S. (2009). Influence of bank vegetation and gravel bed on velocity and Reynolds stress distributions. *International Journal of Sediment Research*, *24*(2), 236–246.

Arcement, G. J., & Schneider, V. R. (1989). *Guide for selecting Manning's roughness coefficients for natural channels and flood plains*. US Government Printing Office Washington, DC. Retrieved from http://ponce.sdsu.edu/usgs_report_2339.pdf

Baptist, M. J., Babovic, V., Rodríguez Uthurburu, J., Keijzer, M., Uittenbogaard, R. E., Mynett, A., & Verwey, A. (2007). On inducing equations for vegetation resistance. *Journal of Hydraulic Research*, *45*(4), 435–450. https://doi.org/10.1080/00221686.2007.9521778

Breda, N. J. J. (2003). Ground-based measurements of leaf area index: a review of methods, instruments and current controversies. *Journal of Experimental Botany*, *54*(392), 2403–2417. https://doi.org/10.1093/jxb/erg263

Busari, A. O., & Li, C. W. (2015). A hydraulic roughness model for submerged flexible vegetation with uncertainty estimation. *Journal of Hydro-Environment Research*, *9*(2), 268–280. https://doi.org/10.1016/j.jher.2014.06.005

Byrne, Colin F. (2017). "A Numerical Investigation of the Implications of Altered Channel-Floodplain Connectivity on Hydrodynamic Flood Wave Processes." http://digitalrepository.unm.edu/ce_etds/191

Casas, A., Lane, S. N., Yu, D., & Benito, G. (2010). A method for parameterising roughness and topographic sub-grid scale effects in hydraulic modelling from LiDAR data. *Hydrology and Earth System Sciences*, *14*(8), 1567–1579. https://doi.org/10.5194/hess-14-1567-2010

Chow, V. T. (1959). *Open-channel hydraulics*. McGraw-Hill.

Cleverly, J. R., Dahm, C. N., Thibault, J. R., McDonnell, D. E., & Allred Coonrod, J. E. (2006). Riparian ecohydrology: regulation of water flux from the ground to the atmosphere in the Middle Rio Grande, New Mexico. *Hydrological Processes*, *20*(15), 3207–3225. https://doi.org/10.1002/hyp.6328

Dombroski, D. (2017). *Remote Sensing of Vegetation Characteristics for Estimation of Partitioned Roughness in Hydraulic and Sediment Transport Modeling Applications* (RESEARCH). Denver, CO: Bureau of Reclamation, Denver Technical Service Center.

Dorn, H., Vetter, M., & Hoefle, B. (2014). GIS-Based Roughness Derivation for Flood Simulations: A Comparison of Orthophotos, LiDAR and Crowdsourced Geodata. *Remote Sensing*, *6*(2), 1739–1759. https://doi.org/10.3390/rs6021739

FathiMaghadam, M., & Kouwen, N. (1997). Nonrigid, nonsubmerged, vegetative roughness on floodplains. *Journal of Hydraulic Engineering-Asce*, *123*(1), 51–57. https://doi.org/10.1061/(ASCE)0733-9429(1997)123:1(51)

Fathi-Moghadam, M. (1996). *Momentum absorption in non-rigid, non-submerged, tall vegetation along rivers* (Ph.D.). University of Waterloo (Canada), Canada. Retrieved from https://search-proquest-

com.libproxy.unm.edu/pqdtglobal/docview/304340364/abstract/4551D1E548654172PQ/1

Forzieri, G., Degetto, M., Righetti, M., Castelli, F., & Preti, F. (2011). Satellite multispectral data for improved floodplain roughness modelling. *Journal of Hydrology*, *407*(1–4), 41–57. https://doi.org/10.1016/j.jhydrol.2011.07.009

Forzieri, G., Moser, G., Vivoni, E. R., Castelli, F., & Canovaro, F. (2010). Riparian Vegetation Mapping for Hydraulic Roughness Estimation Using Very High Resolution Remote Sensing Data Fusion. *Journal of Hydraulic Engineering-Asce*, *136*(11), 855–867. https://doi.org/10.1061/(ASCE)HY.1943-7900.0000254

Gillihan, T. (2013). Dynamic vegetation Roughness in the riparian zone. *Civil Engineering ETDs*. Retrieved from http://digitalrepository.unm.edu/ce_etds/82

Gould, G. K., Liu, M., Barber, M. E., Cherkauer, K. A., Robichaud, P. R., & Adam, J. C. (2016). The effects of climate change and extreme wildfire events on runoff erosion over a mountain watershed. *Journal of Hydrology*, *536*, 74–91. https://doi.org/10.1016/j.jhydrol.2016.02.025

Hartwell, S., Morino, K., Nagler, P. L., & Glenn, E. P. (2010). On the irrigation requirements of cottonwood (Populus fremontii and Populus deltoides var. wislizenii) and willow (Salix gooddingii) grown in a desert environment. *Journal of Arid Environments*, *74*(6), 667–674. https://doi.org/10.1016/j.jaridenv.2009.12.007

Horritt, M. S., & Bates, P. D. (2002). Evaluation of 1D and 2D numerical models for predicting river flood inundation. *Journal of Hydrology*, *268*(1–4), 87–99. https://doi.org/10.1016/S0022-1694(02)00121-X

Isaacson, K., & Coonrod, J. (2011). USGS Streamflow Data and Modeling Sand-Bed Rivers. *Journal of Hydraulic Engineering-Asce*, *137*(8), 847–851. https://doi.org/10.1061/(ASCE)HY.1943-7900.0000362

Isenburg,M., 2014. "LAStools - efficient LiDAR processing software"

Jalonen, J., Jarvela, J., & Aberle, J. (2013). Leaf Area Index as Vegetation Density Measure for Hydraulic Analyses. *Journal of Hydraulic Engineering-Asce*, *139*(5), 461–469. https://doi.org/10.1061/(ASCE)HY.1943-7900.0000700

Järvelä, J. (2002). Flow resistance of flexible and stiff vegetation: a flume study with natural plants. *Journal of Hydrology*, *269*(1–2), 44–54. https://doi.org/10.1016/S0022-1694(02)00193-2

Järvelä, J. (2004). Determination of flow resistance caused by non-submerged woody vegetation. *International Journal of River Basin Management*, *2*(1), 61–70.

Jarvela, J. (2005). Effect of submerged flexible vegetation on flow structure and resistance. *Journal of Hydrology*, *307*(1–4), 233–241. https://doi.org/10.1016/j.jhydrol.2004.10.013

Jensen, J. R. (2016). *Introductory Digital Image Processing: A Remote Sensing Perspective* (fourth edition). Pearson.

Jeong, S. G., Mo, Y., Kim, H. G., Park, C. H., & Lee, D. K. (2016). Mapping riparian habitat using a combination of remote-sensing techniques. *International Journal of Remote Sensing*, *37*(5), 1069–1088. https://doi.org/10.1080/01431161.2016.1142685

Kouwen, N., Li, R. M., & Simons, D. B. (1981). Flow resistance in vegetated waterways. *Transactions of the ASAE [American Society of Agricultural Engineers] (USA)*. Retrieved from http://agris.fao.org/agris-search/search.do?recordID=US8123000

Lai, Y. G. (2008). SRH-2D version 2: Theory and User's Manual. Sedimentation and River Hydraulics–Two-Dimensional River Flow Modeling. US Bureau of Reclamation, Technical Service Center, Denver, CO.

Leopold, L. B. (1994). *A View of the River*. Cambridge, Mass: Harvard University Press.

Luo, S., Chen, J. M., Wang, C., Gonsamo, A., Xi, X., Lin, Y., … Qin, H. (2018). Comparative Performances of Airborne LiDAR Height and Intensity Data for Leaf Area Index

Estimation. *Ieee Journal of Selected Topics in Applied Earth Observations and Remote Sensing*, *11*(1), 300–310. https://doi.org/10.1109/JSTARS.2017.2765890

Mason, D. C., Cobby, D. M., Horritt, M. S., & Bates, P. D. (2003). Floodplain friction parameterization in two-dimensional river flood models using vegetation heights derived from airborne scanning laser altimetry. *Hydrological Processes*, *17*(9), 1711–1732. https://doi.org/10.1002/hyp.1270

Mussetter Engineering, Inc. (2006). *Evaluation of Bar Morphology, Distribution and Dynamics as Indices of Fluvial Processes in the Middle Rio Grande, New Mexico* (p. 156). Fort Collins, Colorado.

Nepf, H. M. (1999). Drag, turbulence, and diffusion in flow through emergent vegetation. *Water Resources Research*, *35*(2), 479–489. https://doi.org/10.1029/1998WR900069

Poff, N. L., Allan, J. D., Bain, M. B., & Stromberg, J. C. (1997). The Natural Flow Regime: A Paradigm for River Conservation and Restoration, *47*(11). Retrieved from http://wec.ufl.edu/floridarivers/RiverClass/Papers/Poff%20et%20al.%2097%20natflow_paradigm.pdf

Ree, W. O., & Palmer, V. J. (1949). Flow of water in channels protected by vegetative linings. *U S Dept Agric Tech Bull*, *967*, 1–115.

Richard, G., & Julien, P. (2003). *A. Reservoir Effects of Stream Channels DAM IMPACTS ON AND RESTORATION OF AN ALLUVIAL RIVER*.

Richardson, J. J., Moskal, L. M., & Kim, S.-H. (2009). Modeling approaches to estimate effective leaf area index from aerial discrete-return LIDAR. *Agricultural and Forest Meteorology*, *149*(6–7), 1152–1160. https://doi.org/10.1016/j.agrformet.2009.02.007

Soil Conservation Service. (1954). *Handbook of channel design for soil and water conservation.* Stillwater, OK.: SCS-TP-61 Stillwater Outdoor Hydraulic Laboratory Stillwater Oklahoma:

Solberg, S., Næsset, E., Hanssen, K. H., & Christiansen, E. (2006). Mapping defoliation during a severe insect attack on Scots pine using airborne laser scanning. *Remote Sensing of Environment*, *102*(3–4), 364–376. https://doi.org/10.1016/j.rse.2006.03.001

Stone, M. C., Byrne, C. F., & Morrison, R. R. (2017). Evaluating the impacts of hydrologic and geomorphic alterations on floodplain connectivity. *Ecohydrology*. Retrieved from http://doi.org/10.1002/eco.1833

Stone, M. C., Chen, L., Kyle McKay, S., Goreham, J., Acharya, K., Fischenich, C., & Stone, A. B. (2013). Bending of submerged woody riparian vegetation as a function of hydraulic flow conditions: bending of submerged woody riparian vegetation. *River Research and Applications*, *29*(2), 195–205. https://doi.org/10.1002/rra.1592

Straatsma, M., & Huthoff, F. (2011). Uncertainty in 2D hydrodynamic models from errors in roughness parameterization based on aerial images. *Physics and Chemistry of the Earth*, *36*(7–8), 324–334. https://doi.org/10.1016/j.pce.2011.02.009

Straatsma, M. W., & Baptist, M. J. (2008). Floodplain roughness parameterization using airborne laser scanning and spectral remote sensing. *Remote Sensing of Environment*, *112*(3), 1062–1080. https://doi.org/10.1016/j.rse.2007.07.012

Straatsma, M. W., Warmink, J. J., & Middelkoop, H. (2008). Two novel methods for field measurements of hydrodynamic density of floodplain vegetation using terrestrial laser scanning and digital parallel photography. *International Journal of Remote Sensing*, *29*(5), 1595–1617. https://doi.org/10.1080/01431160701736455

Straatsma, Menno W. (2008). Quantitative mapping of hydrodynamic vegetation density of floodplain forests under leaf-off conditions using airborne laser scanning. *Photogrammetric Engineering and Remote Sensing*, *74*(8), 987–998.

Stromberg, J. C., Beauchamp, V. B., Dixon, M. D., Lite, S. J., & Paradzick, C. (2007). Importance of low-flow and high-flow characteristics to restoration of riparian vegetation

along rivers in arid south-western United States. *Freshwater Biology*, *52*(4), 651–679. https://doi.org/10.1111/j.1365-2427.2006.01713.x

Temple, D. M., Service, U. S. A. R., & Station, O. A. E. (1987). *Stability design of grass-lined open channels*. U.S. Dept. of Agriculture, Agricultural Research Service.

Tseng, Y.-H., Lin, L.-P., & Wang, C.-K. (2016). Mapping CHM and LAI for Heterogeneous Forests Using Airborne Full-Waveform LiDAR Data. *Terrestrial Atmospheric and Oceanic Sciences*, *27*(4), 537–548. https://doi.org/10.3319/TAO.2016.01.29.04(ISRS)

Uotani, T., Kanda, K., & Michioku, K. (2014). Experimental and numerical study on hydrodynamics of riparian vegetation. *Journal of Hydrodynamics, Ser. B*, *26*(5), 796–806. https://doi.org/10.1016/S1001-6058(14)60088-3

van Dijk, W. M., Teske, R., van de Lageweg, W. I., & Kleinhans, M. G. (2013). Effects of vegetation distribution on experimental river channel dynamics. *Water Resources Research*, *49*(11), 7558–7574. https://doi.org/10.1002/2013WR013574

Vargas-Luna, A., Crosato, A., & Uijttewaal, W. S. J. (2015). Effects of vegetation on flow and sediment transport: comparative analyses and validation of predicting models: EFFECTS OF VEGETATION ON FLOW AND SEDIMENT TRANSPORT. *Earth Surface Processes and Landforms*, *40*(2), 157–176. https://doi.org/10.1002/esp.3633

Weiss, J. L., Gutzler, D. S., Allred Coonrod, J. E., & Dahm, C. N. (2004). Seasonal and inter-annual relationships between vegetation and climate in central New Mexico, USA. *Journal of Arid Environments*, *57*(4), 507–534. https://doi.org/10.1016/S0140-1963(03)00113-7

Wilson, C. A. M. E., & Horritt, M. S. (2002). Measuring the flow resistance of submerged grass. *Hydrological Processes*, *16*(13), 2589–2598. https://doi.org/10.1002/hyp.1049

Wilson, C., Stoesser, T., Bates, P. D., & Pinzen, A. B. (2003). Open channel flow through different forms of submerged flexible vegetation. *Journal of Hydraulic Engineering-Asce*, *129*(11), 847–853. https://doi.org/10.1061/(ASCE)0733-9429(2003)129:11(847)

Wu, F.-C., Shen, H. W., & Chou, Y.-J. (1999). Variation of Roughness Coefficients for Unsubmerged and Submerged Vegetation. *Journal of Hydraulic Engineering*, *125*(9). Retrieved from http://ascelibrary.org.libproxy.unm.edu/doi/10.1061/%28ASCE%290733-9429%281999%29125%3A9%28934%29

Wu, W., & He, Z. (2009). Effects of vegetation on flow conveyance and sediment transport capacity. *International Journal of Sediment Research*, *24*(3), 247–259.

Yi, Y., Wang, Z., Zhang, K., Yu, G., & Duan, X. (2008). Sediment pollution and its effect on fish through food chain in the Yangtze River. *International Journal of Sediment Research*, *23*(4), 338–347.

Zahidi, I., Yusuf, B., Hamedianfar, A., Shafri, H. Z. M., & Mohamed, T. A. (2015). Object-based classification of QuickBird image and low point density LIDAR for tropical trees and shrubs mapping. *European Journal of Remote Sensing*, *48*, 423–446. https://doi.org/10.5721/EuJRS20154824